

THIS FILE IS MADE AVAILABLE THROUGH THE DECLASSIFICATION EFFORTS AND RESEARCH OF:

THE BLACK VAULT

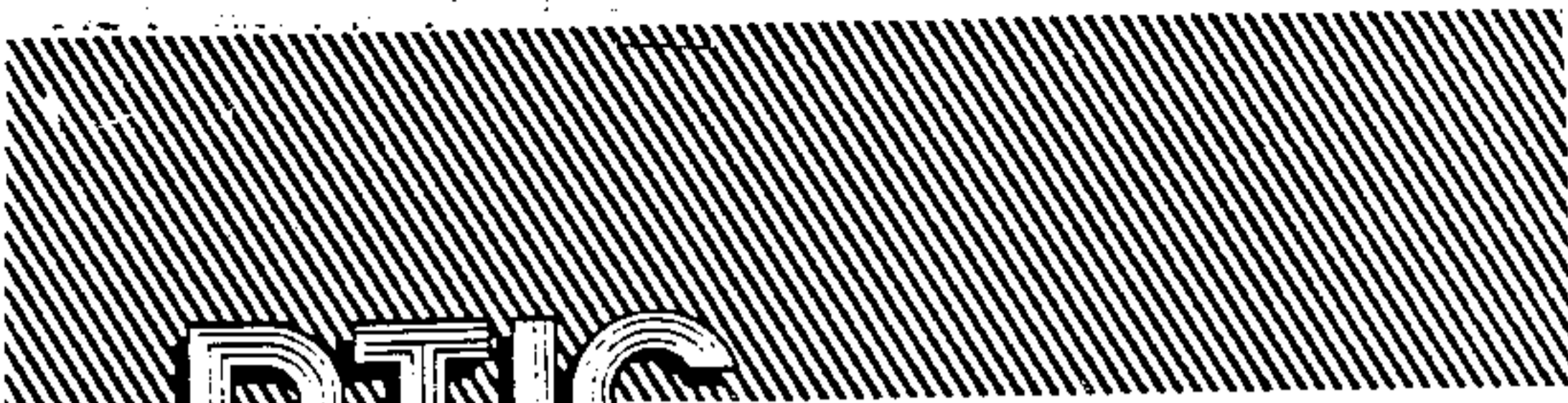
THE BLACK VAULT IS THE LARGEST ONLINE FREEDOM OF INFORMATION ACT / GOVERNMENT RECORD CLEARING HOUSE IN THE WORLD. THE RESEARCH EFFORTS HERE ARE RESPONSIBLE FOR THE DECLASSIFICATION OF THOUSANDS OF DOCUMENTS THROUGHOUT THE U.S. GOVERNMENT, AND ALL CAN BE DOWNLOADED BY VISITING:

[HTTP://WWW.BLACKVAULT.COM](http://www.blackvault.com)

YOU ARE ENCOURAGED TO FORWARD THIS DOCUMENT TO YOUR FRIENDS, BUT PLEASE KEEP THIS IDENTIFYING IMAGE AT THE TOP OF THE .PDF SO OTHERS CAN DOWNLOAD MORE!

UNCLASSIFIED

AD515 288 L
196



DTIC

690602

EXCISED UNDER THE PROVISIONS OF THE
FREEDOM OF INFORMATION ACT 5USC552
(b) (1)

Technical Report

APR 22 1993

THIS DOCUMENT HAS BEEN DOWNGRADED
TO ~~UNCLASSIFIED~~
Per Director ARPA S&IO/TIC

12418

distributed by

~~2) [unclear]~~



**Defense Technical Information Center
DEFENSE LOGISTICS AGENCY**

CAMERON STATION, ALEXANDRIA, VIRGINIA 22304-6145

UNCLASSIFIED

DARPA DO NOT REMOVE DARPA
EDARPA00052482A
ZODARPA00031535L

NOTICE

We are pleased to supply this document in response to your request.

The acquisition of technical reports, notes, memorandums, etc., is an active, ongoing program at the Defense Technical Information Center (DTIC) that depends, in part, on the efforts and interests of users and contributors.

Therefore, if you know of the existence of any significant reports, etc., that are not in the DTIC collection, we would appreciate receiving copies or information related to their sources and availability.

The appropriate regulations are Department of Defense Directive 3200.12, DoD Scientific and Technical Information Program; Department of Defense Directive 5200.20, Distribution Statements on Technical Documents (amended by Secretary of Defense Memorandum, 18 Oct 1983, subject: Control of Unclassified Technology with Military Application); Military Standard (MIL-STD) 847-B, Format Requirements for Scientific and Technical Reports Prepared by or for the Department of Defense; Department of Defense 5200.1R, Information Security Program Regulation.

Our Acquisition Section, DTIC-DDAB, will assist in resolving any questions you may have. Telephone numbers of that office are: (202)274-6847, 274-6874 or Autovon 284-6847, 284-6874.

FEBRUARY 1984

U.S. GOVERNMENT PRINTING OFFICE: 1983-551 165 30047



STATE OF TEXAS

ADULTS 15288

10	11	12	13	14	15
16	17	18	19	20	21
22	23	24	25	26	27

SECURITY MARKING

The classified or limited status of this report applies to each page, unless otherwise marked.
Separate page printouts **MUST** be marked accordingly.

THIS DOCUMENT CONTAINS INFORMATION AFFECTING THE NATIONAL DEFENSE OF THE UNITED STATES WITHIN THE MEANING OF THE ESPIONAGE LAWS, TITLE 18, U.S.C., SECTIONS 793 AND 794. THE TRANSMISSION OR THE REVELATION OF ITS CONTENTS IN ANY MANNER TO AN UNAUTHORIZED PERSON IS PROHIBITED BY LAW.

NOTICE: When government or other drawings, specifications or other data are used for any purpose other than in connection with a definitely related government procurement operation, the U.S. Government thereby incurs no responsibility, nor any obligation whatsoever; and the fact that the Government may have formulated, furnished, or in any way supplied the said drawings, specifications, or other data is not to be regarded by implication or otherwise as in any manner licensing the holder or any other person or corporation, or conveying any rights or permission to manufacture, use or sell any patented invention that may in any way be related thereto.

UNCLASSIFIED

Sylvania Electronic Systems-Western Division
Electronic Defense Laboratories
Mountain View, California

APR 22 1993

THIS DOCUMENT HAS BEEN DOWNGRADED
TO **UNCLASSIFIED**

Per Director, ARPA, S&ID/TIO

EDL-E184

Project Aquarius Final Report (U)

Project Engineer: K. Snow 415/966-3186

ARPA Order No. 1459

Effective Date of Contract: 2 June 1969

Contract Expiration Date: 31 May 1971

Amount of Contract: \$118,864

DDC
PREMISE
MAY 24 1971
RECEIVED
D

ARPA - TIO ARL: VA 22209

This research was supported by the Advanced Research
Projects Agency of the Department of Defense and was monitored
by the Office of Naval Research under Contract No. N00014-69-C-0446

DDC CONTROL
NO. 11391

UNCLASSIFIED

UNCLASSIFIED

~~SECRET~~

(U) TABLE OF CONTENTS (U)

<u>Section</u>	<u>Title</u>	<u>Page</u>
1.	INTRODUCTION AND SUMMARY	1-1
1.1	General	1-1
1.2	Early Warning System - Summary	1-3
1.3	Fleet Air Defense - Summary	1-8
1.4	Recommendations	1-12
2.	EARLY WARNING SYSTEMS	2-1
2.1	Predicted Detection Performance	2-1
2.2	Detection Experiment	2-8
2.3	Conclusions of EW Study	2-16
3.	FLEET AIR DEFENSE	3-1
3.1	Polystatic System Detection Feasibility	3-1
3.2	Target Location Methods	3-16
3.3	Error Analysis	3-33
4.	EXPERIMENTAL TESTING OF FAD POLYSTATIC TECHNIQUES	4-1
4.1	Objectives	4-1
4.2	Experimental Considerations	4-2
4.3	System Design	4-8
4.4	Design Concept	4-11
4.5	Detailed Design Specifications	4-14
4.6	Computer Hardware Description	4-19
	APPENDIX A	A-1

UNCLASSIFIED

~~SECRET~~

UNCLASSIFIED

(U) ILLUSTRATIONS (U)

<u>Figure</u>	<u>Title</u>	<u>Page</u>
1-1	Basic Geometric Configurations	1-2
1-2	Illustration of Buoy Tactical Early Warning Concept	1-4
1-3	Network Geometry	1-5
1-4	FAD Polystatic System	1-9
2-1	Detection Regions	2-7
2-2	Block Diagram for High Dynamic Range Receiving System	2-10
2-3	Block Diagram of Twelve Channel Analog Receiving System	2-11
2-4	Event 1 Flight Pattern	2-13
2-5	Predicted and Observed Detection Regions	2-14
3-1	FAD Polystatic System	3-2
3-2	Located Sources	3-5
3-3	Source Schedule	3-6
3-4	Typical Geometry	3-7
3-5	Basic Transmission Loss for a Groundwave Along the Ocean	3-9
3-6	Typical Fleet Protection Areas in the Mediterranean Ocean	3-11
3-7	Skywave-Groundwave Example	3-13
3-8	Skywave-Groundwave Coverage	3-14
3-9	Double-Baseline, Two-Measurements Model	3-17
3-10	Double-Baseline, One-Measurement Model	3-18
3-11	Single Baseline Model	3-20
3-12	Variables for Double-Baseline, Two-Measurements Model	3-21

UNCLASSIFIED

(U) ILLUSTRATIONS (U)

--Continued.

<u>Figure</u>	<u>Title</u>	<u>Page</u>
3-13	Variables for Double-Baseline, One-Measurement Model	3-25
3-14	Variables for Single Baseline Model	3-28
3-15	Variables for Doppler Location Finder	3-32
3-16a	Range Estimation Errors for Double Baseline, Single Measurement Technique--Geometry No. 1	3-40
3-16b	Range Estimation Errors for Double Baseline, Single Measurement Technique--Geometry No. 2	3-40
3-16c	Range Estimation Errors for Double Baseline, Single Measurement Technique--Geometry No. 3	3-41
3-16d	Range Estimation Errors for Double Baseline, Single Measurement Technique--Geometry No. 4	3-41
3-16e	Range Estimation Errors for Double Baseline, Single Measurement Technique--Geometry No. 5	3-42
3-16f	Range Estimation Errors for Double Baseline, Single Measurement Technique--Geometry No. 6	3-42
3-16g	Range Estimation Errors for Double Baseline, Single Measurement Technique--Geometry No. 7	3-43
3-16h	Range Estimation Errors for Double Baseline, Single Measurement Technique--Geometry No. 8	3-43
3-17	Range Estimation Errors for Single Baseline, Double Measurement Technique	3-46
3-18	Range Estimation Errors for Single Baseline, Double Measurement Technique	3-46
3-19	Location Error for Doppler Location Finder--Geometry No. 1	3-50
3-20	Location Error for Doppler Location Finder--Geometry No. 2	3-50
3-21	Location Error for Doppler Location Finder--Geometry No. 3	3-51

UNCLASSIFIED

(U) ILLUSTRATIONS (U)

--Continued.

<u>Figure</u>	<u>Title</u>	<u>Page</u>
3-22	Location Error for Doppler Location Finder-- Geometry No. 4	3-51
3-23	Location Error for Doppler Location Finder-- Geometry No. 5	3-52
3-24	Location Error for Doppler Location Finder-- Geometry No. 6	3-52
3-25	Location Error for Doppler Location Finder-- Geometry No. 7	3-53
3-26	Location Error for Doppler Location Finder-- Geometry No. 8	3-53
3-27	Location Error for Doppler Location Finder-- Geometry No. 9	3-54
3-28	Location Error for Doppler Location Finder-- Geometry No. 10	3-54
4-1	System Block Diagram	4-10
4-2	Artist's Concept of Data Collection System	4-15
4-3	Fathometer Display	4-20

UNCLASSIFIED

(U) TABLES (U)

<u>Table</u>	<u>Title</u>	<u>Page</u>
2-1	Predicted System Performance for November 1969 for Carter Cay Transmitter Using Frequencies near the MUF	2-3
2-2	Summary of Detection Region Calculations	2-6
3-1	Mediterranean Transmitters	3-4
3-2	Additional Transmitters	3-15
4-1	Experimental Factors	4-3
4-2	Candidate Sources for FAD Polystatic Experiment	4-4
4-3	Typical Aircraft and Missile Threats	4-5
4-4	Test Parameters for Experiment	4-9
4-5	Spectrum Analysis Specifications	4-14
4-6	Computer Core Requirements	4-18

UNCLASSIFIED

UNCLASSIFIED

Section 1

INTRODUCTION AND SUMMARY

1.1 (U) **GENERAL (U)**

Project AQUARIUS is a part of the Advanced Research Projects Agency (ARPA) sponsored ocean surveillance and tactical early warning program under Project MAY BELL. The primary goal of Project MAY BELL was to investigate the feasibility of detecting and tracking aircraft, missiles, and ships at over-the-horizon distances using high frequency (HF) monostatic and bi-static radars. Concepts using the basic geometric configurations shown in Figure 1-1 have been explored. The MAY BELL program emphasis has been directed towards determining the attenuation, clutter and propagation aspects that apply to concepts using surface waves; and investigating the basic feasibility of detecting and tracking aircraft and SLBM's for Fleet Air Defense (FAD) and Buoy Tactical Early Warning.

Sylvania's primary efforts under Project AQUARIUS have been to determine the feasibility of:

- (1) detecting both submarine launched ballistic missiles (SLBMs) and aircraft using surface wave propagation to the target and sky wave propagation from the target to the receiver, and
- (2) providing detection and tracking information under electromagnetic control (EMCON) conditions for FAD using shore-based HF (CW) sources and shipboard receivers.

Both analytical and experimental work have been accomplished to arrive at the conclusions included in this report. The principal results of the investigation are summarized in the remainder of this section: results related to early warning (EW) systems and results associated with Fleet Air Defense. The detailed presentation is included in Sections 2 and 3, respectively. Based on these findings recommendations are made in Section 4 for subsequent experiments and investigations associated with aircraft tracking under EMCON conditions using a polystatic configuration.

The concepts explored under Project AQUARIUS can be applied to tactical early warning systems employed against aircraft and submarine

UNCLASSIFIED

UNCLASSIFIED

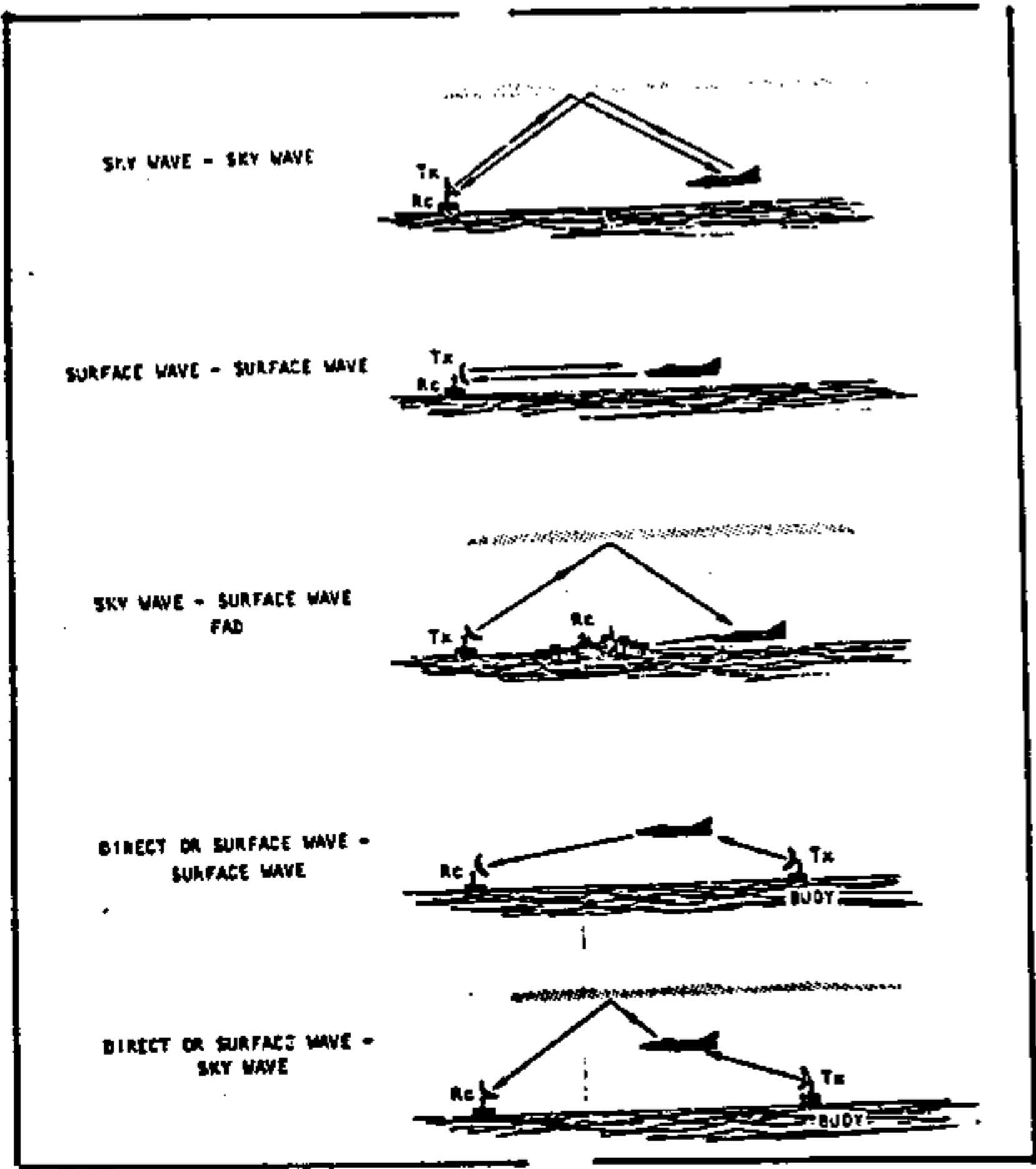


Figure 1-1 ^(U) Basic Geometric Configurations. (U)

UNCLASSIFIED

~~SECRET~~

UNCLASSIFIED

1.1 (U) ~~SECRET~~ --Continued.

launched ballistic missiles (SLBMs) and fleet air defense (FAD) systems that must cope with hostile aircraft and missiles under both friendly and enemy EMCON conditions.

1.2 (U) ~~SECRET~~ EARLY WARNING SYSTEM - SUMMARY. (U)

The early warning system configuration considered under Project AQUARIUS is depicted in Figure 1-2. It consists of low power buoy and land based transmitters that illuminate the target (an aircraft or SLBM) via a ground or surface wave. Target detection is accomplished via a sky wave reflection to a highly sensitive receiver located on the coast. The primary goals of this effort were to experimentally demonstrate the feasibility of detecting both SLBMs and low-flying aircraft and to compare the experimentally observed detection ranges to theoretically predicted detection ranges. The targets were detected by observing the scattered doppler shifted signal from the moving targets.

1.2.1 (U) ~~SECRET~~ Predicted Detection Performance. (U)

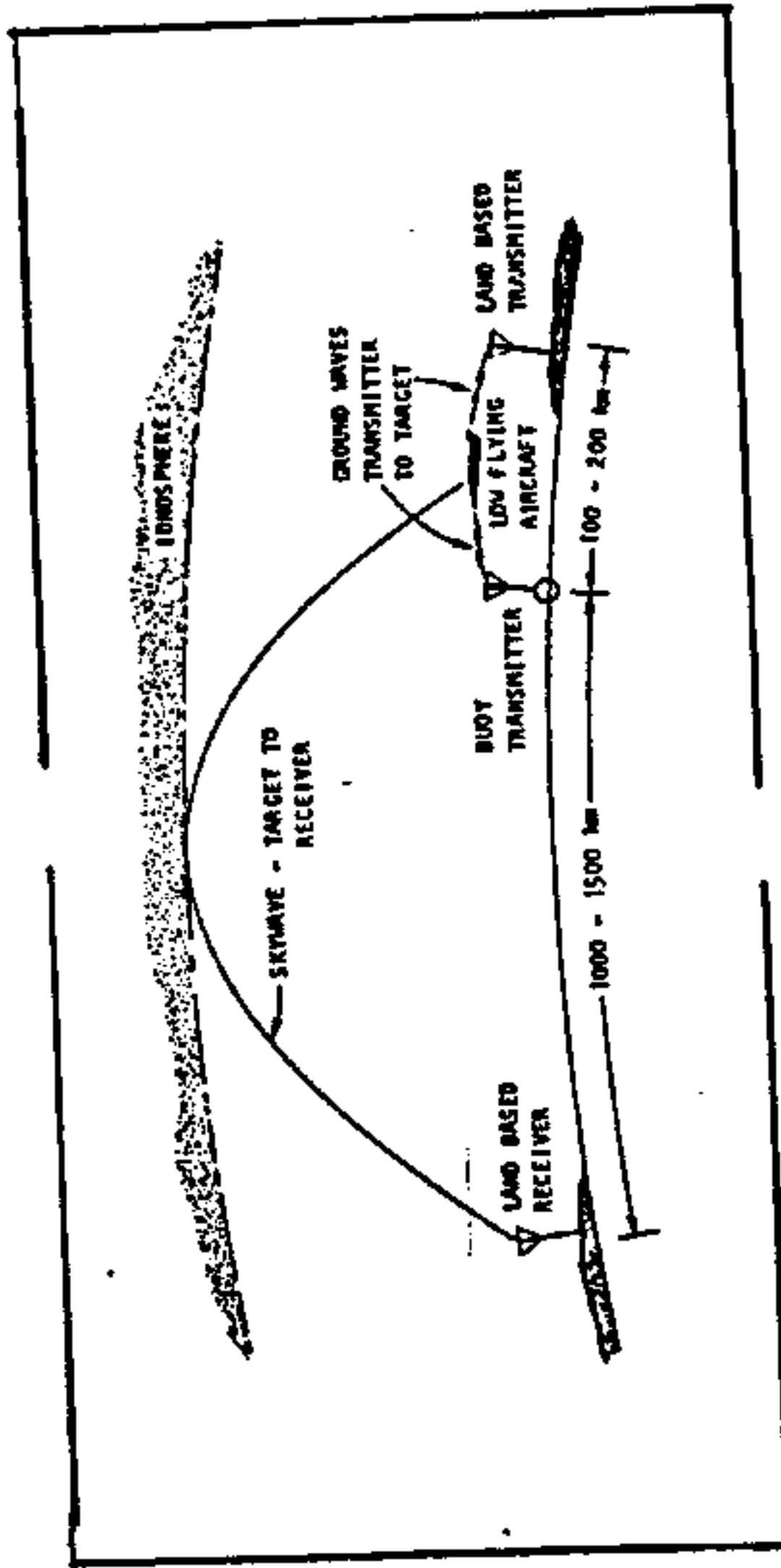
Propagation calculations to predict system detection performance using a modified version of the ESSA skywave propagation program were made for both the direct and the scatter-paths between the receiver site at Vint Hill Farms Station (VHFS) and the buoy transmitter off the Florida coast and the Carter Cay transmitter (see Figure 1-3). Separate prediction analyses were made for SLBMs and aircraft.

A constant scattering cross section of 100 M^2 was assumed for the SLBM at all altitudes below 100 km. Above 100 km altitude enhanced cross section values of 10^4 to 10^5 m^2 were used. Because of the relatively low (10 watts) powers (and low frequency) of the buoy transmitters, the signal-to-noise ratio of the reflected doppler is almost negligible below 100 km altitude for any time of the day for either 5.8 or 9.295 MHz (the frequencies used in the experiment). Only above 100 km with the enhanced target cross section is there any substantial chance of SLBM detection using buoy transmitters. However, with the Carter Cay transmitter using 3 kw and transmitting on frequencies near the MUF, the signal-to-noise ratio and thus the probability of detection even at low altitudes is generally above 0.8. Thus, the Carter Cay transmitters operating on frequencies near the IF hop MUF between Carter Cay and VHFS, should provide low altitude SLBM detections in the afternoon.

~~SECRET~~

UNCLASSIFIED

UNCLASSIFIED



(U) Figure 1-2. Illustration of Buoy Tactical Early Warning Concept (U).

SECRET

UNCLASSIFIED

UNCLASSIFIED

[REDACTED]
(This page is UNCLASSIFIED)

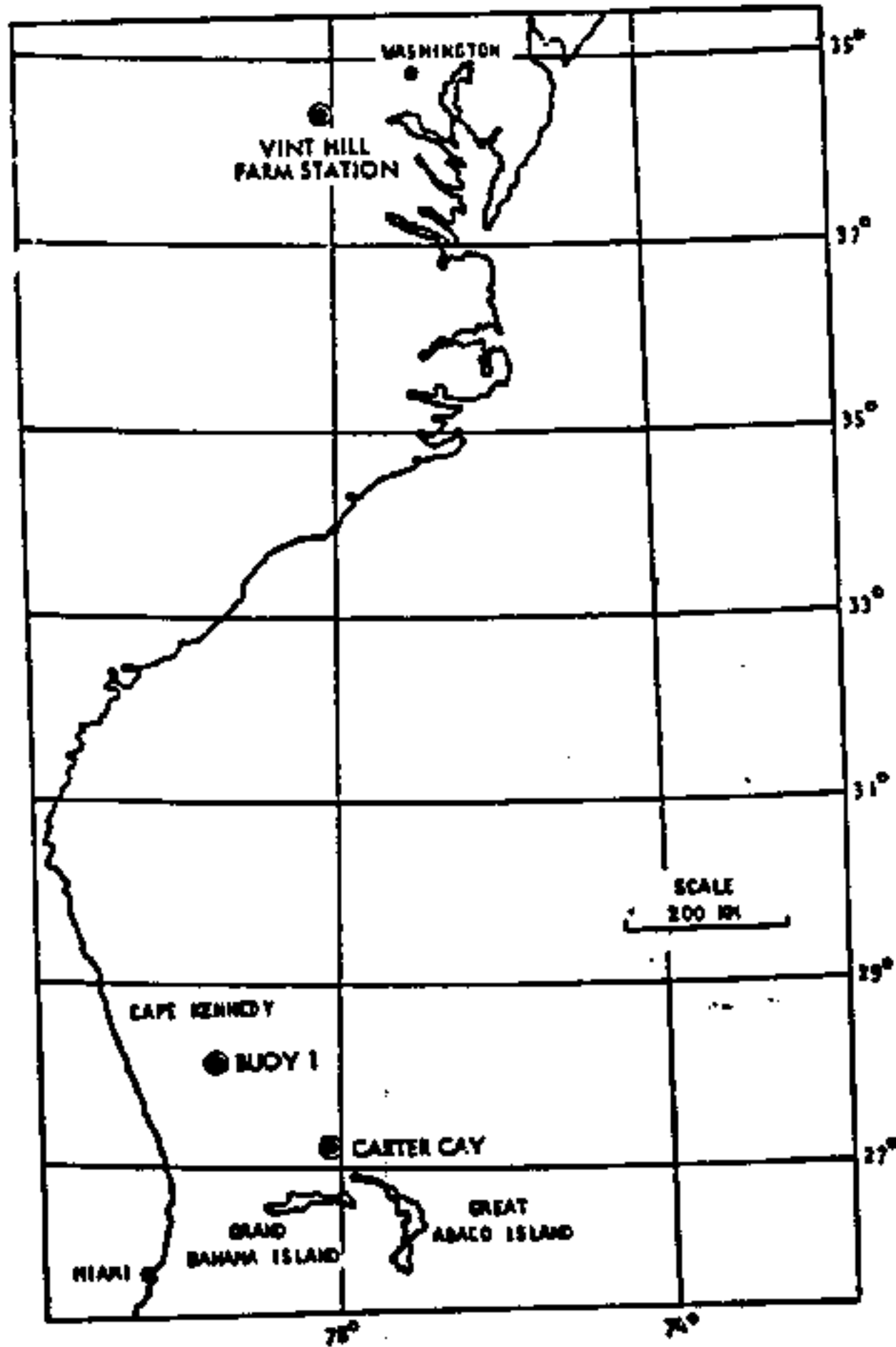


Figure 1-3. (U) Network Geometry (U).

1-5

[REDACTED]
UNCLASSIFIED

~~SECRET~~

UNCLASSIFIED

1.2.1 (U) ~~SECRET~~ --Continued.

The predicted detection performance for low flying aircraft was also examined because it is important to determine whether or not aircraft flying controlled patterns near the buoys and Carter Cay can be detected. This was done by computing the expected detection regions around the transmitter using median operating values. The results indicate that aircraft with 100 m² cross sections can be expected to be detected at distances in the range of 11-67 km from the transmitter; depending on the frequency and time of operation and hop structure.

1.2.2 (U) ~~SECRET~~ Experimental Results. (U)

The principal experiments consisted of two separate controlled aircraft flights of a Navy P3B aircraft to examine the detection capability of the bistatic configurations and two propagation measurements between the Carter Cay transmitter and the Vint Hill Farm Station receiver. Figure 1-3 describes the network geometry.

The first flight employing a 10-watt buoy transmitter resulted in a detected aircraft doppler signature. However, it was not the P3B aircraft used in the test but an aircraft flying near the receiver at VHFS. This conclusion is reached because the time of the signature does not coincide with the time the P3B was closest to the buoy. Also, the predicted detectability region for the existing operating conditions (noise, etc.) extended at best to only 11 km while the P3B aircraft approached the buoy to within only 30 km. Thus, due to timing, geometry, and transmitter power constraints, the detected signature is not considered to be due to the test aircraft.

The second flight test employed the higher powered (3 kw) Carter Cay transmitter to illuminate the aircraft flying at several altitudes from 2,000 to 24,000 feet. From this test it was concluded that aircraft below 2,000 feet and within the predicted detectability regions (approximately 11 km from the transmitter) can be detected using the buoy concept if at least 3 kw is transmitted.

Signal strength tests were performed to determine how accurately the prediction techniques correlate with measured values and to estimate the hop structures for various frequencies. Tests were performed for two frequencies and at two times during the day. It was found that there was good agreement between predicted and observed carrier levels for 1E, 1F, and 2F hop structures.

~~SECRET~~

UNCLASSIFIED

UNCLASSIFIED

1.2.3 (3) System Parameter Considerations. (U)

While the experimental results described herein indicate the basic feasibility of the ground-wave/sky-wave configuration, there remains a need for additional information to design a complete coastal defensive system. In particular, there are many parameters that inter-relate the ground-wave/sky-wave mode that were not examined or tested in detail during this experiment. These include variations in frequency, path loss with time of day, season, etc. To perform an adequate design of an early warning system an examination of six areas was required:

- (1) effective radiated power and surface wave from a buoy mounted antenna,
- (2) surface-wave losses to the target,
- (3) scattering or reflection coefficient of the target,
- (4) sky-wave losses to the receiver,
- (5) effective noise at the receiver, and
- (6) receiver antenna gain.

These areas were examined and the specific parameters that contribute the most uncertainty in specifying system design values were identified. They include frequency, path length, target aspect angles, null depth variations, receiving site noise environment, absorption, target altitude measurement tolerances, and interference. A proposed experimental program was recommended that could be accomplished in four phases. First, analysis and measurements are to be made to evaluate the coupling between the buoy-mounted transmitter and the surface wave which is vertically polarized. Second, additional analysis using modeling experiments is to be carried out to evaluate the difference between backscatter and forward scatter target cross section. Third, the path losses for both sky wave and surface wave are to be measured for an optimal set of frequencies and modes of propagation. Fourth, a preliminary system is to be defined as a result of the first three phases. This design would include coverage area, control requirements, and an estimate of detection probability and false alarm rate.

UNCLASSIFIED

~~SECRET~~

UNCLASSIFIED

1.3 (U) ~~SECRET~~ FLEET AIR DEFENSE - SUMMARY. (U)

In lieu of pursuing the experiments needed to specify a coastal tactical early warning system, Sylvania was redirected to focus attention on the Fleet Air Defense (FAD) problem.

The detection of low-flying threats to surface vessels at a range sufficient to give useful warning time and tracking information is a problem which must be solved if the surface navy is to survive. In detecting these threats the enemy must not be given the opportunity to use simple direction finding techniques to locate fleet units. Thus, it is desirable that target detection not require radiation from the fleet and that the fleet operate under complete electromagnetic control (EMCON).

The feasibility of using a hybrid (skywave/surface-wave) system to help solve this problem has been demonstrated as part of the MAY BELL program. In this concept, the target is illuminated by skywaves from transmitters (either shipborne or land-based) located at over-the-horizon (OTH) ranges. Surface waves which propagate from the target to a receiving system aboard a ship permit detections to be made even when the target is below the line-of-sight radar horizon.

Experiments performed at Cape Kennedy, Florida, with a shore-based receiving station simulating the shipboard environment, a Navy P3B aircraft as a controlled target, and illumination provided by the MADRE (pulse) and CHAPEL BELL (phase code) transmitters, located respectively in Maryland and Virginia, have shown the technique to be feasible. For most of the flights of the target its altitude was 200 feet, and detections were made at ranges as great as 100 kilometers (km) from the receiver.

Sylvania's investigations in this area were divided into two parts. The first was to examine the feasibility of using transmitters of opportunity as sources for a polystatic doppler radar system for FAD in the Mediterranean Sea. The second part consisted of examining target tracking methods for use with such a doppler radar problem. Recommendations for follow-on experiments were then made to verify the tracking techniques (Section 4.2).

1.3.1 (U) ~~SECRET~~ Polystatic System Detection Feasibility. (U)

The polystatic radar system that employs HF broadcast transmitters of opportunity and a shipborne receiver (see Figure 1-4) was examined to determine the availability of sources for illuminating airborne threats to the U. S. fleet so that a shipborne receiver can be employed to detect the target

~~SECRET~~

UNCLASSIFIED

UNCLASSIFIED

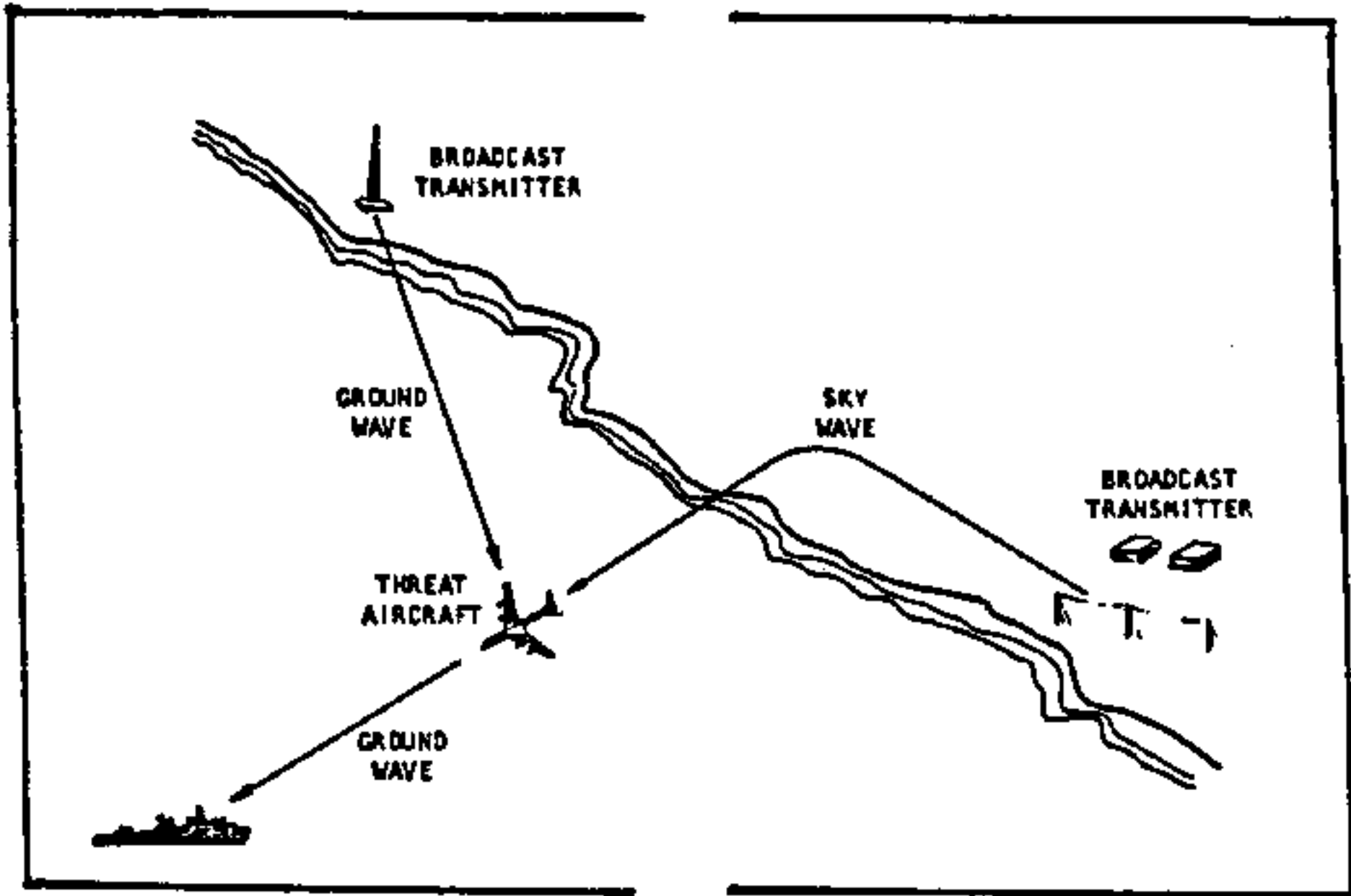


Figure 1-4 (U) FAD Polystatic System. (U)

~~SECRET~~

UNCLASSIFIED

~~SECRET~~
UNCLASSIFIED

1.3.1 (U) ~~SECRET~~ --Continued.

at over-the-horizon (OTH) ranges. This study was constrained to the Mediterranean region. The sources were examined to determine the effective radiated power of the transmitter in various directions, especially over the Mediterranean Sea, the propagation modes, and the operating schedule of the transmitter. Propagation losses from the transmitter to the target, loss due to the scattering geometry, and losses from the target to the receiver were examined to determine predicted detectability regions. The results indicate that the sources studies can provide sufficient coverage for the fleet over approximately one half of the Mediterranean Sea some of the time. More study is needed to evaluate other sources with different transmission schedules to provide round-the-clock coverage. The large number of known transmitters that have not yet been evaluated and tentative knowledge of their characteristics and schedules appear to be sufficient to provide the additional coverage needed. The studies indicate that detection ranges on the order of 100 km from the fleet should be possible. Section 3.1 contains the details of this analysis.

1.3.2 (U) ~~SECRET~~ Target Location Methods. (U)

To provide tracking information for FAD, target location techniques using the basic polystatic configuration described previously were examined. For low-flying aircraft (below 1000 feet) and surface-wave propagation for the target-receiver half path, the location estimation problem can be considered to be a two-dimensional problem. Models for location estimation were developed for three configurations: a two-transmitter, one-receiver (double baseline) case, a one-transmitter, one-receiver (single baseline) case, and a four transmitter, one-receiver case (doppler location finder). For the double baseline case two techniques were developed, one in which azimuthal and doppler measurements are made at two different time points for each baseline and a second to represent a single set of measurements for each baseline. For the single baseline case a third technique requiring two sets of azimuthal and doppler measurements was developed. For the four-transmitter, one-receiver case, four doppler measurements are made to provide an estimate of target range and azimuth. Section 3.2 contains a detailed description of the techniques.

~~SECRET~~
UNCLASSIFIED

~~SECRET~~
UNCLASSIFIED

1.3.3 (U) ~~SECRET~~ Error Analysis. (U)

A detailed error analysis was conducted of three of the four techniques. This effort excluded an examination of the first technique (double baseline, double measurement) because the other techniques are simpler to implement.

For the double baseline, single measurement technique it is shown that although the technique is not completely satisfactory under all circumstances, it is fairly successful for certain geometries and parameters. Both bias and random errors arise because of the need for approximations and measurement errors. For RMS measurement accuracies of 1 degree in azimuth and 0.1 Hz in doppler frequency range estimate errors of less than 15 percent of the true range can be achieved.

For the single baseline, double measurement technique range estimate errors of less than 15 percent can also be achieved for the same bearing and doppler measurement accuracies (1 degree and 0.1 Hz). However, the error is especially sensitive to transmitter-target-receiver geometry for this technique. Errors in excess of 80 percent can arise when the shipborne receiver is located between the target and the transmitter. Bias errors are eliminated for target trajectories aimed directly at the ship.

The errors associated with the doppler location finder technique were examined for a doppler measurement accuracy of 0.1 Hz RMS. The RMS range estimate error is less than 15 percent in many cases and the RMS bearing estimate error is less than 6°. In one case the range estimate error is less than 5 percent. This latter case assumes that four transmitters are distributed at the corners of a square centered around the ship with the target approaching from outside the square. This technique results in no bias errors and the random errors are generally less than those for the other techniques. If bearing measurements with 1 degree RMS error are used with the doppler location finder technique then the location accuracies are quite good.

The principal conclusions that can be drawn from the error analysis is that target location can be estimated with reasonable accuracy (15 percent of true target range) using a number of techniques for a variety of FAD operational conditions. The most promising approach for implementation is a hybrid of the techniques considered. For example, for a given transmitter-receiver geometry the doppler location finder that estimates range and azimuth from four doppler measurements may be used with separate azimuthal measurements to estimate a target's location. Because each of the techniques is sensitive to transmitter-target-receiver geometry,

~~SECRET~~
UNCLASSIFIED

UNCLASSIFIED

1.3.3 (U) ~~SECRET~~ --Continued.

the target location system should include an algorithm for selecting the estimation method(s) for a set of operating conditions and combining the estimated results using tests for accuracy. The estimation method(s) would be selected to minimize the errors for targets from different quadrants around the ship for a given transmitter-receiver configuration. The results of the different estimation methods would be compared and combined to provide the "best" estimate.

Section 3.3 contains the details of the error analysis.

1.3.4 (U) Prototype Aircraft Detection System Design. (U)

The results of the investigation of transmitter sources for the FAD system and the evaluation of target location methods were employed as inputs for a prototype aircraft detection system design. This system would provide a test bed to verify the detection capability of the polystatic doppler radar system for FAD. In addition, the prototype system can be used to demonstrate the accuracies of the various target location techniques and select parameters for a final FAD system. Section 3.4 contains the details of the prototype system design.

1.4 (U) RECOMMENDATIONS. (U)

Based on the early warning and Fleet Air Defense (FAD) investigations under Project AQUARIUS recommendations are made that apply principally to FAD systems. They include the development of a prototype aircraft detection system, the experimental testing of the FAD polystatic techniques using this system, and the conduct of subsequent investigations necessary for system implementation.

The prototype system and experimental tests are necessary to demonstrate the detection range of the polystatic technique and to verify the accuracies of the target location estimation methods examined under Project AQUARIUS. The prototype system to be employed for the tests can be readily implemented as described in Section 3.4. As mentioned previously, such a system can provide a test bed for final system parameter selection, especially in the areas of man-machine interface. In addition, it can be used to evaluate hardware and software tradeoffs prior to the final system design.

~~SECRET~~

UNCLASSIFIED

[REDACTED]

UNCLASSIFIED

1.4 (U) [REDACTED] --Continued.

The subsequent FAD investigations recommended, based on the results of this study are to evaluate transmitter sources for use in the polystatic system for fleet operations in other parts of the world, to refine the target location techniques, and to examine the multiple signature discrimination problem. The source evaluation effort is needed to identify transmitters to be used for fleet early warning when the fleet operates in other areas of the world. The target location technique refinement study is intended to employ the results of the four methods examined under Project AQUARIUS for the development of a hybrid target location system that will perform satisfactorily under a greater variety of fleet operating geometries. The study should incorporate the four techniques to develop a composite method for reducing the sensitivity of target location estimation accuracy to transmitter-target-receiver geometry. The experimental tests that are recommended should be closely coordinated with this effort so that the refined target location techniques can be tested.

The multiple signature discrimination problem consists of the need to identify threats to the US Fleet and to distinguish them from other aircraft, objects, and false alarms. Investigation of methods to efficiently discard the false alarms and to verify that an aircraft is hostile needs to be conducted.

A more detailed description of these recommendations is included in Section 4.

UNCLASSIFIED

[REDACTED]

(This Page is Unclassified)

UNCLASSIFIED

This Page Intentionally Blank

[REDACTED]

(This Page is Unclassified)

UNCLASSIFIED



UNCLASSIFIED

Section 2

EARLY WARNING SYSTEMS

(U) As described in Figure 1-2, the early warning system configuration considered for investigation under Project AQUARIUS consists of low power HF buoy and land-based transmitters that illuminate the target (an aircraft or SLBM) via a ground or surface wave and a highly sensitive receiver located on the coast that detects the sky-wave target reflection from the target. The primary goals of this effort were to experimentally demonstrate the feasibility of detecting both SLBMs and low-flying aircraft and to compare the experimentally observed detection ranges to theoretically predicted detection ranges. The early warning system investigation was divided into three parts:

- a. a predicted detection performance evaluation,
- b. experimentation in the field to meet the primary goals of demonstration and verification of theoretically predicted detection ranges, and
- c. evaluation of early warning system parameters for design.

These efforts are described in the following subsection, (Sections 2.2 and 2.3). The conclusions of these efforts are contained in Section 2.4.

2.1 (U) PREDICTED DETECTION PERFORMANCE. (U)

Propagation calculations to predict early warning system performance using a modified version of the ESSA skywave propagation program (described in Appendix A) have been made for both the direct and the scatter paths between the receiver site at Vint Hill Farm Station and the buoy transmitters off the Florida coast. The purpose of these calculations was to estimate the feasibility of detecting SLBM missile launchings from Cape Kennedy and controlled aircraft targets using buoys at ranges of 100, 200 and 300 km from Cape Kennedy and the Carter Cay transmitter. The geometry and parameters were selected to provide theoretically predicted detection ranges for comparison with experimental results.

UNCLASSIFIED

UNCLASSIFIED

2.1.1 (U) Missile Detection Performance. (U)

Several sets of calculations using the computer predictions were performed. The receiving antenna at Vint Hill Farms Station used for all tests is a tulip element LDAA built by ITT with an assumed maximum gain of 16 dbi. A constant scattering cross section of 160 m^2 was assumed for the missile at all altitudes below 100 km. At altitudes above 100 km the bistatic cross section was modelled using a hyperboloid compressed ambient shock surface. The assumed cross section then changes from 10^2 m^2 at low altitude to values of 10^4 to 10^6 m^2 above 100 km. The three buoy transmitter locations are at 100, 200 and 300 km directly down range from the 105° Cape Kennedy launch azimuth. The Carter Cay transmitters are approximately 285 km down range at a 123° azimuth from Cape Kennedy. The transmitted frequencies for the buoys were the presently assigned values of 5.8 and 9.295 MHz. These frequencies, plus frequencies of 15 and 20 MHz were assumed for the Carter Cay transmitters. The buoys were assumed to have a transmitting power of 100 watts radiating from monopole antennas. The Carter Cay transmitters were assumed to be radiating 3 kw into monopole antennas.

Because of the low power and relatively low frequency from the buoy transmitters, the target signal-to-noise ratio was generally found to be negligible when the target is below 100 km for any time of the day for either frequency. Only above 100 km with the enhanced target cross section does there appear to be any substantial chance of target detection using the buoy transmitters. However, with the Carter Cay transmitter using 3 kw and transmitting on frequencies near the MUF as shown in Table 2-1 the signature-to-noise ratio and thus the probability of detection at even low altitudes is quite substantial. In fact, there are many cases for which the signal-to-noise ratio exceeds 15 db. Thus, if the high power Carter Cay transmitters continue to operate and transmit on frequencies near the 1 F hop MUF between Carter and VHFS then low altitude SLBM detections in the afternoon should be possible.

2.1.2 (U) Aircraft Detection Areas. (U)

Even though the probability of detecting SLBM launchings from Cape Kennedy is quite low (due to the relatively long range from the buoy to the target) it is important to determine whether or not aircraft flying controlled patterns near the buoys and Carter Cay can be detected. A way to evaluate this and to clearly display the results is to compute expected detection regions around the transmitter position. Variables that must be considered when calculating detectability regions are bistatic geometry, frequency, transmitter power, target cross section, skywave hop structure, sea state, local time of day and noise level. By choosing median values for all the variables and changing the values of a single variable at a time, regions where detections

SECRET

UNCLASSIFIED

TABLE 2-1.

(U) Predicted System Performance for November 1969
for Carter Cay Transmitter Using Frequencies near the MUF. (U)

(This page is UNCLASSIFIED)

Altitude	Frequency MHz	0000Z MUF		0400 MUF		0800 MUF		1200 MUF		1600 MUF		2000 MUF	
		S/N	PC/SB	S/N	PC/SB	S/N	PC/SB	S/N	PC/SB	S/N	PC/SB	S/N	PC/SB
5 KM	15	9.93	13.56	-	-	-	-	13.4	21.80	10.4	21.07	10.4	21.07
	20	-	60.3	-	-	-	-	59.2	-	60.7	-	60.7	-
10 KM	15	-	-	-	-	-	-	16.5	21.77	11.3	21.03	11.3	21.03
	20	-	-	-	-	-	-	73.3	-	74.8	-	74.8	-
40 KM	15	10.0	13.65	-	-	-	-	12.3	22.07	10.4	21.28	10.4	21.28
	20	-	60.2	-	-	-	-	60.2	-	60.7	-	60.7	-
119 KM	15	-	-	-	-	-	-	16.5	22.00	11.3	21.21	11.3	21.21
	20	-	-	-	-	-	-	73.4	-	74.8	-	74.8	-
40 KM	15	11.3	14.20	-	-	19.3	12.99	12.0	23.73	9.2	22.60	9.2	22.60
	20	-	59.0	-	-	60.6	-	60.6	-	61.8	-	61.8	-
40 KM	15	-	-	-	-	-	-	18.2	23.51	13.2	22.38	13.2	22.38
	20	-	-	-	-	-	-	71.7	-	72.9	-	72.9	-
119 KM	15	26.7	15.83	-	-	47.1	14.70	33.5	14.53	51.1	26.40	51.1	26.40
	20	-	43.6	-	-	32.8	-	39.2	-	20.0	-	20.0	-
119 KM	15	18.6	15.55	-	-	-	-	56.6	28.16	48.7	25.80	48.7	25.80
	20	-	190.4	-	-	-	-	33.2	-	37.4	-	37.4	-

S/N = Target signal-to-noise ratio (db)
PC/SB = Carrier-to-target signal ratio (db)

UNCLASSIFIED

UNCLASSIFIED

UNCLASSIFIED

2.1.2 (U) [REDACTED] -- Continued.

are most likely to occur can be generated, as well as obtaining an understanding of how a particular variable affects the overall detection area.

Detectability regions have been calculated for various frequencies, hop structures and noise levels using a buoy located 120 km from Cape Kennedy as the transmitter and VHFS, Virginia, as the receiver. A sea state of 5, transmitter power of 50 watts, ground-wave propagation from transmitter to target and sky-wave propagation from target to receiver and a required signal-to-noise ratio of 3 db have been assumed.

The following technique is applied to find the area of detectability. From the bistatic radar equations*, the total power loss over the scatter path is:

$$L = P_T - P_R = L_T + L_R + L_S - G_T - G_R - 10 \log \frac{4\pi\sigma}{\lambda^2} \quad (2-1)$$

- where:
- P_T = power transmitted;
 - P_R = power received;
 - L_T = loss over transmitter half path, T;
 - L_R = loss over receiver half path, R;
 - L_S = system loss;
 - G_T = gain of transmitter antenna;
 - G_R = gain of receiver antenna;
 - σ = target cross-section (meters); and
 - λ = wavelength (meters).

Assuming a minimum allowable scatter path signal-to-noise ratio of 3 db, the required power received would be at least $N + 3$ db, where N is the noise level at the receiver.

*See Skolnik, Merrill L., Introduction to Radar Systems, McGraw-Hill Book Company, Inc., New York, New York, 1955.

UNCLASSIFIED

UNCLASSIFIED

2.1.2 (U) [REDACTED] -- Continued.

$$P_R = N + 3 \text{ db} \quad (2-2)$$

From (2-1)

$$L = P_T - P_R$$

and hence:

$$L = P_T - N - 3 \text{ db} \quad (2-3)$$

Substituting equation (2-3) into equation (2-1) and solving for $L_T + L_R$ results in:

$$L_T + L_R = P_T - N - 3 - L_S + G_T + G_R + 10 \log \frac{4\pi\sigma}{\lambda^2} \quad (2-4)$$

Equation (2-4) provides an expression for calculating the total allowable scatter path loss between a transmitter and receiver while still maintaining sufficient signal strength to detect the target. Using different values for D-layer loss and sky-wave propagation over the transmitter-target half path, $\sigma = 100 \text{ m}^2$, and the appropriate transmitter/receiver gain parameters, the maximum loss associated with the target-receiver half path (L_R) can be obtained for various conditions. These L_R losses can be converted to receiver-target ranges using Barrick's loss tables* and the detection regions can be obtained. This technique was used to calculate the detection area around the transmitter for various frequencies and atmospheric noise conditions. The results of the detection area calculations are tabulated in Table 2-2 and a vertical projection of some of the regions onto the ground is shown in Figure 2-1. The reason for the egg-like shape is that the area boundary is the locus of points such that the product $R_1 R_2$ is equal to a constant (see Section 3.1.3 for a more detailed description of the evaluation method).

Referring to Figure 2-1 we see that the largest area of detection is for 2F hop cases for both 5.8 and 9.259 MHz, as compared to the 1E hop situation. This is because there is substantially less D-layer loss for the 2F hop mode than the 1E hop mode due primarily to the different path lengths in the D-region itself. With higher modes the incident angle through the D-layer is higher, thus the loss on these paths due to D-layer absorption is smaller.

*Barrick, D. E., "Theory of Ground-Wave Propagation Across a Rough Sea at VHF/UHF", Battelle Memorial Institute, Draft Report (1970).

UNCLASSIFIED

[REDACTED]

(This page is UNCLASSIFIED)

Table 2-2

(U) Summary of Detection Region Calculations (U)

Freq MHz	Hop Structure	R ₁ Km	R ₁ Loss db	D- Layer Loss db	R ₂ Loss db	L _{BT} +L _{BR} Loss db	Atmos Noise dbw
5.800	1E	11	61.0	48.5	102.2	211.7	-180(B)
5.800	2F	67	79.1	30.4	102.2	211.7	-180(B)
5.800	1E	10	59.5	34.0	102.2	195.7	-153(M)
9.259	1E	34	80.1	21.9	108.7	210.7	-172(B)
9.259	2F	48	86.2	15.8	108.7	210.7	-172(B)
9.259	1E	44	84.7	15.3	108.7	208.7	-169(M)
9.259	1F	65	90.8	9.2	108.7	208.7	-169(M)
15.000	1F	60	101.0	4.0	112.0	216.9	-174(M)
15.000	1F	67	103.6	5.9	112.0	221.5	-176(B)
20.000	1F	66	113.9	3.1	114.5	231.5	-186(B)
20.000	1F	66	113.6	2.1	114.5	230.1	-185(M)

B = Best noise case 0800-1200 Local Time

M = Medium noise case 1600-1200 Local Time

See Figure 2-1 for R₁ and R₂ definition

[REDACTED]

UNCLASSIFIED

[REDACTED]
(This page is UNCLASSIFIED)

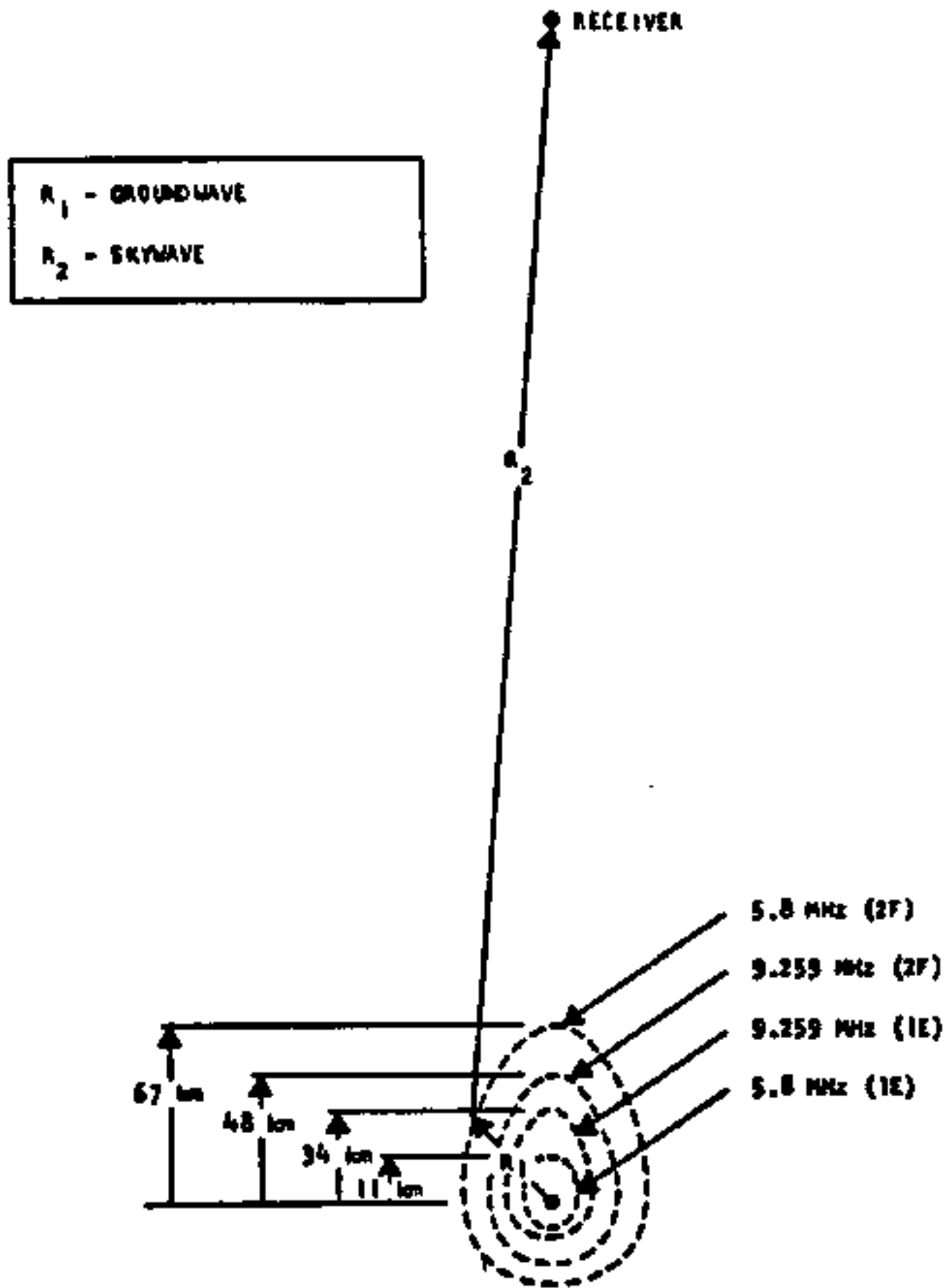


Figure 2-1. (U) Detection Regions (U).

UNCLASSIFIED

UNCLASSIFIED

2.1.2 (U) Continued.

For the 2F hop modes the region at 5.8 MHz is larger than the region at 9.259 MHz. This is due to the fact that the loss is greater at higher frequencies. However, for the 1E modes the situation is reversed. The higher frequency also results in the larger detection area. This is because the D-layer loss on the 9.259 MHz frequency is substantially less than the D-layer loss at 5.8 MHz and this dominates the ground-wave propagation advantage at the lower frequency.

From Table 2-2 we see that the detectability radii (R_1) tend to increase with increasing transmitted frequency. However, once the frequency increases to approximately 15 MHz, the spreading losses over the transmitter-target half path cancel the effect of decreasing D-layer loss and decreasing atmospheric noise so that the growth of the detectability region virtually stops. Note that the detectable radii (R_1) are approximately the same at 15 and 20 MHz for the best noise case. It is also observed that varying transmitter power and transmitter or receiver antenna gains have the same effect on the size of the detectability regions. That is a db of gain or loss whether generated from varying transmitter power or antenna gain enters the radar range equation in the same way.

2.2 (U) DETECTION EXPERIMENT. (U)

2.2.1 (U) General. (U)

Due to the nature and the time frame of this project, the experimental data were collected by using equipment developed by other Project MAY BELL participants or by using hardware developed for other programs. Both the buoy and the CW transmitters at Carter Cay used in these tests, were also used for the ground-wave measurements which Raytheon was conducting. The receiving system in use belongs to the USASA field station located at Vint Hill Farms Station, Virginia, and consisted of a linear disposed antenna array and multichannel HF receiving and recording equipment.

In the description of the detection experiment the transmitter and receiver site characteristics are first described. Then the receiving system calibration and experimental geometry are discussed. The results of the experiment are then presented.

2.2.2 (U) Transmitter Characteristics. (U)

Two different types of transmitters were used in the experiment. Those tests conducted prior to December 1969 used a buoy-mounted transmitter of approximately 10 watts radiating at 5.8 and 9.259 MHz. The

UNCLASSIFIED

2.2.2 (U) -- Continued.

antenna on the buoy consists of a top-loaded vertical monopole cut for a quarter wavelength at 7.5 MHz. This buoy was anchored off the coast of Florida approximately 120 kilometers downrange, and at an azimuth of 113 degrees from Cape Kennedy. The tests conducted in January and February 1970, used the CW transmitters on Carter Cay. The power of these CW transmissions ranged from 100 watts up to 3 kilowatts depending upon time and the particular transmitter in use. All of these transmissions radiate into quarter-wave vertical monopoles cut for the frequency in use.

2.2.3 (U) Receiver Site Characteristics. (U)

Two separate receiving systems were used at the receiver site located at Vint Hill Farms Station. One receiving system was a van-mounted high dynamic range digital processing system containing synthesizer controlled receivers (Sylvania R-27A receivers); digital spectrum analysis* using a CDC 1700 general-purpose computer and both analog and digital PCM recording capability. The second receiver system is located in two back-to-back house trailers, and consists of a DF set connected to an LDAA steerable beam antenna and 12 analog receiving channels using R390A receivers. The R390A receivers connect to both a real-time analog spectral display and a 12 channel analog tape recorder. The block diagrams of these two receiving systems are shown in Figures 2-2 and 2-3.

2.2.4 (U) Receiver System Calibration. (U)

One important goal of this project is to be able to predict the detection performance of the buoy tactical early warning system. Thus, it is desired to compare predicted signal and noise values to actual measured data. Then, if there exist significant discrepancies between the actual and observed data, the predictions must be modified to correct this difference.

The standard calibrations performed on the system included a measurement of the received carrier strength and also the received noise power referenced to a 1-Hertz bandwidth. The process of measuring the received carrier strength was a simple procedure of comparing the receiver IF output signal level when it was connected to the antenna, to the IF output level when the receiver was connected to a synthesizer having the same HF frequency as the carrier signal being measured. The average IF output level for that

* Digital Spectrum Analysis not available after January, 1970, due to termination of the computer lease.

UNCLASSIFIED

(This page is UNCLASSIFIED)

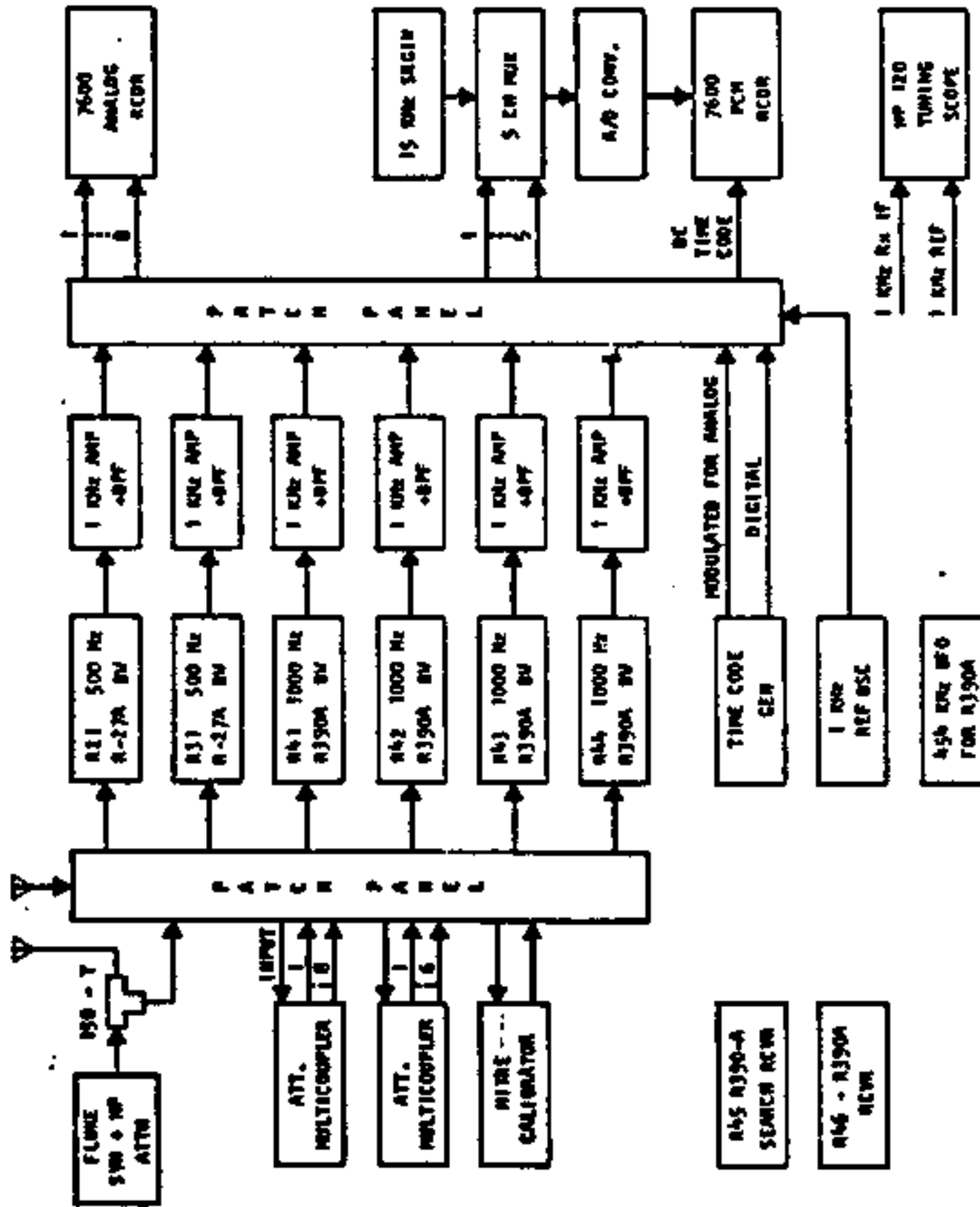


Figure 2-2. (U) Block Diagram for High Dynamic Range Receiving System (U).

UNCLASSIFIED

(This page is UNCLASSIFIED)

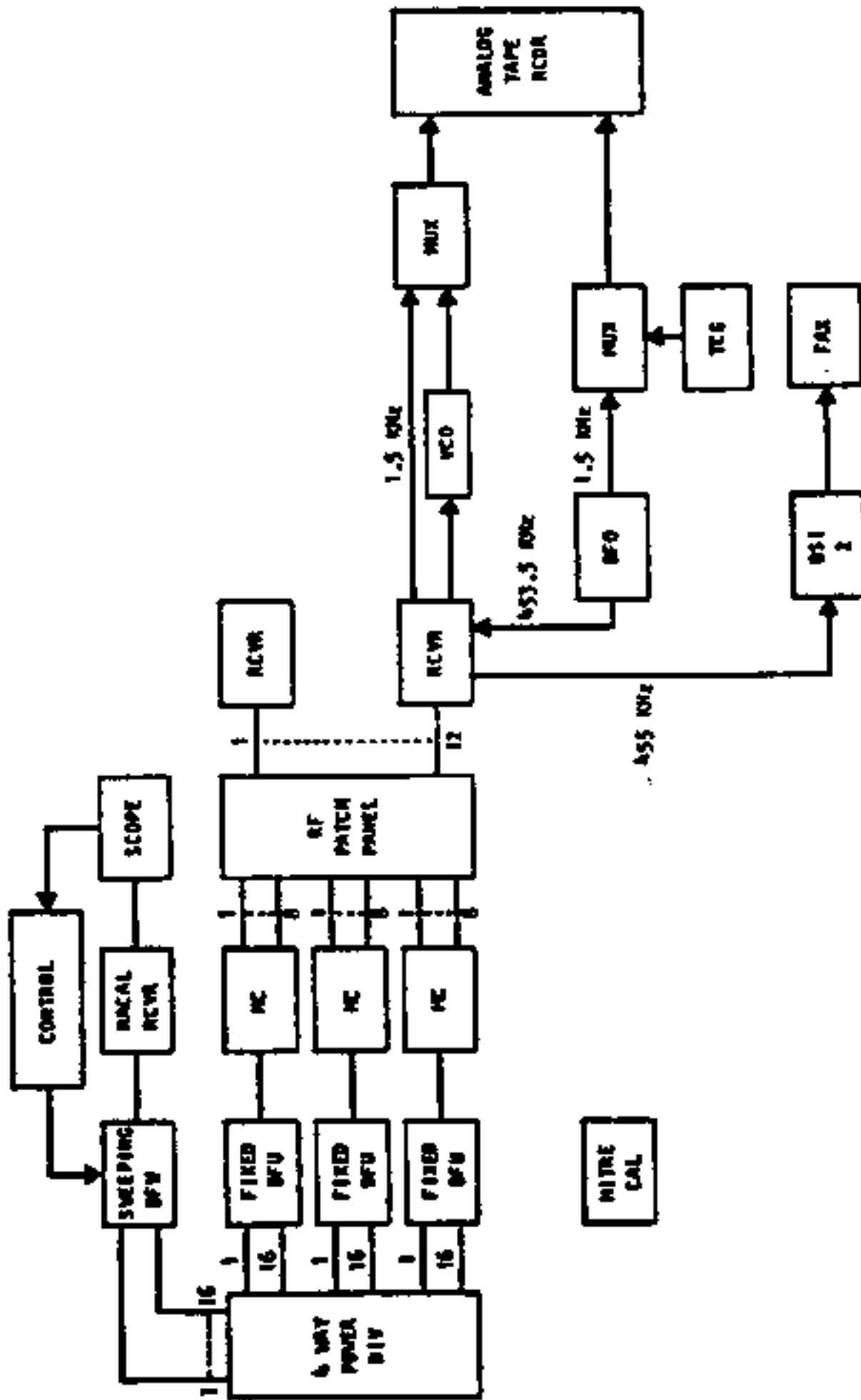


Figure 2-3. (U) Block Diagram of Twelve Channel Analog Receiving System (U).

UNCLASSIFIED

UNCLASSIFIED

2.2.4 (U) -- Continued.

particular carrier signal was noted. Then the synthesizer at the same frequency was fed to the antenna terminals and the output amplitude adjusted until the receiver IF output signal strength was the same. The synthesizer signal level was then measured and converted to db with respect to a watt. This signal substitution method gave the received carrier strength in dbw and was measured within the narrow IF receiver bandwidth.

The determination of the noise level at frequencies near the carrier was done by AM modulating the on-air carrier signal with an audio frequency square wave using a very small percentage modulation. The amplitude of these modulation tones was observed at the output of the real-time spectrum analysis display. The modulation percentage was then reduced until the modulation tones disappear into the background noise of the display. Because the modulation percentage is easily converted to signal level in db below the carrier and the spectrum analysis bandwidth was 1 Hz, the relative carrier-to-noise power was directly obtained referenced to a 1 Hz bandwidth. Thus, if the calibration tone disappeared into the noise at a level of 64 db below the carrier, it was assumed that the noise value was also 64 db below the carrier value. This carrier-to-noise ratio was then subtracted from the received carrier strength to obtain the measured noise power in dbw per Hz.

2.2.5 (U) Results of Experiment. (U)

The principal experiments consisted of two separate controlled aircraft flights of a Navy P3B aircraft to examine the detection capability of the bistatic configurations, and two propagation measurements between the Carter Cay transmitter and the Vint Hill Farm Station receiver. The two flights, denoted as Events 1 and 2, are shown in Figure 2-4 and 2-5, respectively. The network geometry is shown in Figure 1-3.

The first event on 18 December 1969 employed a 10-watt buoy transmitter (instead of a 100-watt transmitter as examined in the prediction analysis*) located 120 km from Cape Kennedy on an azimuth of 113°. A Navy P3B aircraft was flown at an altitude between 300 to 600 feet, and speed between 200 and 400 knots, along the flight path shown in Figure 2-4. A signature was detected on 5.8 MHz between 1750-1755Z and 2000-2005Z. The propagation conditions are summarized below--

RF: 5.8 MHz
Transmitter Power: 10 W.
Carrier Level: -92 dbw
Noise Level: -160 dbw
Calculated detection radii: 3 km (1E Hop), 6 km (2F Hop)

*The 10-watt buoy transmitter was built after the analysis using the 100-watt value was completed.

UNCLASSIFIED

SECRET

UNCLASSIFIED

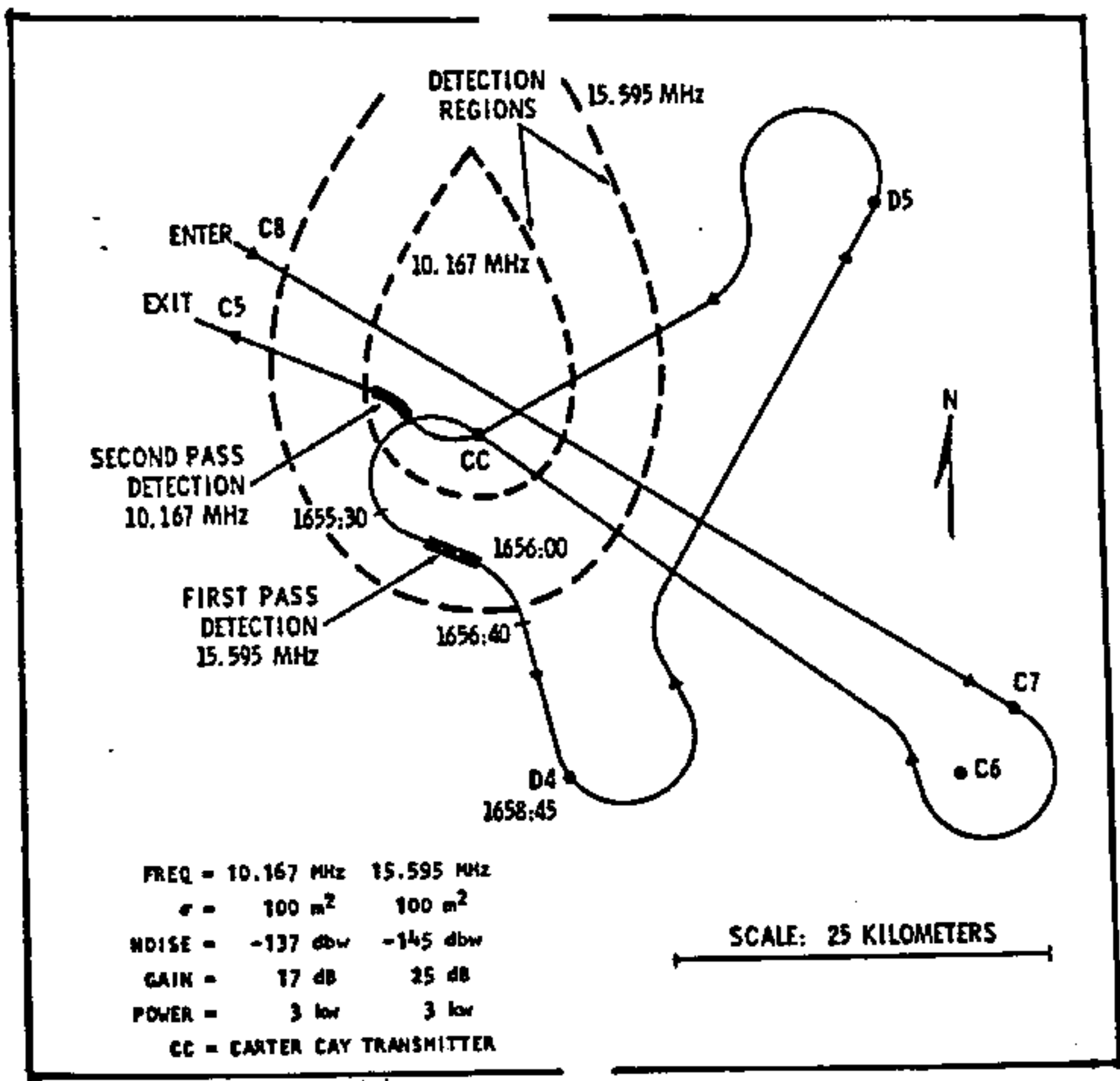


Figure 2-5 (U) Predicted and Observed Detection Regions. (U)

SECRET

UNCLASSIFIED

~~SECRET~~

UNCLASSIFIED

2.2.5 (U) ~~SECRET~~ -- Continued.

The detected signature is not considered to be the P3B test aircraft, but an aircraft flying near the receiver at VHS. The predicted detectability region for this day extends at best only to 11 km. The P3B's closest approach to the buoy is only 30 km. Also, the period of the first Doppler signature's sign change occurs 2.8 minutes earlier than the predicted closest approach. In addition, the Doppler signatures obtained (although consistent with those for an aircraft) were much stronger than could be expected from the test aircraft using a 10-watt transmitter to illuminate the target. Therefore, because of inconsistent timing the distances of aircraft from the transmitter and receiver, and the strength of the detected signatures using a 10-watt transmitter, it is concluded that the detected signatures were not the P3B test aircraft, but rather another aircraft flying over the receiving antenna.

The second event on January 27, 1970, employed the 3 kw Carter Cay transmitter and a P3B test flight at a speed between 200-300 knots. The aircraft flew the pattern shown in Figure 2-5 at successive altitudes of 24,000, 14,000, 12,000, and 2,000 feet. The propagation conditions are summarized below:

<u>RF (MHz)</u>	<u>XMTR Power (watts)</u>	<u>Receiving Antenna Gain (db)</u>	<u>Noise Level (dbw)</u>
10.167	3,000	17	-137
15.595	3,000	25	-145

The detections for the first and second passes of the aircraft near the transmitter at 15.595 MHz and 10.167 MHz, respectively, are shown in Figure 2-3. The predicted detection regions for these frequencies are also included in the figure for comparison. The experimental data generally agree with the predicted results except that the detections are expected sooner during the flight. The lack of a signature during aircraft flight at high altitudes (e.g., 20,000 ft.) over the Carter Cay transmitter may be attributed to aircraft flight in the vertical null of the antenna. Both signatures were obtained for aircraft flight below 2,000 feet. Therefore, it can be concluded that aircraft detection below this altitude and within the predicted detectability regions can be detected using the buoy concept if sufficient power is transmitted (e.g., 3 kw).

~~SECRET~~

UNCLASSIFIED

[REDACTED]

UNCLASSIFIED

2.3 (U)

CONCLUSIONS OF EW STUDY. (U)

The conclusions derived from the early warning system study are:

- a. Detection of SLBMs at altitudes below 100 km is unlikely using buoy transmitters with 100 watts or less, and a landbased receiving system for the network geometry shown in Figure 1-3. However, with the missile at altitudes above 100 km (at which the missile radar cross section is enhanced) detection appears possible.
- b. For buoy (or landbased) transmitters with 3 kw power and transmitting near the MUF, SLBM detection is probable for the network geometry in Figure 1-3 at both low and high altitudes.
- c. Aircraft detection regions can be estimated with fair accuracy because the experimental results generally agree with the predicted results. Using a 3 kw transmitter (Carter Cay) aircraft can be detected at distances as great as 60 km with a receiving site at VHFS.

The conclusions indicate that it is basically possible to detect aircraft and SLBMs using a bistatic HF radar configuration in which a buoy transmitter is employed with ground- or surface-wave propagation to the target and sky-wave propagation between the target and the receiver. However, transmitter power on the order of 3 kw or more is required. In addition, it may be necessary to judiciously select the frequency of operation to minimize the D-layer and spreading losses for target detection under different transmitter-target-detection geometries.

[REDACTED]

UNCLASSIFIED

~~SECRET~~

CONFIDENTIAL

Section 3

FLEET AIR DEFENSE

(U) The detection of low-flying threats to surface vessels at a range sufficient to give useful warning time and tracking information is a problem for which over-the-horizon detection (OHD) systems can offer a solution. A polystatic system such as portrayed in Figure 3-1 is especially desirable because it not only provides greater lead time for fleet air defense (FAD) by detecting targets at long ranges, but also provides the detection information without requiring active radiation from the fleet. Thus, the enemy is not given an opportunity to locate the fleet by employing direction-finding techniques against a fleet monostatic radar transmitter.

(U) The results of the investigations for FAD are presented in four parts. The first describes the feasibility of using a polystatic system to protect the fleet in the Mediterranean Sea. Aircraft detection regions are examined for transmitters of opportunity that presently exist, and receivers located in the fleet. In addition, the operating schedules of the transmitter sources were examined to determine the degree of 24 hour coverage possible. The second part of the FAD investigation describes target location methods that can be employed using the basic polystatic configuration. Equations are derived for each technique to show how the target range can be estimated using measured and known parameters. The third part is the results of an error analysis of those target location techniques that are feasible. The bias and random errors associated with each technique are discussed. The fourth part describes the design for a prototype aircraft detection system. This system can serve as the test bed for experimental verification of polystatic techniques and system evaluation to select the parameters for the final system design.

3.1 (U) ~~SECRET~~ POLYSTATIC SYSTEM DETECTION FEASIBILITY. (U)

3.1.1 (U) ~~SECRET~~ General. (U)

The polystatic system for FAD consists of HF broadcast transmitters of opportunity for illuminating the target and a shipborne receiver (see Figure 3-1) for detecting the target-reflected Doppler signature. The detectability of this system was investigated for FAD operations in the Mediterranean Sea.

Two types of propagation mechanism were considered. The first consists of ground-wave propagation between the transmitter and the target

[REDACTED]

UNCLASSIFIED

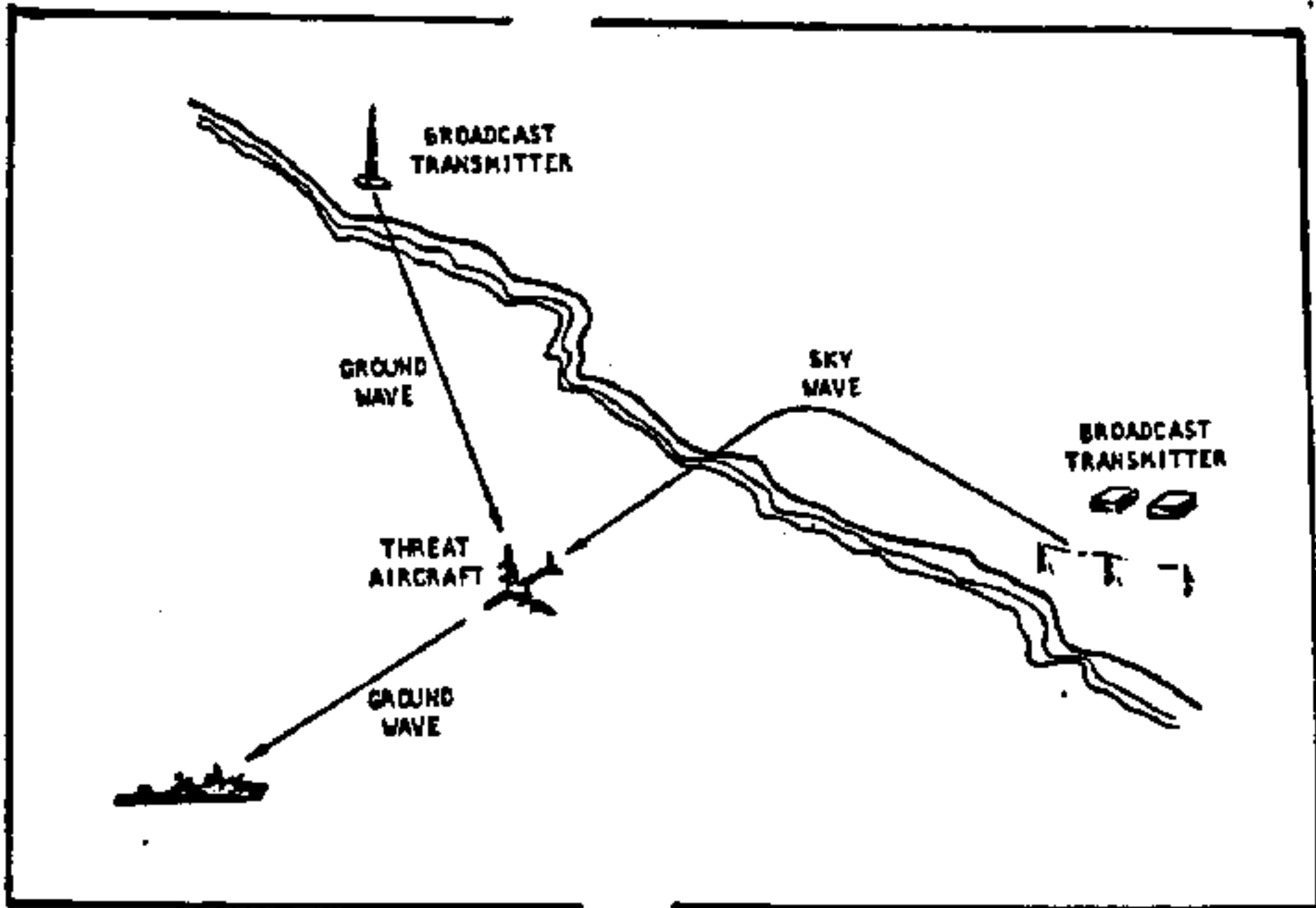


Figure 3-1 (U) FAD Polystatic System. (U)

[REDACTED]

UNCLASSIFIED

UNCLASSIFIED

3.1.1 (U)  -- Continued.

and also between the target and the shipborne receiver. The second consists of sky-wave propagation between the transmitter and the target and ground-wave propagation between the target and receiver. These two types are denoted as ground-ground and sky-ground modes, respectively.

To accomplish this feasibility study the efforts considered three aspects: source availability, the operating schedules of sources, and the coverage provided by available sources. These are described below.

3.1.2 (U)  Available Transmitters. (U)

The transmitters were categorized into two groups based on the polarization of their radiated signals. Horizontally polarized signals were considered for sky-wave propagation only on the transmitter-target half path since the attenuation of the horizontal component of a ground-wave over sea water is very large. The vertically polarized signals, on the other hand, were considered for both sky-wave and ground-wave propagation for the transmitter-target half path.

Table 3-1 lists some of the transmitters in the immediate vicinity of the Mediterranean which have been evaluated along with transmitter location, selected frequencies, transmitter power, beam information and polarization. The locations of the transmitters are displayed in Figure 3-2.

Transmitter scheduling is also an important factor in the evaluation of these transmitters. Historical records of scheduling were examined along with current information from FBIS to determine the schedules for each transmitter. Figure 3-3 shows the scheduling for the transmitters in Figure 3-2. Transmitters are available around the clock for coverage of some areas of the Mediterranean, but more sources must be located to provide complete around-the-clock coverage of the Mediterranean.

3.1.3 (U)  Coverage. (U)

Figure 3-4 illustrates the geometry for a bistatic radar detection. Several requirements must be satisfied in order to make a detection. First, the received scatter path signal, T-R, must be above the noise level present at the receiver. Second, the direct path signal must be received. (In the case of transmitters with sufficient frequency stability, a synthesizer signal can be used where the direct path signal cannot be received.) Third, the ratio of the direct path to scatter path signals must fall within the dynamic range limitations of the receiver.

UNCLASSIFIED

(This page is UNCLASSIFIED)

TABLE 3-1 (UNCLASSIFIED). MEDITERRANEAN TRANSMITTERS (U).

City	Latitude	Longitude	Frequency	Power - kw	Azimuth	Polarization
Caltanissetta	37° 30'	14° 04'	4060	25	ND	VEM
			7175	5	ND	VEM
Rome	41° 48'	12° 31'	5960	60	ND	VEM
			4060	5	ND	VEM
			7175	5	ND	VEM
Athina	38° 02'	23° 42'	6085	5	ND	VEM
Lanzetta	39° 48'	30° 49'	6090	3	ND	VEM
			7240	1	ND	VEM
Kosani	40° 20'	21° 48'	7215	3	ND	VER
Lavio	39° 32'	32° 25'	5923	2	ND	VER
Rhodes	36° 29'	30° 34'	4011	35	ND	VEM
			7125	35	ND	VER
			7260	35	ND	VER
Serrai	41° 08'	13° 31'	7160	2	ND	VER
			7165	2	ND	VER
Tripoli	37° 35'	31° 23'	5585	1	ND	VER
Beirut	33° 52'	35° 25'	5580	100	ND	HOR
Damascus	33° 30'	36° 07'	6165	50	ND	HOR
Tel Aviv	32° 0'	34° 59'	6370	20	ND	HOR
			7189	20	ND	HOR
Cairo			7050			
			7075			
Tripoli	32° 42'	13° 12'	7165	100	ND	HOR
Tunis	36° 50'	9° 54'	5905	50	102-252	HOR
Algiers	37°	3°	6581	50	ND	HOR
			9518	50	ND	HOR
Tangier	35° 41'	5° 56'	6170	100	40°	HOR
			6190	100	40°	HOR
			7225	100	40°	HOR
Lidou	38° 45'	8° 40'	6025	50	54	HOR
Madrid	40° 16'	3° 21'	6130	100	300	HOR
Tirane	41° 30'	20°	5945	50	ND	ND
			6020			
			7060			
Sofia	43°	24°	5920	50	ND	ND
			6020			
			7670			

ND: Non-Directional

UNCLASSIFIED

UNCLASSIFIED

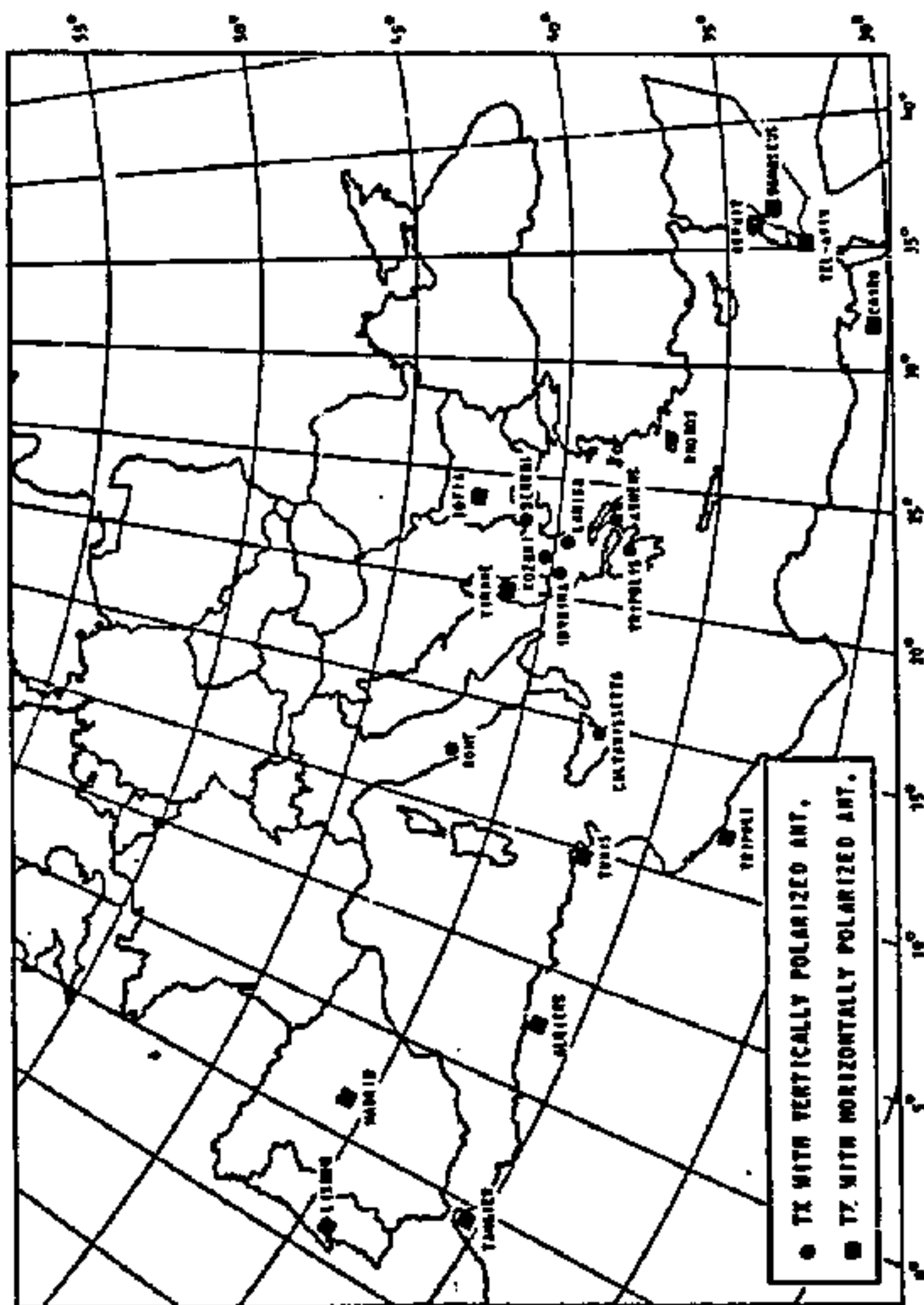


Figure 3-2 (UNCLASSIFIED). Located Sources (U).

UNCLASSIFIED

UNCLASSIFIED

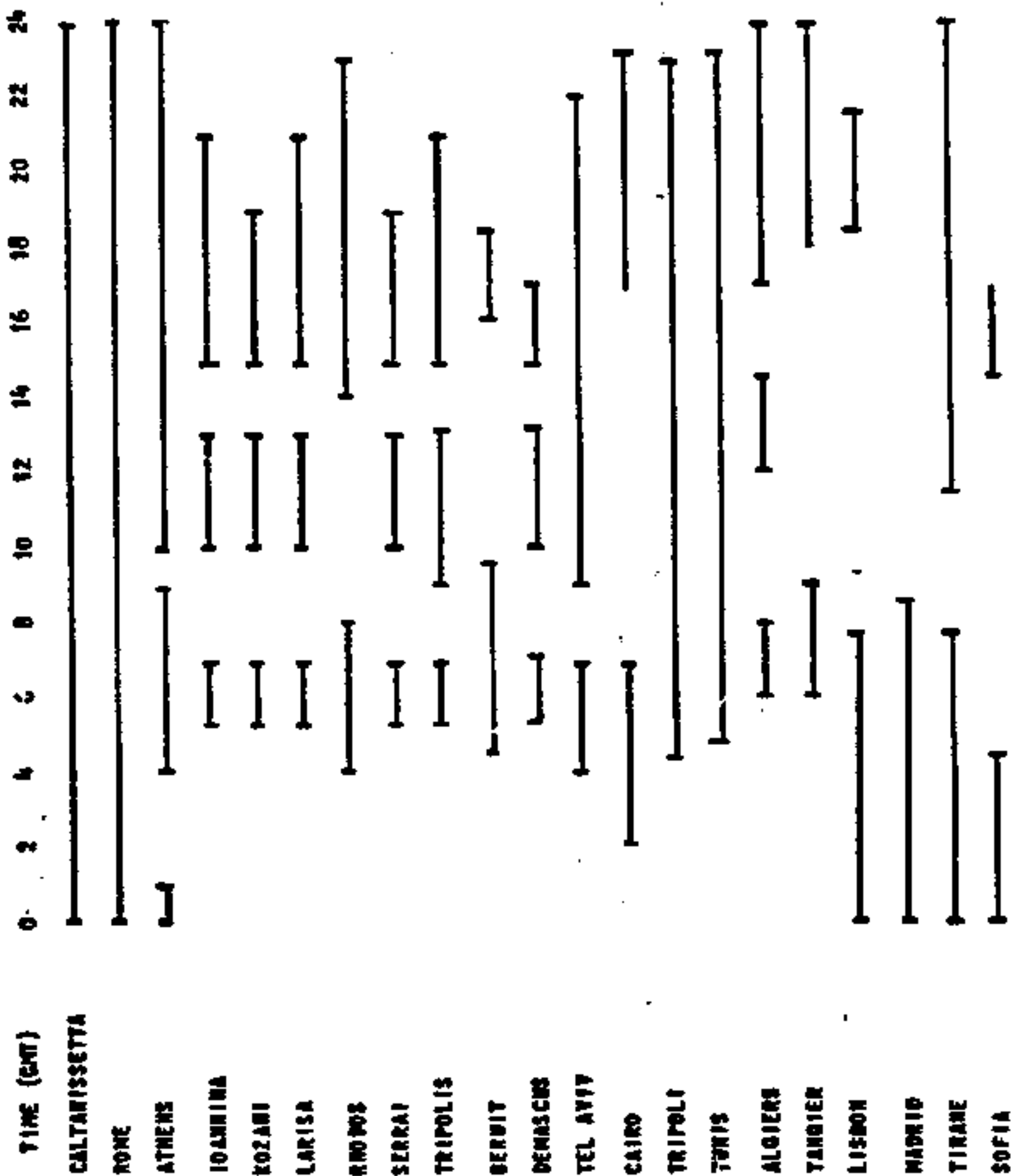


Figure 3-3 (UNCLASSIFIED). Source Schedule (U).

[REDACTED]
(This page is UNCLASSIFIED)

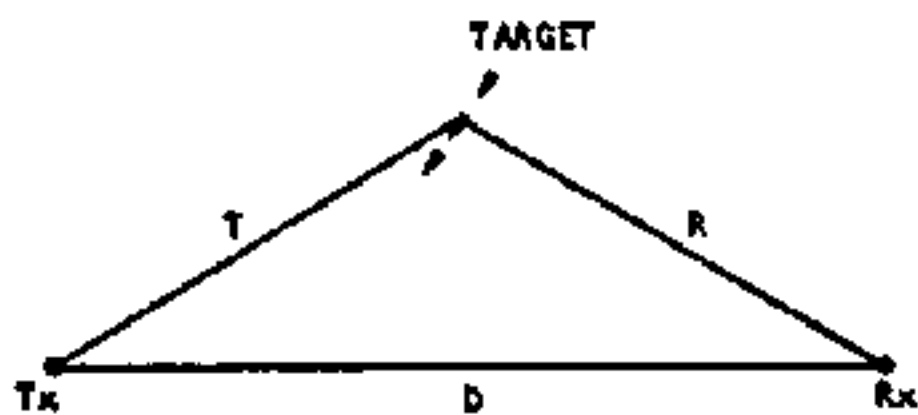


Figure 3-4 (7). Typical Geometry. (U)

UNCLASSIFIED

3.1.3.1

(U)

Evaluation. (U)

Actual propagation losses for each half path have been calculated for selected transmitter-target-receiver geometries to evaluate the coverage available to the fleet. For sky-wave propagation, the losses were calculated using the propagation prediction package by ITSA/ESSA*. For ground-wave propagation, the losses are taken from Barrick's table**.

Figure 3-5 shows an example of one of Barrick's tables. This particular table is for 7 MHz, Sea State 4, 20-knot wind, and propagation in the upwind-downwind direction. The effect of each of these parameters is that increasing frequency increases the loss, rougher sea state increases the loss, and propagation in a crosswind direction has less loss than upwind-downwind propagation.

For organization ease, the Mediterranean was divided into 5 sections. Each section was evaluated individually to determine the amount of coverage protection afforded to a ship while it was located within that area. Evaluations were made for representative transmitter-aircraft-ship positions to see if the detection system was feasible.

3.1.3.2 (U) Ground Wave-Ground Wave Propagation. (U)

For the case in which ground-wave propagation occurs over both half paths, the coverage provided by transmitters with vertically polarized signals was evaluated using the following parameters:

- a. target cross-section $\sigma = 100 \text{ M}^2$;
- b. $G_T = G_R = 0 \text{ db}$;
- c. $N = -150 \text{ dbw}$ and -170 dbw ;
- d. frequency--7 MHz, and
- e. system loss $L_S = 3 \text{ db}$.

* Barghausen, A. F., et al, Predicting Long-Term Operational Parameters of High Frequency Skywave Telecommunication Systems, ESSA Technical Report, LRL 110-ITS 7B, U.S. Department of Commerce; May 1969.

** Barrick, D. E., "Theory of Groundwave Propagation Across a Rough Sea at Dekameter Wavelengths", Battelle Memorial Institute, Columbus Laboratories; January 1970.

UNCLASSIFIED

UNCLASSIFIED

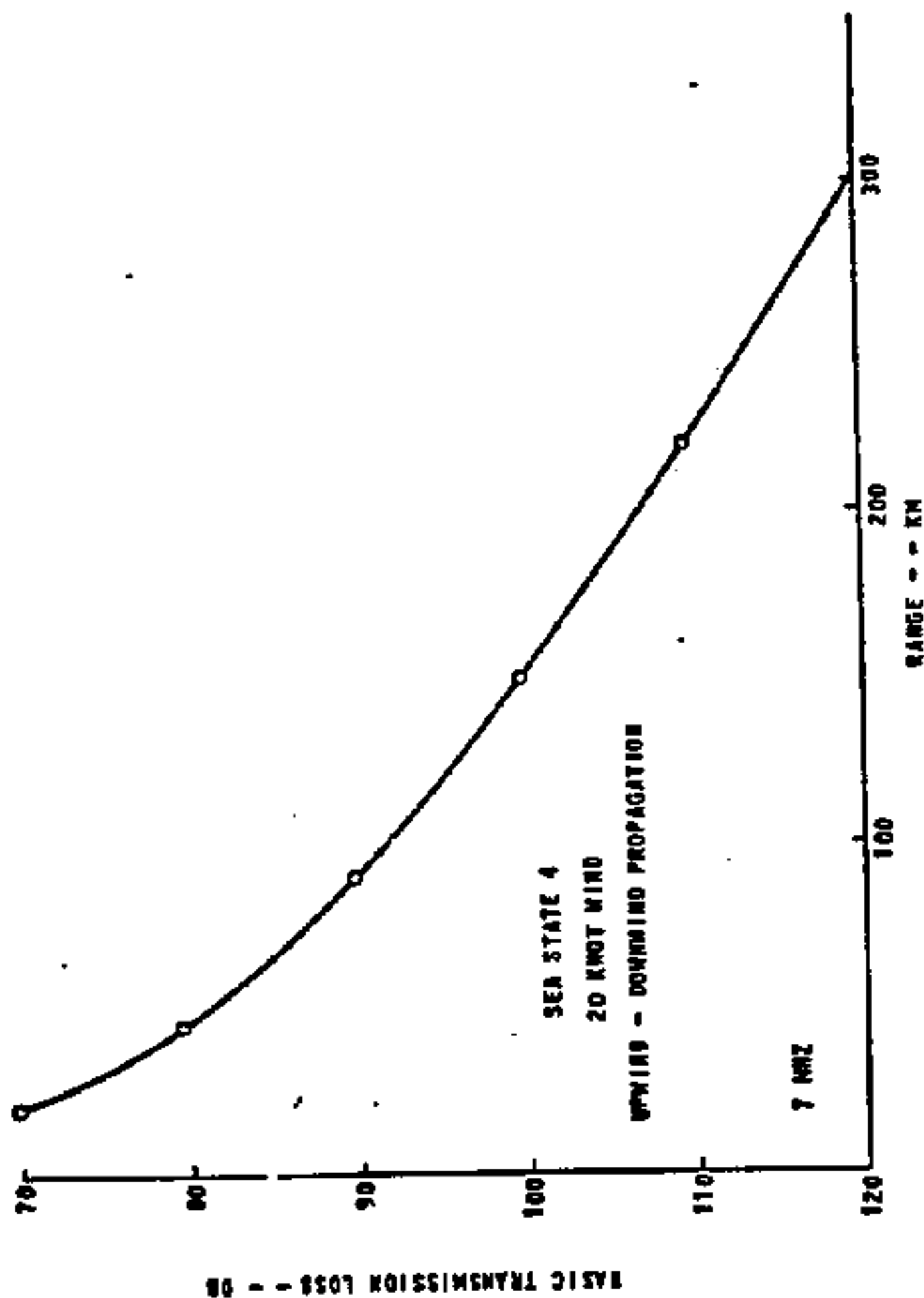


Figure 3-5 (U). Basic Transmission Loss for a Groundwave Along the Ocean (U).

UNCLASSIFIED

UNCLASSIFIED

3.1.3.2 (U) -- Continued.

The two noise levels account for diurnal changes in the noise level of the receiver. The frequency of 7 MHz was selected since it is low enough to provide reasonable ground-wave losses and high enough to have reasonably low noise levels for the detection of aircraft. To determine the region of coverage provided by this propagation mechanism, the shipboard receivers were assumed to be 200 km from the transmitters. With this assumption, a contour of constant sensitivity (Oval of Cassini) was constructed around the transmitter and receiver which determines the region of detectability of an aircraft for that transmitter-receiver combination. This was done in a number of transmitter-receiver cases and the results (Figure 3-6) indicate that coverage is quite good in the northern central part of the Mediterranean Ocean.

3.1.3.3 (U) Sky Wave-Ground Wave Propagation. (U)

For each of the five areas in the Mediterranean, propagation predictions were made for selected transmitters to evaluate the use of sky-wave propagation. Target illumination by line of sight and one F-hop propagation is feasible for detection purposes, but hop structures with more than 1 F-hop for the date and time evaluated incur too much loss over the transmitter half path to afford any reasonable protection. Noise calculations and propagation conditions were calculated for 15 September 1970 at 0800Z (N = -165 dbw).

Five aircraft positions were evaluated with shipboard receivers located at selected positions around the aircraft. The regions of detectability for each transmitter-receiver combination (Ovals of Cassini) were not calculated at this time, but as a first estimate of the protection provided by each transmitter, the following technique was used. For a specific aircraft position (altitude 3,000 feet), loss over the transmitter-target half path was evaluated from the ITSA ESSA prediction program. L_R was then calculated and converted into a distance D_R , using Figure 3-5. Assuming the target scatters equally in all directions, a circle of coverage can be drawn around the aircraft of distance D_R . Any receiver located within the circle should detect the aircraft.

For example, consider transmitters located at Algiers and Madrid, an aircraft located at 37-99N, 2-07E, and a receiver located at 38N, 0E. The predicted losses over the transmitter half path are 116 db for the 1 F-hop mode from Madrid and 91 db for a line-of-sight mode from Algiers. Solving for L_R and converting to a target-receiver distance from Figure 3-4 gives 70 km for the Madrid signal and 205 km for the Algiers

UNCLASSIFIED

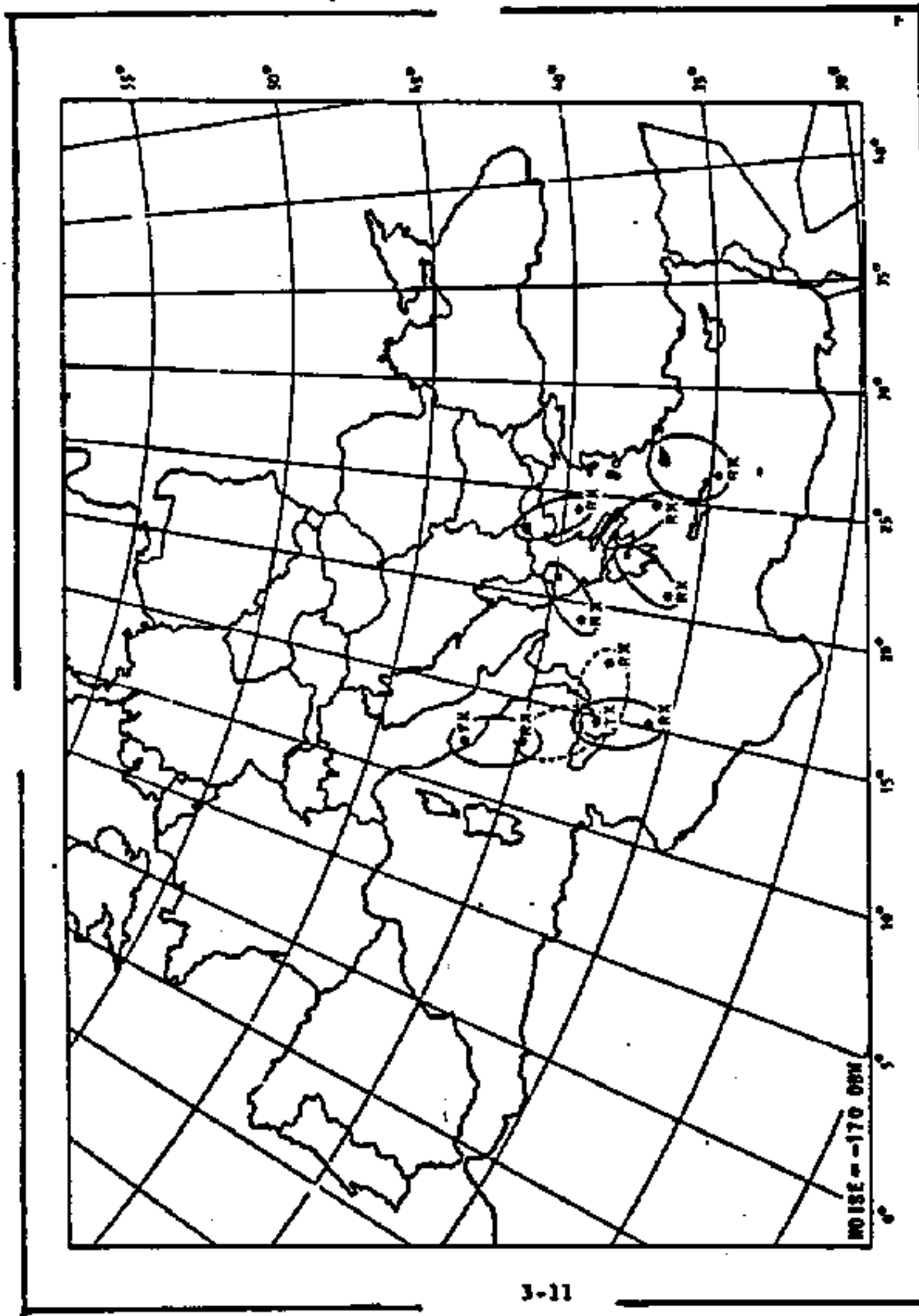


Figure 3-6 (U) Typical Fleet Protection Areas in the Mediterranean Ocean. (U)

UNCLASSIFIED

[REDACTED]
(This page is UNCLASSIFIED)

3.1.3.3 (U) -- Continued.

signal. Any receiver within these distances from the aircraft should be able to detect the aircraft. Figure 3-7 illustrates this example. In this example the shipboard receiver located at 38N, 0E, would detect the aircraft on the Algiers frequency, but not on the frequency from Madrid. As the aircraft closed on the ship, the Madrid frequency would also make a detection.

Using these methods to evaluate the coverage for each area, the following results were found (see Figure 3-8). For area one, transmitters located at Lisbon, Madrid, Tangier, and Algiers were evaluated for the receiver and target position given in the example. The transmitters afforded protection at distances from this aircraft of 10, 20, 70, and 205 km, respectively.

For area 2, transmitters located at Algiers and Rome were evaluated for two different ship positions. Algiers provided detectability at 70 km from the aircraft while Rome provided detectability at 100 km.

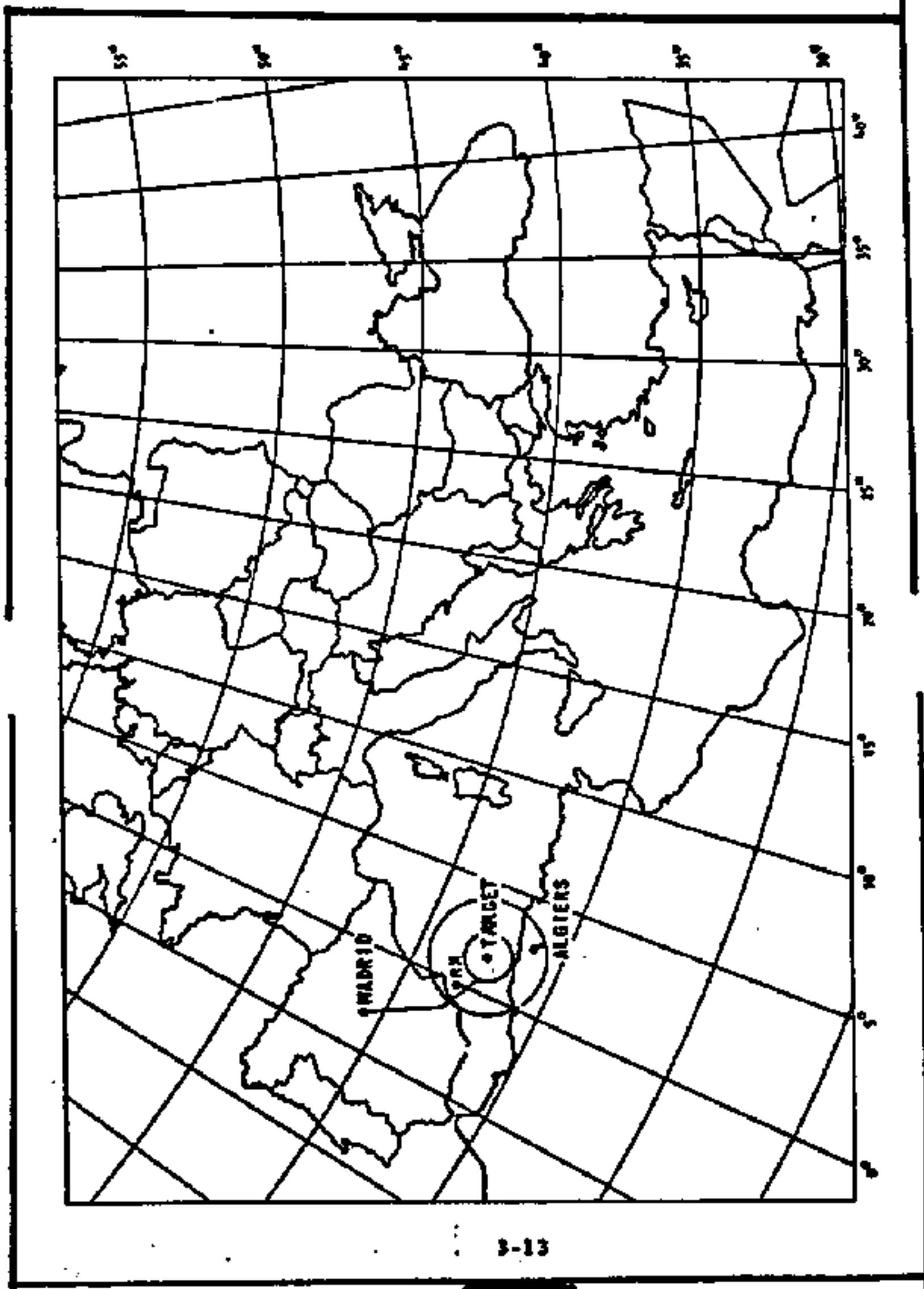
For area 3, transmitters were evaluated at Caltanissetta, Alma Ata, Rome, Tunis, Tirane, and Tripoli. Tripoli provided the greatest detection range at 80 km with Rome and Tirane giving 50 km detection range.

For areas 4 and 5, the greatest detection range for the transmitters evaluated was 100 km in each case.

In addition to the transmitters evaluated, a great number of possible transmitters at other locations still remain to be evaluated around the coast of the Mediterranean. Table 3-2 is a partial listing of these locations. Transmitters with power as low as 1 kw can be used for line-of-sight coverage along the coast and 1F hop propagation into the interior of the sea. Development of these sources is necessary for round-the-clock coverage as well as multiple channel coverage (i. e., on several transmitter frequencies) of a ship at any point in the Mediterranean.

The conclusion that can be drawn from this analysis is that the use of transmitters of opportunity as part of a polystatic HF radar system is feasible for FAD in the Mediterranean Sea. However, before a system is implemented, there is a need to evaluate the transmitter sources that have not been examined to identify the specific transmitters that should be employed by the fleet during operation in different areas of the Mediterranean Sea.

UNCLASSIFIED



3-13

Figure 3-7 (U) Skywave-Groundwave Example. (U)

UNCLASSIFIED

RESTRICTED

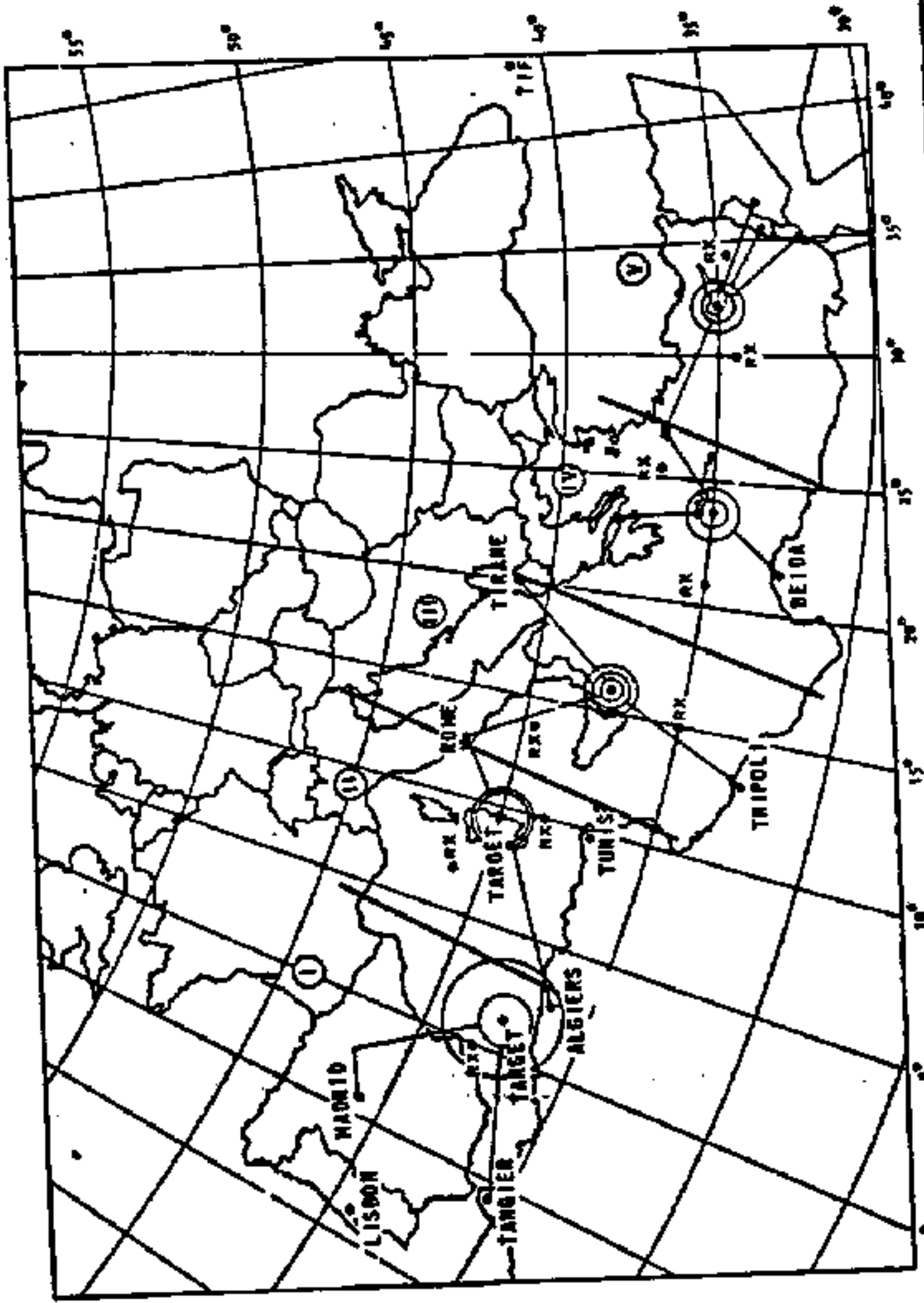


Figure 3-8 Skywave-Groundwave Coverage. (U)

RESTRICTED

[REDACTED]
(This page is UNCLASSIFIED)

Table 3-2

(U) Additional Transmitters (U)

Malaga, Spain	Tobruk, Lybia
Cartagena, Spain	Beida, Lybia
Valencia, Spain	Bengazi, Lybia
Barcelona, Spain	Annaba, Tunisia
Marseille, France	Safaqis, Tunisia
Nice, France	Oran, Algeria
Pisa, Italy	Melilla, Morocco
Naples, Italy	Balearic Island
Izmir, Turkey	Corsica
Latakia, Syria	Sardinia
Port Said, UAR	Crete
Alexandria, UAR	Cyprus

3.2 (U)

TARGET LOCATION METHODS. (U)

As described previously, protection of the fleet against low-flying aircraft and/or cruise missiles may be accomplished using a bistatic radar with a shore-based transmitter for target illumination combined with passive shipboard reception. The target location methods considered in this section appear to eliminate two fundamental problems associated with CW-Doppler bistatic radar:

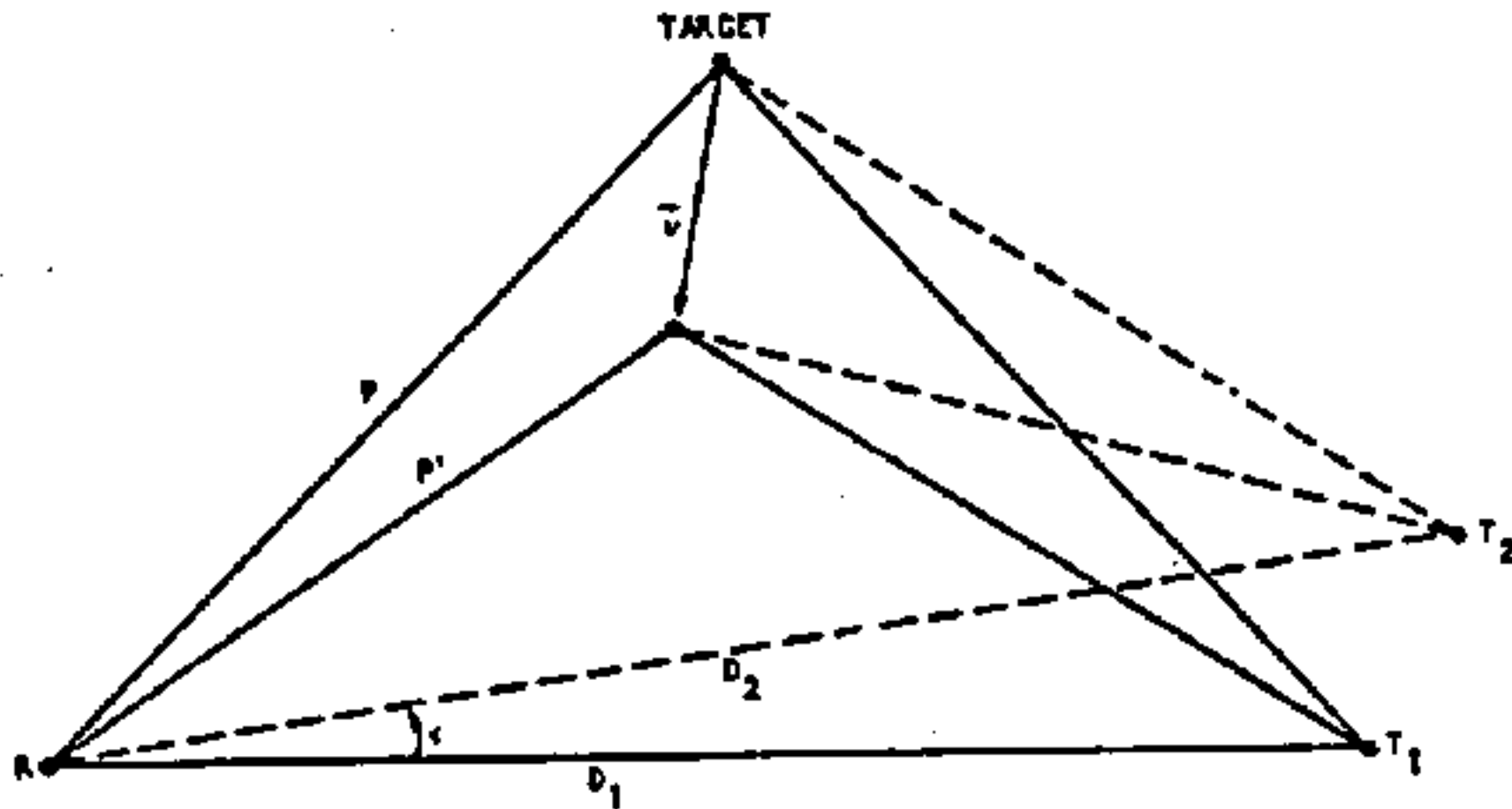
- a. Target signal amplitudes gives no indication of whether the target is near the transmitter or the receiving ship because the bistatic radar range equation is symmetric about the transmitter-target and receiver-target ranges.
- b. Single Doppler measurements alone cannot provide unambiguous target location since single Doppler measurements have a fourfold location ambiguity caused by the geometric symmetry between the transmitter, receiver and target.

Four separate derivations are given describing techniques which may be used to locate and track low-flying targets which may threaten a surface fleet. They all assume a two-dimensional (flat earth) situation that is reasonably accurate (see Section 3.3.4) for low-flying aircraft and cruise missiles. The four techniques are:

- a. the double baseline, double measurement range estimator,
- b. the double baseline, single measurement range estimator,
- c. the single baseline, double measurement range estimator, and
- d. the Doppler location finder.

The first two techniques employ two transmitters and one receiver as shown in Figures 3-9 and 3-10, respectively. For the first method (double baseline, double measurement range estimator) two target-scattered Doppler returns and their directions of arrival are measured at two different points along the target's flight trajectory. Eight measurements are employed to estimate the target's location. For the second method (double baseline, single measurement range estimator) the estimate is essentially made using the two Doppler returns and their associated directions of arrival measured at one flight point. The third technique (single baseline, double measurement range estimator) uses two sets of Doppler returns and associated direction of arrival

UNCLASSIFIED



LEGEND:

- P, P' = GROUND RANGE FROM RECEIVER TO TARGET AT TWO POINTS ON TARGET PATH
- \vec{v} = TARGET VELOCITY VECTOR
- α = ANGLE AT THE RECEIVER BETWEEN THE TWO LOCATION BASELINES
- R = RECEIVER
- T_1, T_2 = TRANSMITTER 1 AND 2, RESPECTIVELY
- D_1, D_2 = ARE THE DISTANCES BETWEEN THE RECEIVER AND TRANSMITTERS T_1 AND T_2 RESPECTIVELY (KNOWN A PRIORI)

Figure 3-9 (U). Double-Baseline, Two-Measurements Model. (U)

UNCLASSIFIED

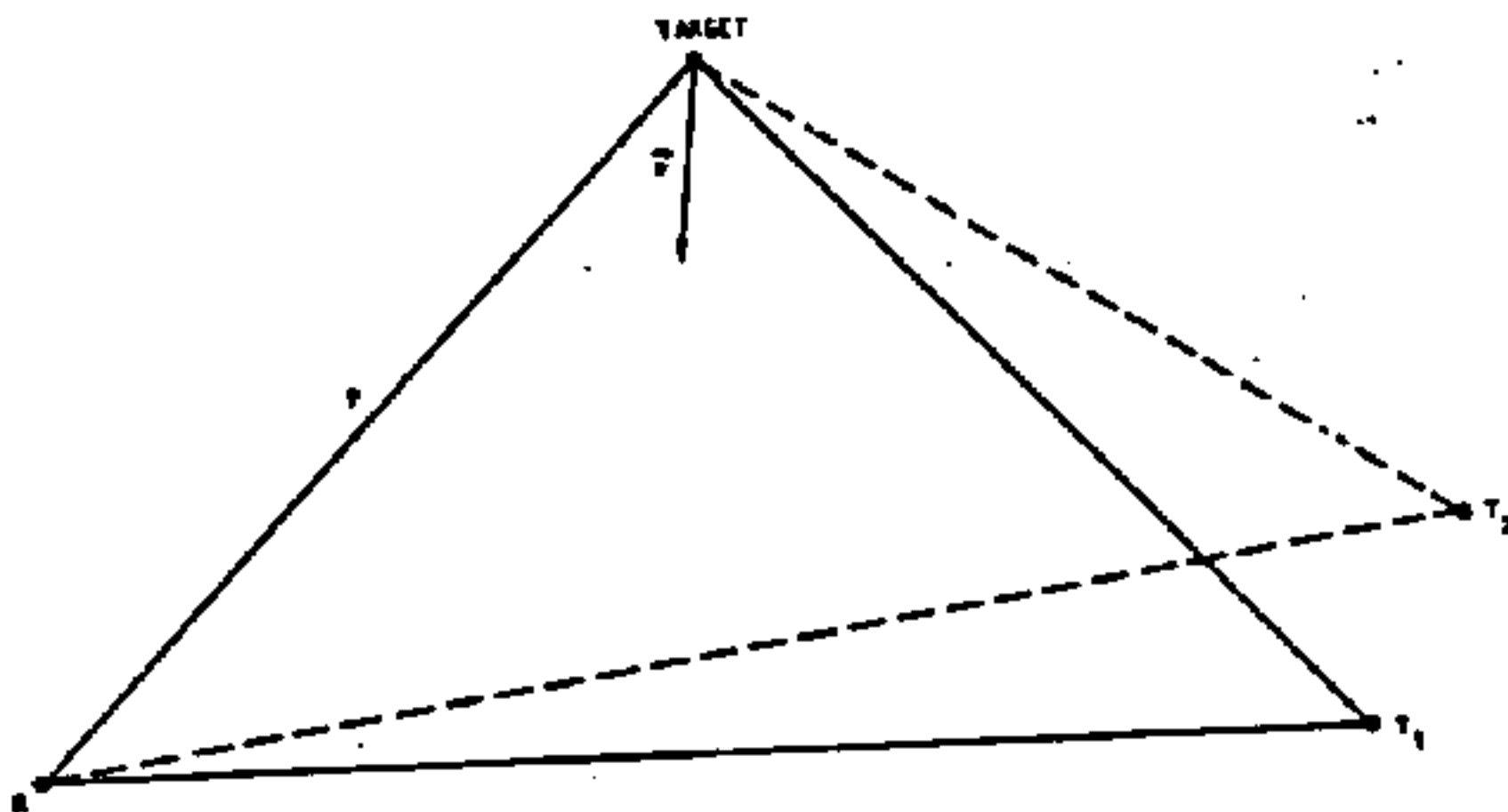


Figure 3-10 (U). Double-Baseline, One-Measurement Model. (U)

3.2 (U) ~~SECRET~~ Continued.

UNCLASSIFIED

and a single transmitter source to estimate the target's range. This method, which uses the configuration in Figure 3-11, is operationally preferred to the first two because of the need for fewer measurements and transmitter sources. The fourth technique (Doppler location finder) employs the Doppler returns from the target illuminated by four transmitters to estimate both range and azimuth. All four techniques provide location information on the detected target.

The derivation of equations for each of the four methods is included below.

3.2.1 (U) Double-Baseline, Two-Measurements Range Estimator. (U)

Consider the single baseline, one time point situation shown in Figure 3-12, where a vehicle is moving at an unknown velocity \bar{U} , the distance between the transmitter and the receiver is assumed known to be D , and the transmitter is broadcasting on a known wavelength λ . The azimuth angle of the target at the receiver, α , and the Doppler shift, Δf , are measured.

The received Doppler shift for this geometry may be written as

$$\begin{aligned}\Delta f &= -\frac{\bar{U}}{\lambda} (f_1 + f_2) \\ &= -\frac{\bar{U}}{\lambda} (\cos \theta_1 + \cos \theta_2)\end{aligned}$$

Angles θ_1 and θ_2 can also be written:

$$\begin{aligned}\theta_1 &= 90 + \alpha + \delta \\ \theta_2 &= 90 + \beta - \delta\end{aligned}$$

Therefore,

$$\Delta f = \frac{\bar{U}}{\lambda} [\sin(\alpha + \delta) + \sin(\beta - \delta)]$$

UNCLASSIFIED

[REDACTED]
(This page is UNCLASSIFIED)

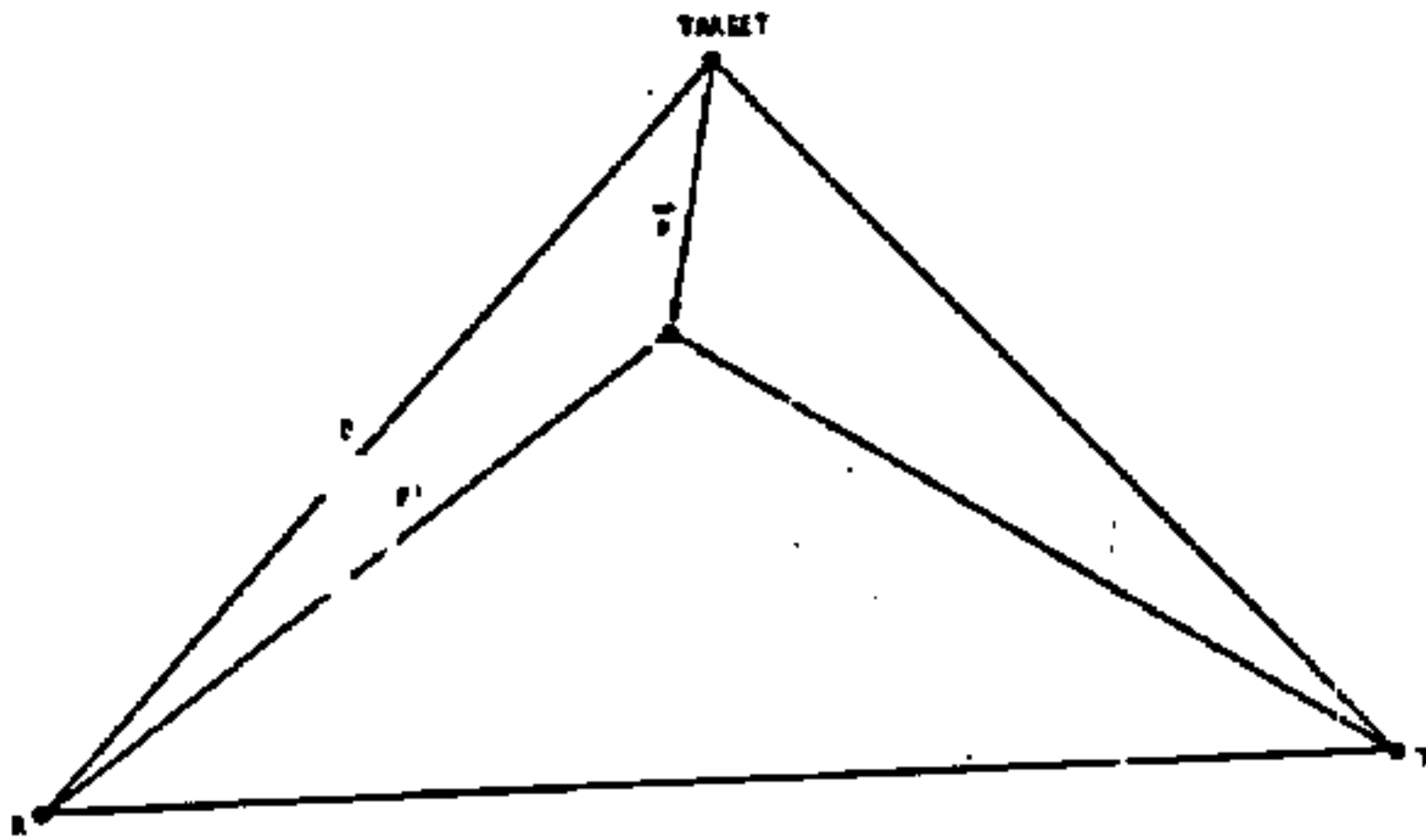


Figure 3-11. (U) Single Baseline Model. (U)

UNCLASSIFIED

UNCLASSIFIED

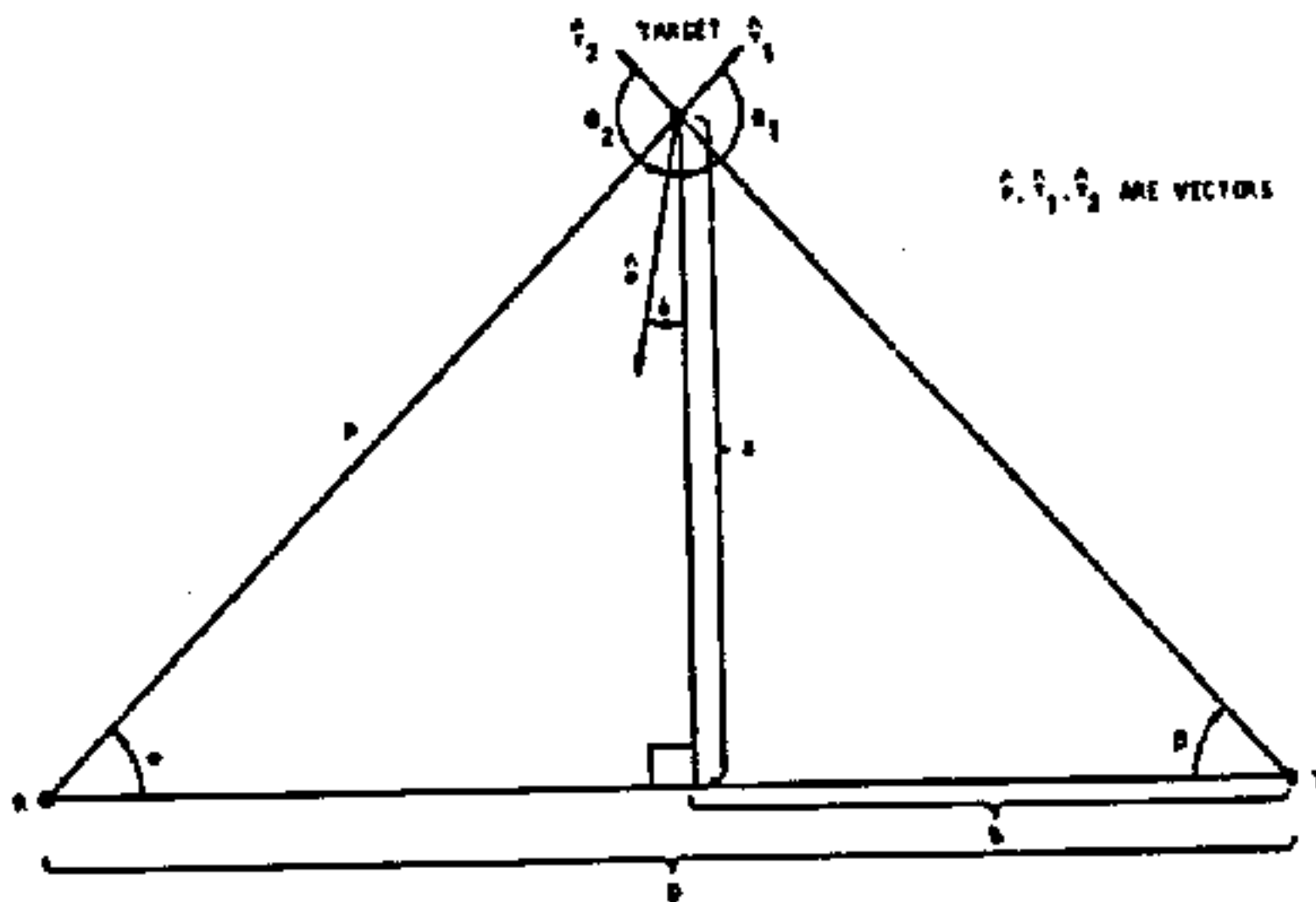


Figure 3-12. (U) Variables for Double-Baseline, Two-Measurements Model. (U)

UNCLASSIFIED

UNCLASSIFIED

3.2.1 (U) -- Continued.

Also,

$$\delta = \tan^{-1} \left(\frac{b}{a} \right)$$

$$= \tan^{-1} \left[\frac{b}{D - \frac{a}{\tan \alpha}} \right] = \tan^{-1} \left[\frac{a \tan \alpha}{D \tan \alpha - a} \right]$$

If there are two transmitter geometries, which shall be distinguished using subscripts, then the following three equations can be written;

$$\Delta f_1 = \frac{v}{\lambda_1} \left\{ \sin(\alpha_1 + \delta_1) + \sin \left[\tan^{-1} \left(\frac{a_1 \tan \alpha_1}{D_1 \tan \alpha_1 - a_1} \right) - \delta_1 \right] \right\} \quad (3-1)$$

$$\Delta f_2 = \frac{v}{\lambda_2} \left\{ \sin(\alpha_2 + \delta_2) + \sin \left[\tan^{-1} \left(\frac{a_2 \tan \alpha_2}{D_2 \tan \alpha_2 - a_2} \right) - \delta_2 \right] \right\} \quad (3-2)$$

and

$$\delta_2 = \delta_1 + \epsilon \quad (3-3)$$

where ϵ is the angle between the two baselines, as shown in Figure 3-9. The value of ϵ may be calculated because the coordinates of the two transmitters and the receivers are assumed known.

If additional azimuth and Doppler measurements are made for these same two geometries at some time Δt later, then four more equations can be written. This set of equations is distinguished by a superscript prime.

$$\Delta f_1' = \frac{v}{\lambda_1} \left\{ \sin(\alpha_1' + \delta_1') + \sin \left[\tan^{-1} \left(\frac{a_1' \tan \alpha_1'}{D_1 \tan \alpha_1' - a_1'} \right) - \delta_1' \right] \right\} \quad (3-4)$$

$$\Delta f_2' = \frac{v}{\lambda_2} \left\{ \sin(\alpha_2' + \delta_2') + \sin \left[\tan^{-1} \left(\frac{a_2' \tan \alpha_2'}{D_2 \tan \alpha_2' - a_2'} \right) - \delta_2' \right] \right\} \quad (3-5)$$

UNCLASSIFIED

3.2.1 (U) -- Continued.

$$a_1' = a_1 - v \Delta t \cos \delta_1 \quad (3-6)$$

$$a_2' = a_2 - v \Delta t \cos \delta_2 \quad (3-7)$$

The last two equations are a result of the constant velocity and direction assumption. All seven equations can be combined into a system of four equations in four unknowns by eliminating δ_2 from the equations. The results are:

$$\Delta f_1 = F_1(v, a_1, \delta_1)$$

$$\Delta f_2 = F_2(v, a_2, \delta_1)$$

$$\Delta f_1' = F_3(v, a_1, \delta_1)$$

$$\Delta f_2' = F_4(v, a_2, \delta_1)$$

where the $F_i(\cdot)$ are different functions of the argument parameters. The unknowns are v , a_1 , a_2 and δ_1 . The measured quantities are α_1 , α_2 , α_1' , α_2' , Δf_1 , $\Delta f_1'$, Δf_2 , and $\Delta f_2'$. The quantities known a priori are D_1 , D_2 , λ_1 , λ_2 , Δt , and c . The above set of simultaneous equations may be solved for the unknowns and the ground range from the receiver to the target could be calculated by

$$P = \frac{a_1}{\sin \alpha_1}$$

Although this procedure yields four independent equations which may be solved for the target position, a slight reformulation of the problem can reduce the number of equations by two as described on the following page. Because this reformulation simplifies the double baseline, two measurement technique, this first target location technique will not be examined further.

UNCLASSIFIED

3.2.2 (U) Double-Baseline, One-Measurement Range Estimator. (U)

The variables for the double-baseline, one-measurement model are defined in Figure 3-13. As in the previous case, the transmitter-receiver distances, D_1 and D_2 , and the transmitter wavelengths, λ_1 and λ_2 , are assumed known a priori. The azimuths, α_1 and α_2 , and Doppler shifts, Δf_1 and Δf_2 , are the only quantities requiring measurement.

From another form of the Doppler equation,

$$\Delta f_1 = \frac{-1}{\lambda_1} (\dot{p} + \dot{n}_1)$$

$$\Delta f_2 = \frac{-1}{\lambda_2} (\dot{p} + \dot{n}_2)$$

where $\dot{p} = dp/dt$ and $\dot{n}_1 = dn/dt$.

From the law of cosines,

$$n_1 = (p^2 + D_1^2 - 2pD_1 \cos \alpha_1)^{1/2}$$

so

$$\dot{n}_1 = \frac{(p\dot{p} - \dot{p}D_1 \cos \alpha_1 + pD_1 \dot{\alpha}_1 \sin \alpha_1)}{(p^2 + D_1^2 - 2pD_1 \cos \alpha_1)^{1/2}} \quad (3-8)$$

where $\dot{\alpha}_1 = d\alpha_1/dt$.

Similarly

$$\dot{n}_2 = \frac{(p\dot{p} - \dot{p}D_2 \cos \alpha_2 + pD_2 \dot{\alpha}_2 \sin \alpha_2)}{(p^2 + D_2^2 - 2pD_2 \cos \alpha_2)^{1/2}} \quad (3-9)$$

Note that $\dot{\alpha}_1 = \dot{\alpha}_2 = \dot{\alpha}$. The quantity $\dot{\alpha}$ can be estimated using the previous azimuth measurements as follows:

$$\dot{\alpha} = \frac{[\alpha_1(t) - \alpha_1(t-\Delta t)] + [\alpha_2(t) - \alpha_2(t-\Delta t)]}{2\Delta t}$$

UNCLASSIFIED

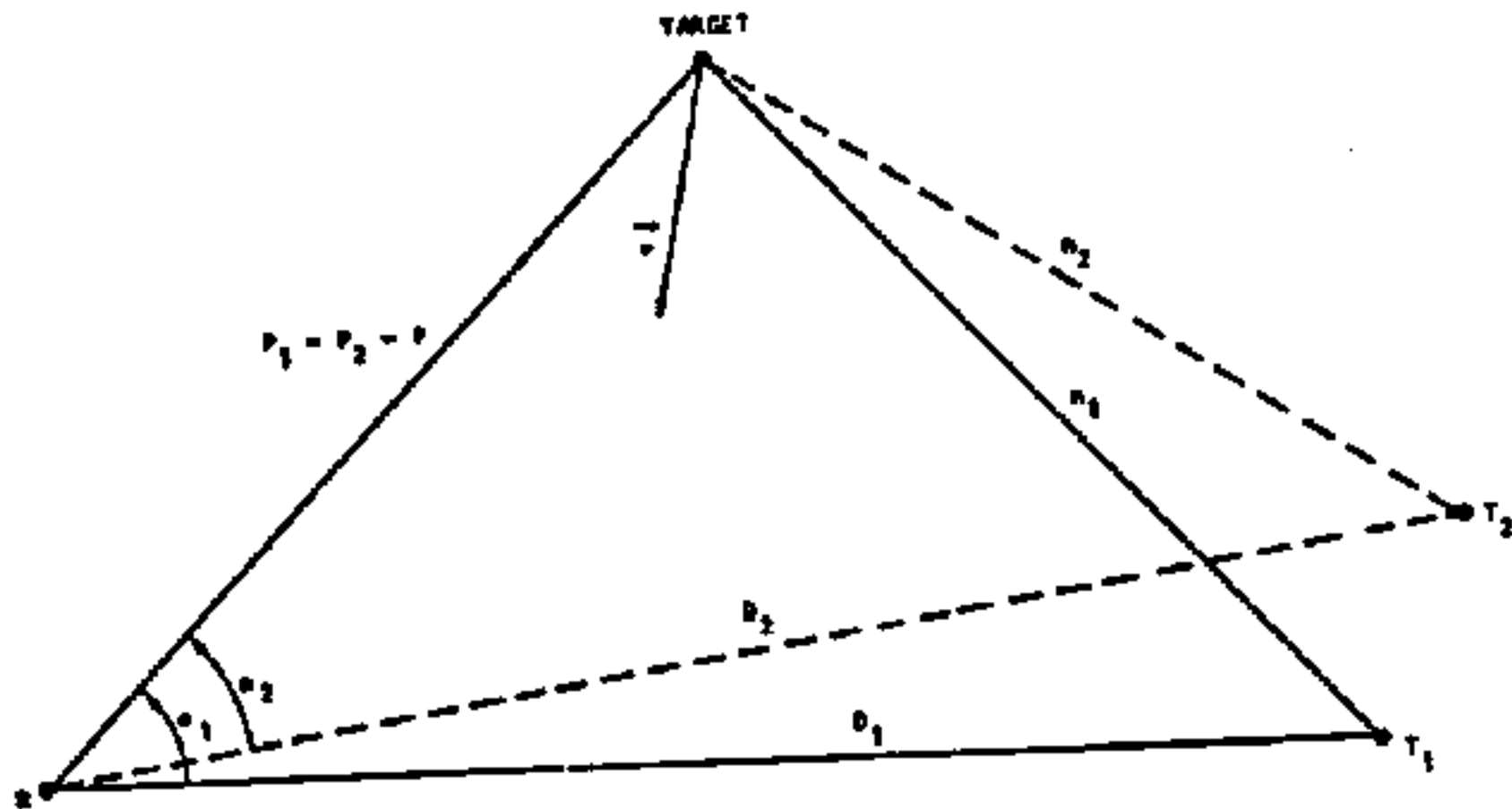


Figure 3-13. (U) Variables for Double-Baseline, One-Measurement Model. (U)

UNCLASSIFIED

UNCLASSIFIED

3.2.2 (U) -- Continued.

Now define h_1 , q_1 , r_1 , and s_1 as follows:

$$h_1 = (p^2 + D_1^2 - 2pD_1 \cos \alpha_1)^{1/2}$$

$$q_1 = \Delta f_1 \lambda_1$$

$$r_1 = D_1 \cos \alpha_1$$

$$s_1 = D_1 \sin \alpha_1$$

The quantities h_2 , q_2 , r_2 , and s_2 are similarly defined. Equations 3-8 and 3-9 can then be written as

$$h_1 = \frac{p\dot{p} - \dot{p}r_1 + ps_1}{h_1}$$

$$h_2 = \frac{p\dot{p} - \dot{p}r_2 + ps_2}{h_2}$$

So Δf_1 can be written

$$\Delta f_1 = \frac{-1}{\lambda_1} \left[\dot{p} + \frac{\dot{p}(p-r_1) + ps_1}{h_1} \right]$$

Similarly

$$\Delta f_2 = \frac{-1}{\lambda_2} \left[\dot{p} + \frac{\dot{p}(p-r_2) + ps_2}{h_2} \right]$$

Solving for \dot{p} .

$$\dot{p} = -\frac{(q_2 h_2 + ps_2)}{(h_2 + p - r_2)}$$

(3-10)

UNCLASSIFIED

3.2.2 (U) -- Continued.

Also,

$$-q_1 h_1 = \dot{p} h_1 + \dot{p} (p - r_1) + p \dot{r}_1$$

and so

$$p = \frac{-[q_1 h_1 + \dot{p} (h_1 - r_1)]}{\dot{r}_1 + \dot{p}} \quad (3-11)$$

Equations (3-10) and (3-11) form a system of two equations in two unknowns (p and \dot{p}) that may be solved using standard iterative techniques. Note also that, for this formulation, the assumption of constant velocity and directions are not necessary.

3.2.3 (U) Single Baseline Model. (U)

The third derivation to be considered is that involving the model using only one transmitter. The variables for the single baseline model are defined in Figure 3-14. As before, the transmitter-receiver distance, D , and the transmitter wavelength, λ , are assumed known. The azimuths, α and α' , and Doppler shifts Δf and $\Delta f'$, are measured quantities where the primes signify measurement at some time Δt after the first (unprimed) measurements. The velocity \bar{v} , of the vehicle is not known.

From the Doppler equation,

$$f = \frac{c}{\lambda} (p + \dot{h})$$

$$f' = \frac{c}{\lambda} (p' + \dot{h}')$$

From the law of cosines,

$$h = (p^2 + D^2 - 2pD \cos \alpha)^{1/2}$$

$$\dot{h} = \frac{(p \dot{p} - \dot{p} D \cos \alpha + p D \dot{\alpha} \sin \alpha)}{(p^2 + D^2 - 2pD \cos \alpha)^{1/2}}$$

UNCLASSIFIED

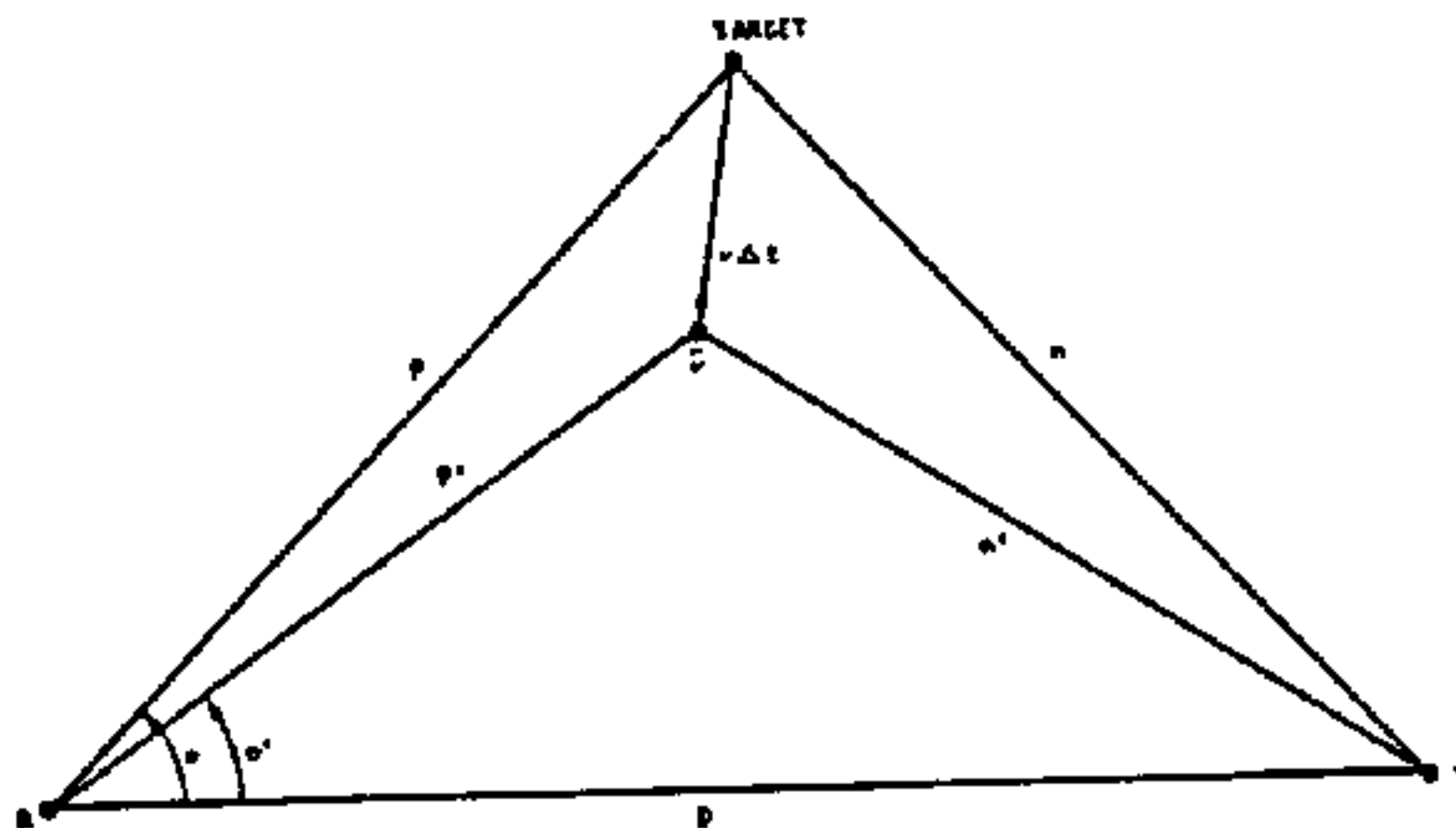


Figure 3-14. (U) Variables for Single Baseline Model. (U)

UNCLASSIFIED

UNCLASSIFIED

3.2.3 (U) -- Continued.

Similarly,

$$h' = \frac{(p' \dot{p}' - b' D \cos \alpha' + p' D \dot{\alpha}' \sin \alpha')}{(p'^2 + D^2 - 2p' D \cos \alpha')^{1/2}}$$

In order to find a solution using only one baseline, two approximations have to be made

(a) \dot{p} is constant; i. e., $\dot{p}' = \dot{p}$ and, furthermore,

$$p = p' + \dot{p} \Delta t$$

(b) $\dot{\alpha}$ is constant; i. e., $\dot{\alpha}' = \dot{\alpha}$

Over short time intervals (small Δt) these assumptions are reasonable. The angular velocity $\dot{\alpha}$ can be estimated as follows:

$$\dot{\alpha} = \frac{\alpha' - \alpha}{\Delta t}$$

These approximations are strictly true if the target is flying on a radial path, toward or away from the ship.

Combining the equations and approximations above gives

$$-\Delta f \lambda = -q = \dot{p} + \frac{\dot{p}(p-r) + ps}{h}$$

where

$$q = \Delta f \lambda$$

$$r = D \cos \alpha$$

$$s = D \dot{\alpha} \sin \alpha$$

$$h = (p^2 + D^2 - 2pD \cos \alpha)^{1/2}$$

UNCLASSIFIED

3.2.3 (U) -- Continued.

Substituting $p = p' - \dot{p}\Delta t$, squaring to eliminate square roots and algebraic manipulation of the results yields the cubic equation

$$Ap^3 + Bp^2 - Cp + D = 0 \quad (3-12)$$

where

$$A = 2\Delta t^2 (q-s)$$

$$B = \Delta t^2 (q^2 - s^2) + \Delta t (4qr - 4qp') + 2s\Delta t (2p' - r) + D^2 - r^2$$

$$C = \Delta t (2q^2 r - 2q^2 p' + 2p's^2) + 2p'^2 (q-s) + 2p'r (s-2q) + 2qD^2$$

$$D = p'^2 (q^2 - s^2) + q^2 (D^2 - 2p'r)$$

This cubic equation can be solved for \dot{p} and the correct root chosen. Also note that \dot{p} is still a function of the single unknown p' .

In similar fashion,

$$\Delta f' = \frac{-1}{\lambda} (p' + h')$$

or

$$-\Delta f' = -q' = \dot{p} + \frac{\dot{p}(p' - r') + p's'}{h'}$$

Where h' , q' , r' and s' are defined similarly to h , q , r and s .
Now

$$-q'h' - \dot{p}(h' - r') = p'(p' + s')$$

or

$$p' = \frac{-q'h' - \dot{p}(h' - r')}{p' + s'} \quad (3-13)$$

Equations (3-12) and (3-13) form a set of simultaneous equations in the two unknowns p' and \dot{p} which may be solved for the target position.

UNCLASSIFIED

3.2.4 (U) Doppler Location Finder (DLF), (U)

The range estimation techniques discussed in the previous sections all utilized measurements of target bearing and Doppler frequency. The Doppler Location Finder (DLF) described in this section uses only Doppler measurements and yields both range and bearing information.

The variables for the DLF are defined in Figure 3-15. The transmitter-receiver distances, D_1 , D_2 , D_3 , and D_4 , and the transmitter wavelengths, λ_1 , λ_2 , λ_3 , and λ_4 , are assumed known a priori. The angles, θ_1 , θ_2 , θ_3 , and θ_4 , formed by the reference baseline with the transmitter-receiver are also assumed known a priori. The only measured quantities are the Doppler shifts, Δf_1 , Δf_2 , Δf_3 , and Δf_4 . The variables estimated by the DLF technique are range p , bearing α , range velocity, \dot{p} , and bearing velocity $\dot{\alpha}$. The latter two variables described the change of target position with time and are of secondary importance. The range and bearing estimates describe the target location and have primary significance.

From the Doppler equation:

$$\Delta f_i = -\frac{1}{\lambda_i} (\dot{p} + \dot{n}_i) \quad (3-14)$$

where

$$\dot{n}_i = dn_i/dt, \quad i = 1, 2, 3, 4$$

From the law of cosines,

$$n_i = [p^2 + D_i^2 - 2pD_i \cos(\alpha + \theta_i)]^{1/2}$$

so

$$\dot{n}_i = \frac{[p\dot{p} - \dot{p}D_i \cos(\alpha + \theta_i) + pD_i \dot{\alpha} \sin(\alpha + \theta_i)]}{[p^2 + D_i^2 - 2pD_i \cos(\alpha + \theta_i)]^{1/2}} \quad (3-15)$$

Thus, from (3-14) and (3-15) it can be seen that

$$\Delta f_i = h(p, \alpha, \dot{p}, \dot{\alpha}; D_i, \theta_i, \lambda_i) \quad (3-16)$$

where h is a function of the argument parameters.

UNCLASSIFIED

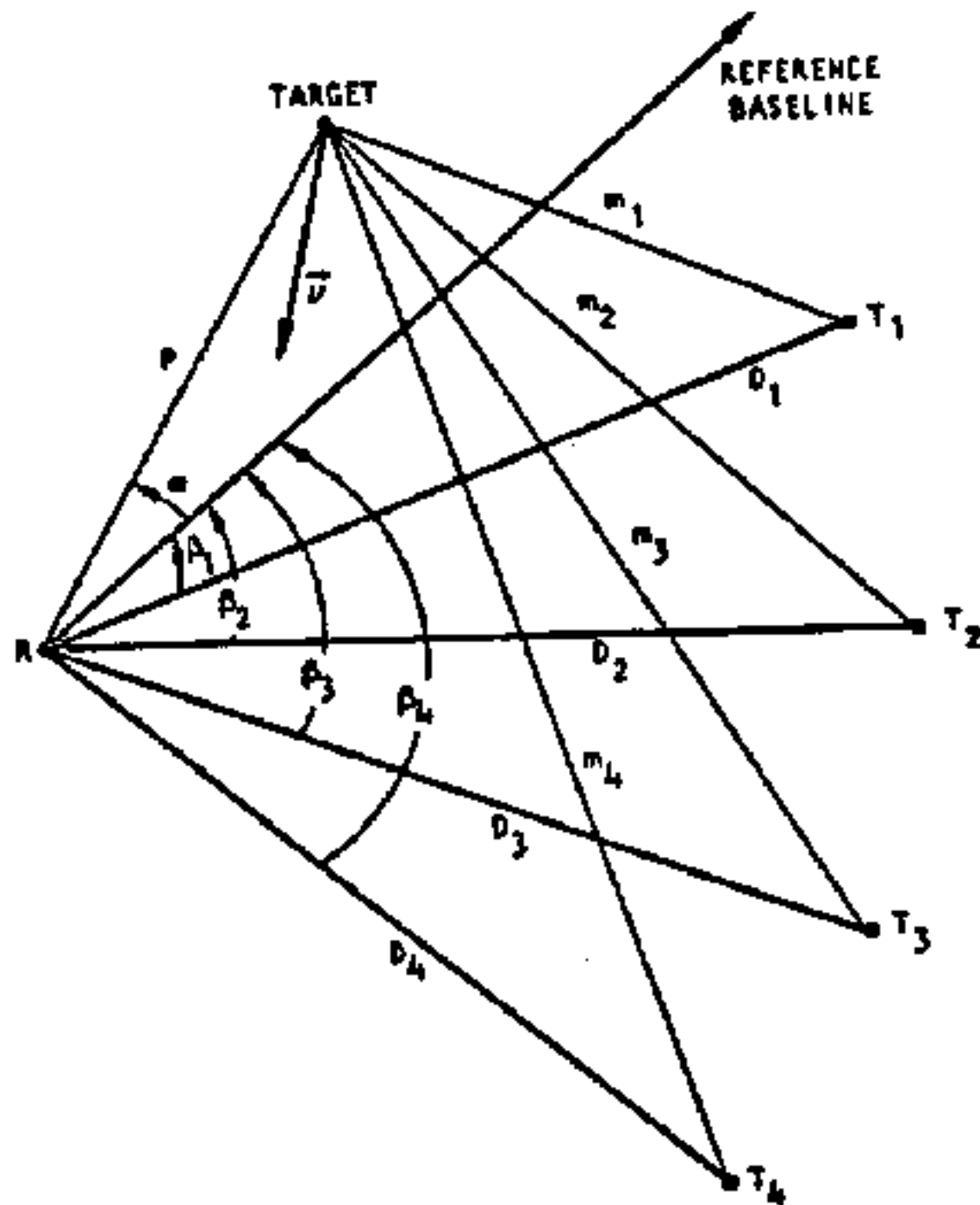


Figure 3-15. (U) Variables for Doppler Location Finder. (U)

UNCLASSIFIED

UNCLASSIFIED

3.2.4 (U) -- Continued.

The desired parameters (p , α , \dot{p} , and $\dot{\alpha}$) can therefore be estimated by the solution of the following system of equations.

$$\begin{aligned}\Delta f_1 &= h(p, \alpha, \dot{p}, \dot{\alpha}; D_1, \theta_1, \lambda_1) \\ \Delta f_2 &= h(p, \alpha, \dot{p}, \dot{\alpha}; D_2, \theta_2, \lambda_2) \\ \Delta f_3 &= h(p, \alpha, \dot{p}, \dot{\alpha}; D_3, \theta_3, \lambda_3) \\ \Delta f_4 &= h(p, \alpha, \dot{p}, \dot{\alpha}; D_4, \theta_4, \lambda_4) .\end{aligned}\tag{3-17}$$

This system of equations can be solved using standard iterative methods. Unlike the other techniques discussed, this method is truly instantaneous; the estimate at one point in time requires no previous measurements. Also, the equations are exact; they require no assumptions as to the constancy of p or $\dot{\alpha}$.

The Doppler Location Finder can thus estimate target range and bearing using only Doppler frequency measurements.

3.3 (U) ERROR ANALYSIS. (U)

The target location estimation techniques discussed in Section 3.2 result in two kinds of errors. One is a bias in the estimate that arises because of one or more approximations that are employed in the technique. This is a systematic error that can, in some cases, be minimized by processing. The second kind of error arises because the inputs needed for the estimate involve measurements that contain random errors. These two kinds of errors generally limit the accuracy of an estimation technique.

In Sections 3.3.1 through 3.3.3 the error expressions for both kinds of errors are derived for:

- a. the double baseline, single measurement range estimator,
- b. the single baseline, double measurement range estimator, and
- c. the Doppler location finder.

Some assumptions on independence of error sources have been made. In Section 3.4 the several other possible sources of error that do not significantly alter the estimate are described.

UNCLASSIFIED

3.3.1 (U) Error Analysis of Double-Baseline, Single-Measurement Range Estimator. (U)

The range estimate given by the Double-Baseline, Single-Measurement technique (Section 3.2.2) is dependent on the measured values of target bearing and Doppler frequency. An expression is derived below relating RMS measurement errors of azimuth and Doppler shift to RMS estimation errors of target range. This error expression is valid at specific target locations and has been evaluated for several configurations of target, ship-board receiver, and transmitters using reasonable values for RMS measurement errors. The bias of the range estimate is also computed. The results indicate that for certain system geometries and parameters, total ranging errors of less than 15% can be achieved.

3.3.1.1 (U) Derivation of Error Expressions. (U)

As shown in Section 3.2.2, the true range p is the solution of the nonlinear system of equations:

$$p = \frac{-(q_1 h_1 + \hat{p}(h_2 - r_2))}{S_1 + \hat{p}}$$

$$\hat{p} = \frac{-(q_2 h_2 + p S_2)}{(h_2 + p - r_2)}$$

where $h_1, h_2, q_1, q_2, r_1, r_2, S_1, S_2$ are functions of $\alpha_1, \alpha_2, \dot{\alpha}, \Delta f_1, \Delta f_2$. The expression for \hat{p} can be substituted into the equation for p and it is seen that p is the solution of

$$G = (p; \alpha_1, \alpha_2, \dot{\alpha}, \Delta f_1, \Delta f_2) = 0 \quad (3-18)$$

where G is a nonlinear function of p and the coefficients involve $\alpha_1, \alpha_2, \dot{\alpha}, \Delta f_1, \Delta f_2$. The parameter $\dot{\alpha}$, however, is estimated by

$$\dot{\alpha} = \frac{1}{2 \Delta t} (\alpha_2 + \alpha_3 - \alpha_1 - \alpha_4)$$

where

$$\alpha_2 = \alpha_1(t - \Delta t)^*$$

*Although the technique is described as a single measurement technique, it does require α_1 and α_2 values at time $t - \Delta t$.

UNCLASSIFIED

3.3.1.1 (U) -- Continued.

and

$$\alpha_4 = \alpha_2(t - \Delta t) .$$

Thus, instead of (3-18) an equation of the following form is solved:

$$H(\hat{p}; \alpha_1, \alpha_2, \alpha_3, \alpha_4, \Delta f_1, \Delta f_2) = 0 \quad (3-19)$$

where \hat{p} is the estimated range. Since the estimated value of \hat{p} may be in error, the solution \hat{p} of (3-19) may be slightly biased away from the true p . Let p_{bias} be this bias in the range estimate. Thus,

$$p_{\text{bias}} = \hat{p} - p .$$

As mentioned previously, this bias from the use of an estimated value of \hat{p} is one of the two important types of errors in this range estimation technique. The other (random) error arises from using measured values of bearing and Doppler. The true α_i and Δf_i are not available; the measured values $\hat{\alpha}_i$ and $\Delta \hat{f}_i$ must be used instead. Thus, the estimate of range is taken to be the solution of

$$H(\hat{p}; \hat{\alpha}_1, \hat{\alpha}_2, \hat{\alpha}_3, \hat{\alpha}_4, \Delta \hat{f}_1, \Delta \hat{f}_2) = 0 .$$

The measurements $\hat{\alpha}_i$ and $\Delta \hat{f}_i$ will generally have mean values of α_i and Δf_i , and standard deviations $\Delta(\alpha)_{\text{RMS}}$ and $\Delta(\Delta f)_{\text{RMS}}$, respectively.

Note that \hat{p} is implicitly a function of the $\hat{\alpha}_i$ and $\Delta \hat{f}_i$; as these measured values change so does \hat{p} in order to keep $H = 0$. Thus,

$$\hat{p} = \hat{p}(\hat{\alpha}_1, \hat{\alpha}_2, \hat{\alpha}_3, \hat{\alpha}_4, \Delta \hat{f}_1, \Delta \hat{f}_2) .$$

The change in \hat{p} due to changes in the $\hat{\alpha}_i$ and $\Delta \hat{f}_i$ is given by

$$\begin{aligned} \Delta(\hat{p}) = & \frac{\partial \hat{p}}{\partial \hat{\alpha}_1} \Delta(\hat{\alpha}_1) + \frac{\partial \hat{p}}{\partial \hat{\alpha}_2} \Delta(\hat{\alpha}_2) + \frac{\partial \hat{p}}{\partial \hat{\alpha}_3} \Delta(\hat{\alpha}_3) + \frac{\partial \hat{p}}{\partial \hat{\alpha}_4} \Delta(\hat{\alpha}_4) \\ & + \frac{\partial \hat{p}}{\partial \Delta \hat{f}_1} \Delta(\Delta \hat{f}_1) + \frac{\partial \hat{p}}{\partial \Delta \hat{f}_2} \Delta(\Delta \hat{f}_2) . \end{aligned} \quad (3-20)$$

UNCLASSIFIED

3.3.1.1 (U) -- Continued.

The preceding equation is the deterministic form of the error equation. Because the measurement errors are random, we must employ a modified version. At each target location the partial derivatives $\partial \hat{p} / \partial \hat{\alpha}_i$ and $\partial \hat{p} / \partial \Delta f_i$ are constant. Using two relations from probability theory*,

a. The RMS value of a zero-mean random variable is the standard deviation (σ).

b. If $x = \sum_i A_i Y_i$, then

$$\sigma = \left(\sum_i A_i^2 \sigma_{Y_i}^2 \right)^{1/2}$$

we can derive from (3-20)

$$\begin{aligned} \Delta(\hat{p})_{\text{RMS}} = & \left[\left(\frac{\partial \hat{p}}{\partial \hat{\alpha}_1} \Delta(\hat{\alpha}_1)_{\text{RMS}} \right)^2 + \left(\frac{\partial \hat{p}}{\partial \hat{\alpha}_2} \Delta(\hat{\alpha}_2)_{\text{RMS}} \right)^2 \right. \\ & + \left(\frac{\partial \hat{p}}{\partial \hat{\alpha}_3} \Delta(\hat{\alpha}_3)_{\text{RMS}} \right)^2 + \left(\frac{\partial \hat{p}}{\partial \hat{\alpha}_4} \Delta(\hat{\alpha}_4)_{\text{RMS}} \right)^2 \\ & \left. + \left(\frac{\partial \hat{p}}{\partial \Delta f_1} \Delta(\Delta f_1)_{\text{RMS}} \right)^2 + \left(\frac{\partial \hat{p}}{\partial \Delta f_2} \Delta(\Delta f_2)_{\text{RMS}} \right)^2 \right]^{1/2} \quad (3-21) \end{aligned}$$

Equation (3-21) simplifies when $\Delta(\hat{\alpha}_i)_{\text{RMS}} = \Delta(\hat{\alpha})_{\text{RMS}}$ and $\Delta(\Delta f_i)_{\text{RMS}} = \Delta(\Delta f)_{\text{RMS}}$ for all i :

$$\begin{aligned} \Delta(\hat{p})_{\text{RMS}} = & \left[\left[\left(\frac{\partial \hat{p}}{\partial \hat{\alpha}_1} \right)^2 + \left(\frac{\partial \hat{p}}{\partial \hat{\alpha}_2} \right)^2 + \left(\frac{\partial \hat{p}}{\partial \hat{\alpha}_3} \right)^2 + \left(\frac{\partial \hat{p}}{\partial \hat{\alpha}_4} \right)^2 \right] \left[\Delta(\hat{\alpha})_{\text{RMS}} \right]^2 \right. \\ & \left. + \left[\left(\frac{\partial \hat{p}}{\partial \Delta f_1} \right)^2 + \left(\frac{\partial \hat{p}}{\partial \Delta f_2} \right)^2 \right] \left[\Delta(\Delta f)_{\text{RMS}} \right]^2 \right]^{1/2} \end{aligned}$$

*Pfeiffer, P. E., Concepts of Probability Theory. McGraw-Hill, N.Y., 1965, pp. 230-2.

UNCLASSIFIED

3.3.1.1 (U) -- Continued.

The only remaining step is the evaluation of $\frac{\partial \hat{p}}{\partial \hat{\alpha}_i}$ and $\frac{\partial \hat{p}}{\partial \Delta \hat{f}_i}$.

If the function $\hat{p}(\hat{\alpha}_1, \hat{\alpha}_2, \hat{\alpha}_3, \hat{\alpha}_4, \Delta \hat{f}_1, \Delta \hat{f}_2)$ were known explicitly, this calculation would be direct. However, the \hat{p} -function is only known implicitly and therefore the Implicit Function Theorem² must be invoked. By this theorem from calculus:

$$\frac{\partial \hat{p}}{\partial \hat{\alpha}_i} = - \frac{\frac{\partial H}{\partial \hat{\alpha}_i}}{\frac{\partial H}{\partial \hat{p}}}$$

and

$$\frac{\partial \hat{p}}{\partial \Delta \hat{f}_i} = - \frac{\frac{\partial H}{\partial \Delta \hat{f}_i}}{\frac{\partial H}{\partial \hat{p}}}$$

where the function $H(\hat{p}; \hat{\alpha}_1, \hat{\alpha}_2, \hat{\alpha}_3, \hat{\alpha}_4, \Delta \hat{f}_1, \Delta \hat{f}_2)$ is known explicitly:

$$H(\hat{p}; \hat{\alpha}_1, \hat{\alpha}_2, \hat{\alpha}_3, \hat{\alpha}_4, \Delta \hat{f}_1, \Delta \hat{f}_2)$$

$$= \hat{p} + \left[q_1 h_1 + \frac{(r_1 - h_1)(q_2 h_2 + (p)(D_2)(\sin \alpha_2) \left(\frac{1}{2\Delta t}\right) (\alpha_1 + \alpha_2 - \alpha_3 - \alpha_4))}{h_2 - p - r_2} \right] /$$

$$\left[(D_1) (\sin \alpha_1) \left(\frac{1}{2\Delta t}\right) (\alpha_1 + \alpha_2 - \alpha_3 - \alpha_4) \right]$$

$$- \left(\frac{q_2 h_2 + (p)(D_2)(\sin \alpha_2) \left(\frac{1}{2\Delta t}\right) (\alpha_1 + \alpha_2 - \alpha_3 - \alpha_4)}{h_2 - p - r_2} \right) \right]$$

where r_1, h_1, q_1 are functions of $\alpha_1, \alpha_2, \Delta f_1, \Delta f_2$ and Δt is the time between measurements. Finally, the above equations can be evaluated for $\Delta(\hat{p})_{RMS}$:

² Protter, M. H. and Morrey, E. B., Modern Mathematical Analysis, Addison-Wesley, Reading, Mass., 1964, p. 492.

UNCLASSIFIED

3.3.1.1 (U) -- Continued.

$$\Delta(\hat{p})_{\text{RMS}} = \left\{ \frac{1}{\left| \frac{\partial H}{\partial p} \right|} \left[\left(\frac{\partial H}{\partial \alpha_1} \right)^2 + \left(\frac{\partial H}{\partial \alpha_2} \right)^2 + \left(\frac{\partial H}{\partial \alpha_3} \right)^2 + \left(\frac{\partial H}{\partial \alpha_4} \right)^2 \right] \right\}^{1/2}$$

$$\left[\Delta(\hat{\alpha})_{\text{RMS}} \right]^2 + \left[\left(\frac{\partial H}{\partial \Delta f_1} \right)^2 + \left(\frac{\partial H}{\partial \Delta f_2} \right)^2 \right] \left[\Delta(\Delta f)_{\text{RMS}} \right]^2 \quad (3-22)$$

In the next section, both the bias (P_{bias}) and the RMS error of range estimate for the double-baseline, single-measurement technique are evaluated for typical cases.

3.3.1.2 (U) Results of Error Analysis. (U)

In this section the bias and RMS error of the range estimate of the double-baseline, single-measurement technique are presented for several different system geometries (locations of radar transmitters and receiver and trajectory of target) and system parameters (operating frequency and time between measurements). It is shown that although the technique is not completely satisfactory under all circumstances, it is fairly successful for certain geometries and parameters.

All numerical calculations for the error analyses were performed on an IBM 360 general purpose digital computer. For any given case, P_{bias} (the range bias caused by using an approximation for \hat{p}) was found by solving for \hat{p} and subtracting the actual range p . $\Delta(\hat{p})_{\text{RMS}}$, the RMS error of the range estimate, was calculated using equation (3-22); the partial derivatives of

$$H \left(\frac{\partial H}{\partial p}, \frac{\partial H}{\partial \alpha_1}, \frac{\partial H}{\partial \Delta f_1} \right)$$

were determined by use of standard numerical differentiation algorithms*.

*Southworth, R. W. and Deleeuw, S. L., Digital Computation and Numerical Methods, McGraw-Hill, N.Y., 1965, pp. 352-363.

UNCLASSIFIED

3.3.1.2 (U) -- Continued.

The computed range estimation errors for the double baseline, single measurement technique are displayed in Figures 3-16. The labeled dots indicate the location of the transmitters (T_1 and T_2) and the shipboard receiver (S). The various trajectories of the target are represented by dashed lines. The errors are represented by solid-line segments at various points along the trajectory. The lengths of these segments are scaled to twice the RMS error, while the offset of the center of the segment from the trajectory represents P_{bias} .

The various system parameters, such as operating frequency of the radar (f), time between measurements (Δt), and standard deviations or RMS errors of the measurements (σ_{α} , $\sigma_{\Delta f}$) are listed on the figures, along with the scale of the drawing and the velocity of the target. Δt is not necessarily equal to the spacing of the displayed error segments.

For all the figures of displayed errors, the measurement uncertainties, $\Delta(\alpha)_{RMS}$ and $\Delta(\Delta f)_{RMS}$ were assumed to be 1 degree and .1 Hz, respectively. If these measurements errors in a particular case are larger, then the RMS error in the range estimate would be proportionately greater.

Several conclusions can be drawn from the figures. First, a particular configuration of transmitters and shipboard receiver may be fairly effective against certain target trajectories while much less successful against other trajectories. Also, performance may be acceptable at certain points in a given trajectory but not at others.

An interesting observation can be made from Figures 3-16. The geometries and parameters for the two configurations in Figures 3-16e and f are the same as for those in Figures 3-16g and h, respectively, except that Δt , the time between measurements, is 20 seconds for the former and 120 seconds for the latter. The interval Δt enters into the estimation of range in only one place: the estimation of \hat{r} from the formula

$$\hat{r} = \frac{1}{2\Delta t} (\alpha_1 + \alpha_2 - \alpha_3 - \alpha_4).$$

As Δt is increased, the RMS errors of the α_i are divided by a larger constant and thus the RMS range error should be less. On the other hand, for larger Δt , the first order approximation becomes weaker for those trajectories where \hat{r} is not constant, implying an increased P_{bias} for those cases.

UNCLASSIFIED

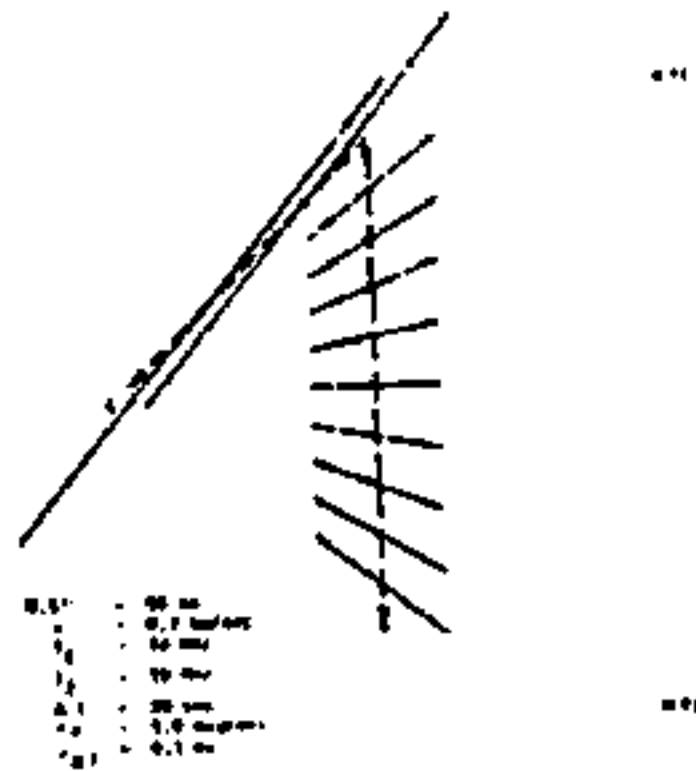


Figure 3-16a (U). Range Estimation Errors for Double Baseline, Single Measurement Technique--Geometry No. 1 (U)

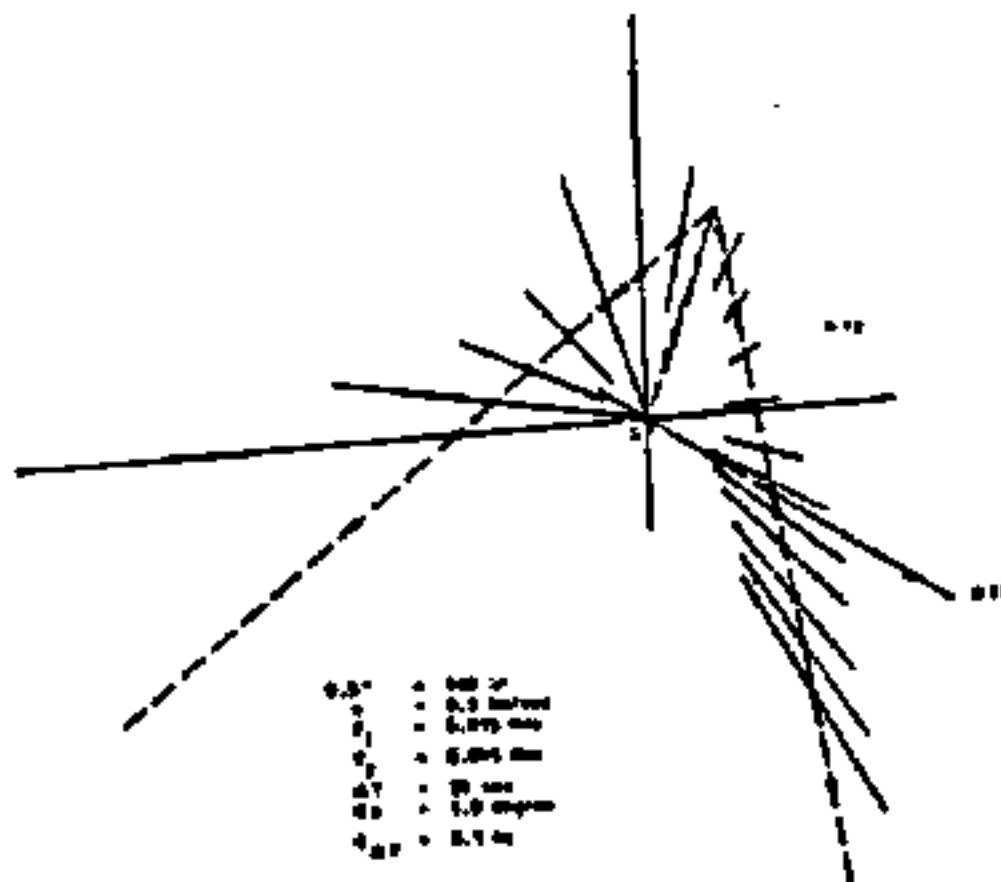


Figure 3-16b (U). Range Estimation Errors for Double Baseline, Single Measurement Technique--Geometry No. 2 (U)

3-40

UNCLASSIFIED

UNCLASSIFIED

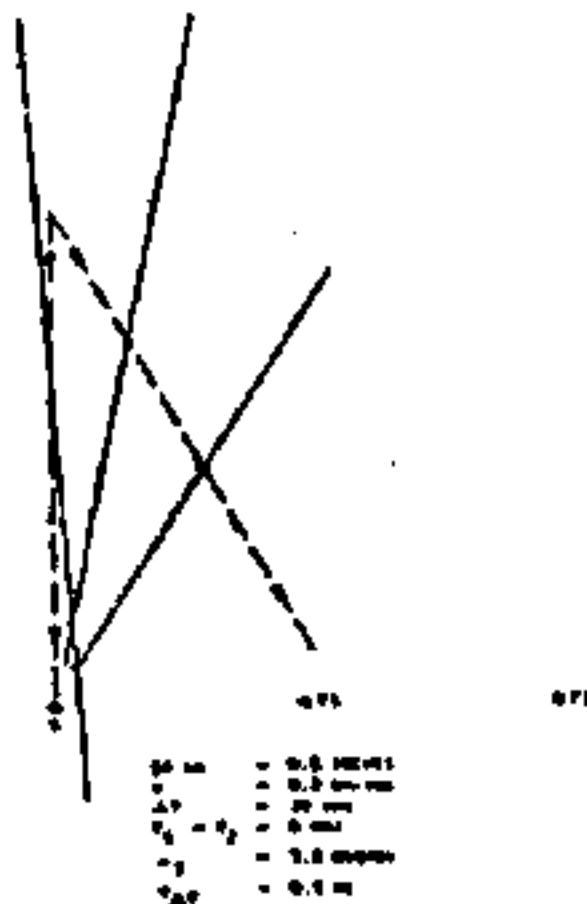


Figure 3-16c (U). Range Estimation Errors for Double Baseline, Single Measurement Technique--Geometry No. 3 (U)

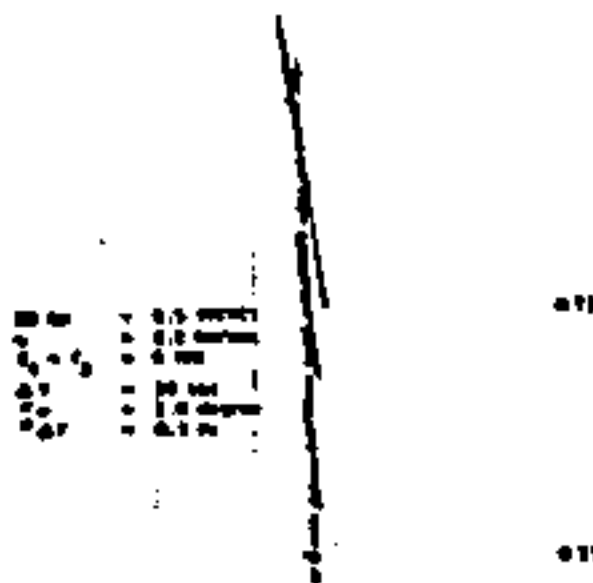


Figure 3-16d (U). Range Estimation Errors for Double Baseline, Single Measurement Technique--Geometry No. 4 (U)

UNCLASSIFIED

UNCLASSIFIED

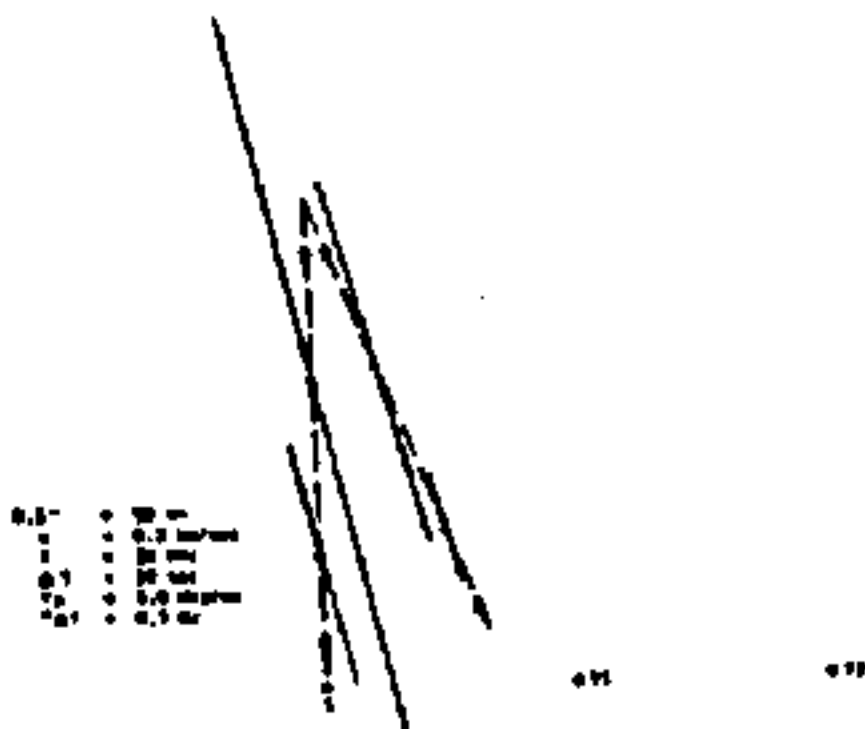


Figure 3-16e (U). Range Estimation Errors for Double Baseline, Single Measurement Technique--Geometry No. 5 (U)

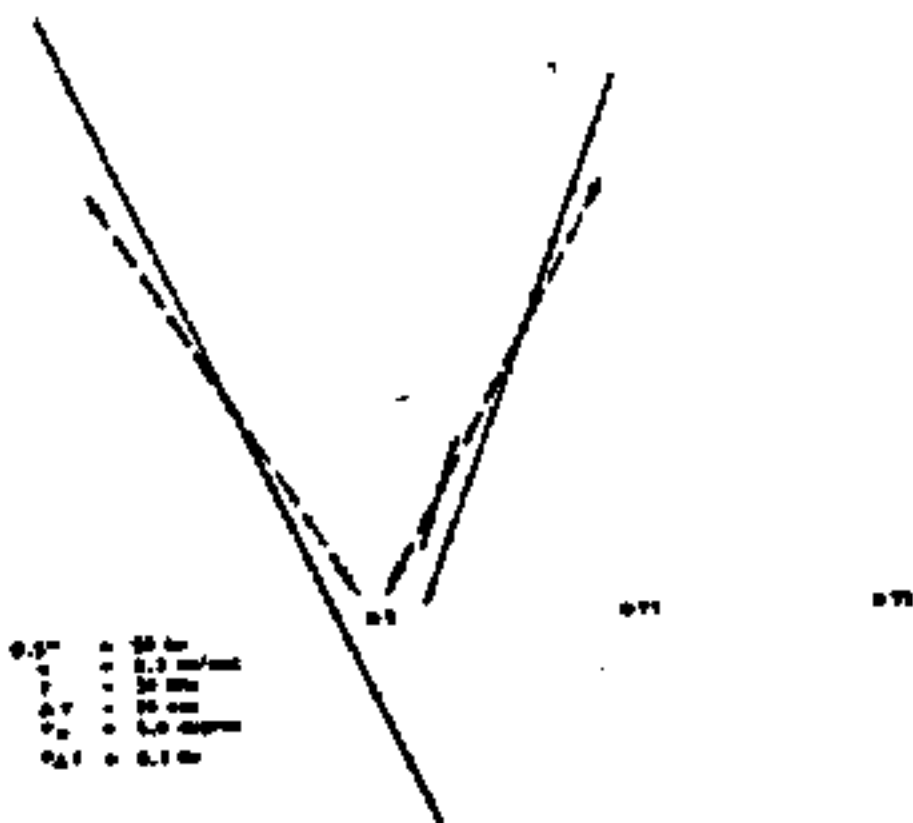


Figure 3-16f (U). Range Estimation Errors for Double Baseline, Single Measurement Technique--Geometry No. 6 (U)

UNCLASSIFIED

UNCLASSIFIED



Figure 3-16g (U). Range Estimation Errors for Double Baseline, Single Measurement Technique--Geometry No. 7 (U)



Figure 3-16h (U). Range Estimation Errors for Double Baseline, Single Measurement Technique--Geometry No. 8 (U)

UNCLASSIFIED

UNCLASSIFIED

3.3.1.2 (U) -- Continued.

Both these effects are observed in Figures 3-16. The RMS errors in Figures 3-16g and h ($\Delta t = 120$ sec.) are generally much less than in Figures 3-16e and f ($\Delta t = 20$ sec.). Yet, also as predicted, in the one trajectory in each pair of figures where the target is not heading at the ship and hence $\dot{\alpha}$ is not constant, there is a significant range bias for $\Delta t = 120$ sec., but not for $\Delta t = 20$ sec. However, the total range estimate error is still much smaller for $\Delta t = 120$ sec.; for several target trajectories, range estimate errors of less than 15 percent are achieved.

3.3.2 (U) Error Analysis of Single-Baseline, Double-Measurement Range Estimator. (U)

The accuracy of the Single-Baseline, Double-Measurement range estimating technique (Section 3.2.3) is also a function of the accuracies of the measurements of target bearing and Doppler frequency. Expressions relating RMS measurement errors to RMS ranging errors are derived and evaluated for several target trajectories. The biases in the estimate are also computed, and it is shown that for several trajectories, the total range estimate errors are less than 15 percent.

3.3.2.1 (U) Derivation of Error Expressions. (U)

As shown in Section 3.2.3, the true range can be estimated by the solution of the set of equations (3-12 and 3-13).

The following approximations are also used to evaluate the RMS range error for this range estimation technique:

$$\hat{\alpha}' = \alpha + \dot{\alpha} \Delta t \quad (3-23)$$

and

$$\hat{\beta}' = \beta + \dot{\beta} \Delta t \quad (3-24)$$

Equation (3-12) is used to find an expression for $\dot{\beta}$ which is then inserted into (3-13) to yield:

$$F(\hat{\beta}'; \alpha', \alpha, \Delta f', \Delta f) = 0 \quad (3-25)$$

a single equation for $\hat{\beta}'$ which depends on the present and past measured values of target bearing and Doppler frequency.

UNCLASSIFIED

3.3.2.1 (U) -- Continued.

The estimate \hat{p}' has, in general, both a bias error and RMS error. The bias arises from the fact that for linear trajectories, $\hat{\alpha}'$ and \hat{p}' are exactly true only when that trajectory is radial with respect to the shipboard receiver. Thus, in most cases, even if the exact values α' , $\Delta f'$, Δf are known, the solution \hat{p}' will be in error by a P'_{bias} . Thus:

$$P'_{\text{bias}} = \hat{p}' - p'$$

An expression for RMS range estimation error in terms of the RMS errors in target bearing and Doppler shift measurements can be obtained by noting the similarity of equations for the double-baseline, single measurement technique and (3-25). Thus, analogous to (3-22), it follows directly that

$$\Delta(\hat{p}')_{\text{RMS}} = \left\{ \left(\frac{1}{\left| \frac{\partial F}{\partial p'} \right|} \right) \left[\left(\frac{\partial F}{\partial \hat{\alpha}'} \right)^2 + \left(\frac{\partial F}{\partial \hat{\Delta} f'} \right)^2 \right] \left[(\Delta(\hat{\alpha}')_{\text{RMS}})^2 \right] + \left[\left(\frac{\partial F}{\partial \hat{\Delta} f'} \right)^2 + \left(\frac{\partial F}{\partial \hat{\Delta} f} \right)^2 \right] \left[(\Delta(\hat{\Delta} f)_{\text{RMS}})^2 \right] \right\}^{1/2}$$

The next section presents the results of evaluating the bias and RMS errors of range estimate for the single-baseline, double-measurement technique.

3.3.2.2 (U) Results of Error Analysis. (U)

The expected errors are presented for two typical cases using the single-baseline, double-measurement range estimator. From Figures 3-17 and 3-18 it can be seen that for two target trajectories (one for each case), the range estimation errors are less than 15 percent. The detection system parameters are the same in all cases. As in the previous section the trajectories are shown by dashed lines and the errors by solid line segments; the length of a segment equals twice the RMS range error, while the displacement of the segment center from the trajectory represents the range estimation bias.

Several observations can be made from the figures. First, of all the trajectories shown, only one shows any bias; this is the trajectory on Figure 3-17 that is not aimed at the ship. This result was predicted in

UNCLASSIFIED

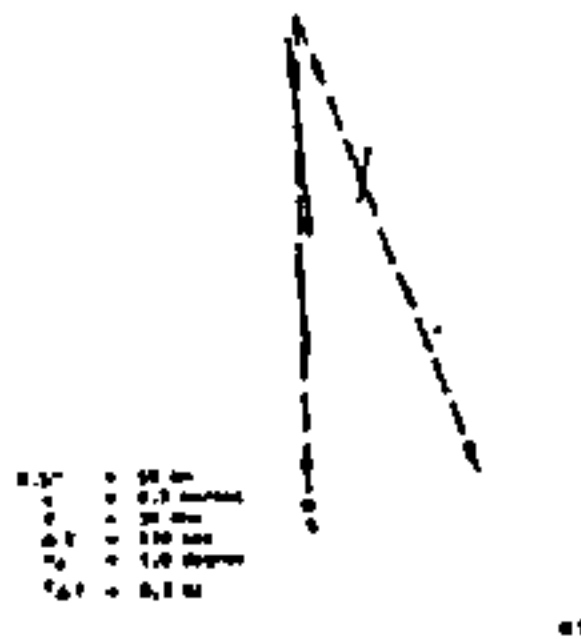


Figure 3-17 (U). Range Estimation Errors for Single Baseline, Double Measurement Technique. (U)

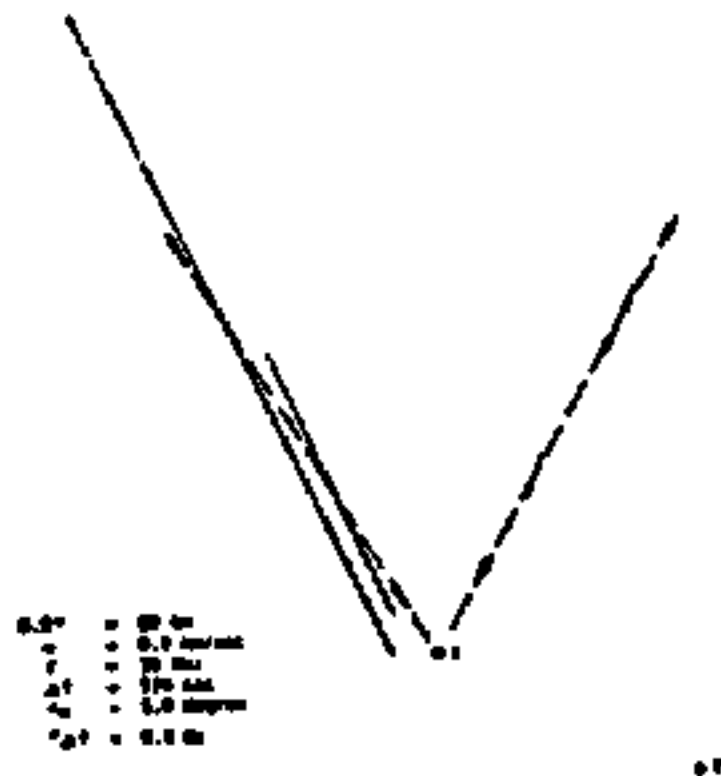


Figure 3-18 (U). Range Estimation Errors for Single Baseline, Double Measurement Technique. (U)

UNCLASSIFIED

UNCLASSIFIED

3.3.2.2 (U) -- Continued.

the last section, because bias errors are caused by the variation of \dot{h} and \dot{p} between measurements. These variations occur only for off-ship trajectories. As shown in Figure 3-17, the bias is about the same magnitude as the RMS error. The bias could be reduced by decreasing the time interval between observations, but at the expense of greater RMS errors. Another observation from the figures is that the estimator's performance depends on the location of the target with respect to the transmitter and shipboard receiver. For example, Figure 3-18 shows a trajectory in which the ship is between the target and transmitter and the target is headed directly at the ship. For this trajectory the range errors are greater than 80 percent. In contrast the two trajectories of Figures 3-17 and 3-18, in which the target is on a fly by trajectory or headed toward the ship in a different geometry resulted in errors of less than 15 percent.

3.3.3 (U) Error Analysis of the Doppler Location Finder. (U)

The range and location estimates given by the Doppler Location Finder (DLF) depend on the measured values of Doppler frequency. An expression is derived below relating measurement uncertainties to estimation errors. Results are presented that demonstrate for a wide class of system geometries range errors of less than 15 percent and bearing errors of less than 6° can be achieved. In addition, for one particular system geometry the range errors are shown to be less than 5 percent.

3.3.3.1 (U) Derivation of Error Expressions. (U)

As described in Section 3.2.4 target location and time derivative variables, p , α , \dot{p} , and $\dot{\alpha}$, are the solution of:

$$\Delta f_i = h(p, \alpha, \dot{p}, \dot{\alpha}; D_i, \theta_i, \lambda_i) \quad i = 1, 2, 3, 4.$$

Because Δf_i will always be measured with some error, it is denoted as $\Delta \hat{f}_i$; the estimates of p , α , \dot{p} , and $\dot{\alpha}$ are similarly denoted by \hat{p} , $\hat{\alpha}$, $\hat{\dot{p}}$, and $\hat{\dot{\alpha}}$ so that

$$\Delta \hat{f}_i = h(\hat{p}, \hat{\alpha}, \hat{\dot{p}}, \hat{\dot{\alpha}}; D_i, \theta_i, \lambda_i) \quad i = 1, 2, 3, 4.$$

As done in the previous sections define

UNCLASSIFIED

3.3.3.1 (U) -- Continued.

$$\Delta(\Delta f_i) = \left(\frac{\partial h}{\partial \hat{p}}\right)_i \Delta \hat{p} + \left(\frac{\partial h}{\partial \hat{c}}\right)_i \Delta \hat{c} + \left(\frac{\partial h}{\partial \hat{p}}\right)_i \Delta \hat{p} + \left(\frac{\partial h}{\partial \hat{c}}\right)_i \Delta \hat{c}$$

Letting the vectors \underline{m} and \underline{v} be defined as

$$\underline{m} = \begin{pmatrix} \Delta f_1 \\ \Delta f_2 \\ \Delta f_3 \\ \Delta f_4 \end{pmatrix} \quad \underline{v} = \begin{pmatrix} \Delta \hat{p} \\ \Delta \hat{c} \\ \Delta \hat{p} \\ \Delta \hat{c} \end{pmatrix}$$

and the matrix A defined as

$$A = \begin{pmatrix} \left(\frac{\partial h}{\partial \hat{p}}\right)_1 & \left(\frac{\partial h}{\partial \hat{c}}\right)_1 & \left(\frac{\partial h}{\partial \hat{p}}\right)_2 & \left(\frac{\partial h}{\partial \hat{c}}\right)_2 \\ \left(\frac{\partial h}{\partial \hat{p}}\right)_3 & \left(\frac{\partial h}{\partial \hat{c}}\right)_3 & \left(\frac{\partial h}{\partial \hat{p}}\right)_4 & \left(\frac{\partial h}{\partial \hat{c}}\right)_4 \\ \left(\frac{\partial h}{\partial \hat{p}}\right)_1 & \left(\frac{\partial h}{\partial \hat{c}}\right)_1 & \left(\frac{\partial h}{\partial \hat{p}}\right)_2 & \left(\frac{\partial h}{\partial \hat{c}}\right)_2 \\ \left(\frac{\partial h}{\partial \hat{p}}\right)_3 & \left(\frac{\partial h}{\partial \hat{c}}\right)_3 & \left(\frac{\partial h}{\partial \hat{p}}\right)_4 & \left(\frac{\partial h}{\partial \hat{c}}\right)_4 \end{pmatrix}$$

then $\underline{m} = A \underline{v}$; assuming A is invertible, $\underline{v} = A^{-1} \underline{m}$.

Evaluating just the first two components of \underline{v} and expressing them in RMS form yields

$$(\Delta \hat{p})_{\text{RMS}} = \left(\sum_{i=1}^4 \left((A^{-1})_{1,i} \right)^2 \cdot \left(\Delta(\Delta f_i) \right)_{\text{RMS}}^2 \right)^{1/2}$$

$$(\Delta \hat{c})_{\text{RMS}} = \left(\sum_{i=1}^4 \left((A^{-1})_{2,i} \right)^2 \cdot \left(\Delta(\Delta f_i) \right)_{\text{RMS}}^2 \right)^{1/2}$$

UNCLASSIFIED

3.3.3.1 (U) Continued.

Assuming $(\Delta(\dot{f}_i))_{\text{RMS}}$ is the same for all i ,

$$(\Delta \hat{r})_{\text{RMS}} = (\Delta(\dot{f}_i))_{\text{RMS}} \cdot \left(\sum_{i=1}^4 \left[((A^{-1})_{1,i})^2 \right] \right)^{1/2}$$

$$(\Delta \hat{\theta})_{\text{RMS}} = (\Delta(\dot{f}_i))_{\text{RMS}} \cdot \left(\sum_{i=1}^4 \left[((A^{-1})_{2,i})^2 \right] \right)^{1/2}$$

These last two equations relate the RMS errors in Doppler frequency measurement to the RMS errors in target range and bearing estimation. The other type of estimation error is a possible bias. For the Doppler Location Finder there are no biases since the equations are exact and use measurements from only one time point. Thus, the RMS error describes the total range and estimation errors of the DLF techniques.

3.3.3.2 (U) Results of Error Analysis. (U)

The expressions for range and bearing uncertainties derived in Section 3.3.3.1 for the Doppler Location Finder were evaluated for a number of configurations. It is shown that with reasonable Doppler measurement errors (i.e., 0.1 Hz) the range error is less than 15 percent and the bearing error is less than 6° in many cases. The error results are presented in Figures 3-19 to 3-28. As with the error analyses for the other techniques, the target trajectories are represented by dashed lines, the transmitters and shipboard receivers are represented by labeled dots, and the assumed system parameters for each case are included. The Doppler measurement RMS error for all cases is assumed to be 0.1 Hz; no value is given for time between measurements because the DLF is an "instantaneous" estimator. For this location estimation technique the errors in both range and azimuth are presented. The RMS range errors are represented by line segments scaled to twice the RMS range error along a radial line from the target to the receiver. The RMS bearing errors are similarly scaled with a line segment perpendicular to the radial line. Note that no biases are shown. The one major observation that can be made is the good performance of the DLF for a variety of receiver-transmitter configurations and against a number of target trajectories. In most cases the range errors were less than 15 percent and the bearing errors less than 6°. Of particular interest is the system geometry shown in Figure 3-28 for which the range errors

UNCLASSIFIED

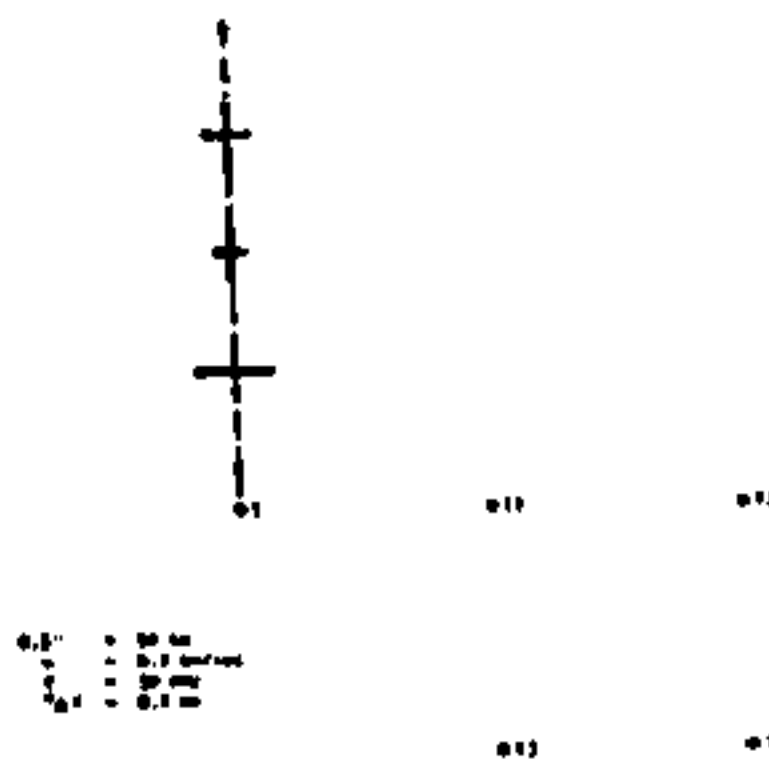


Figure 3-19 (U). Location Error for Doppler Location Finder--Geometry No. 1 (U)

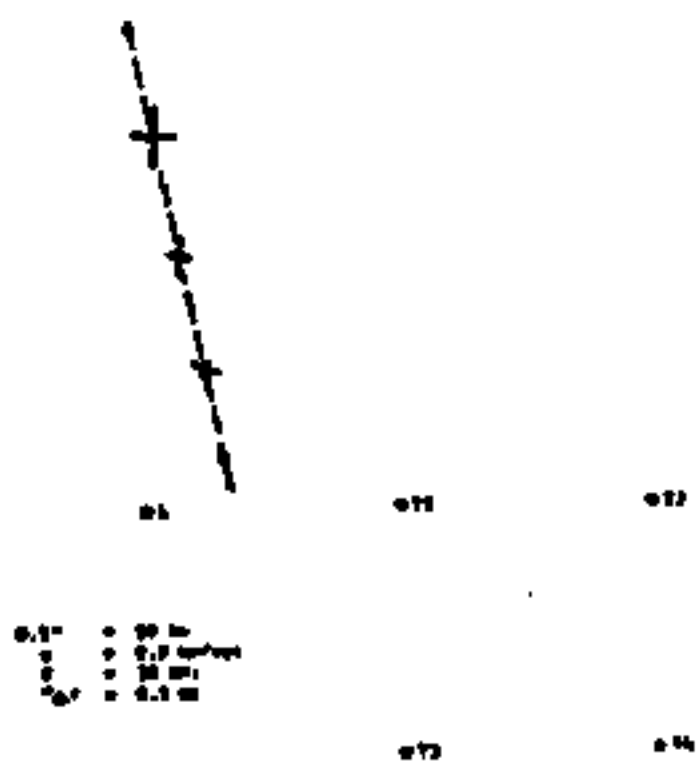


Figure 3-20 (U). Location Error for Doppler Location Finder--Geometry No. 2 (U)

UNCLASSIFIED

UNCLASSIFIED

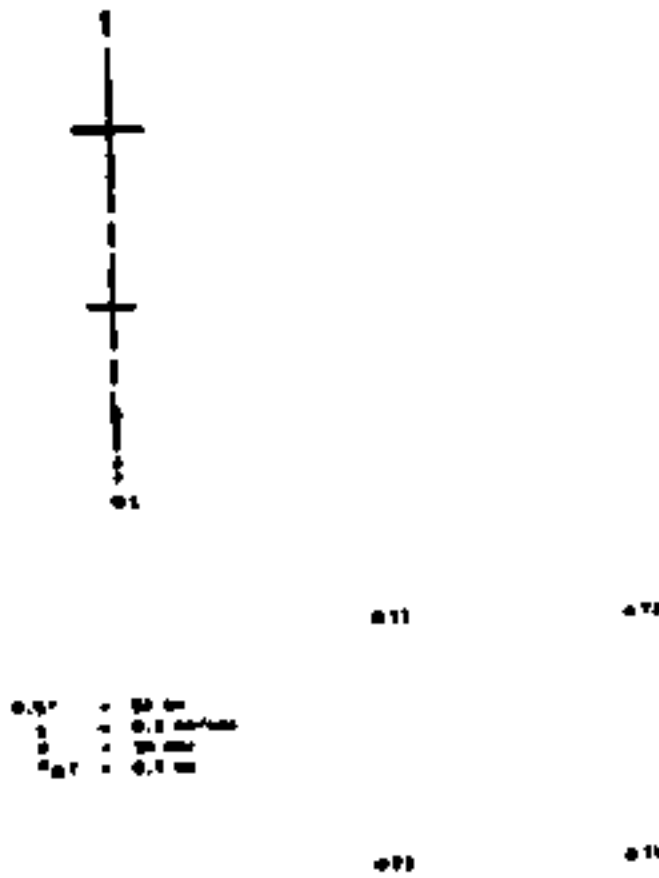


Figure 3-21 (U). Location Error for Doppler Location Finder--Geometry No. 3 (U)

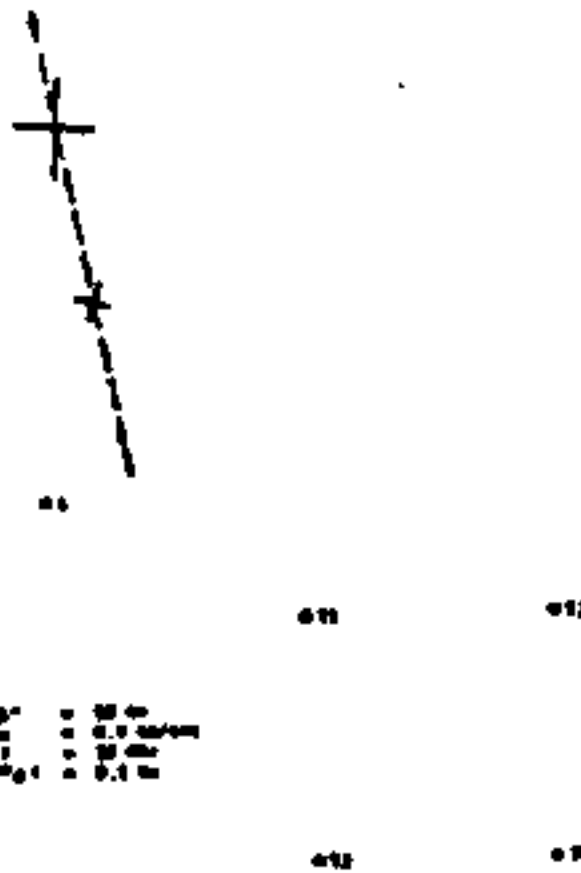


Figure 3-22 (U). Location Error for Doppler Location Finder--Geometry No. 4 (U)

3-51

UNCLASSIFIED

UNCLASSIFIED

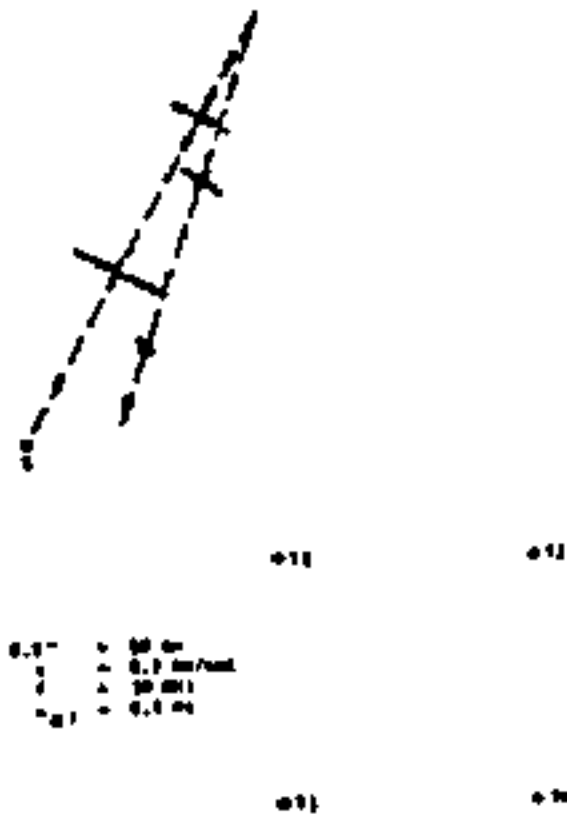


Figure 3-23 (U) Location Error for Doppler Location Finder-- Geometry No. 5 (U)

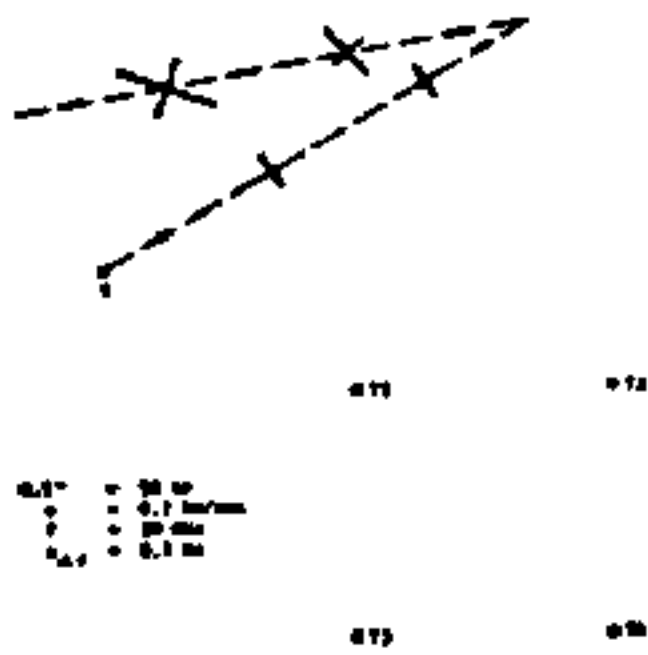


Figure 3-24 (U) Location Error for Doppler Location Finder-- Geometry No. 6 (U)

UNCLASSIFIED

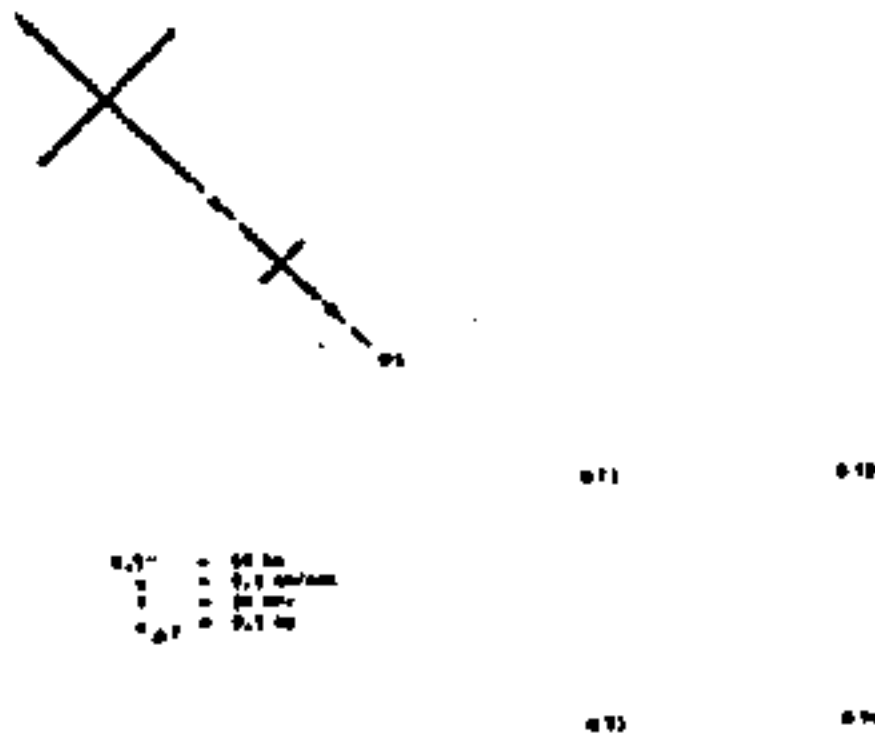


Figure 3-25 (U). Location Error for Doppler Location Finder--Geometry No. 7 (U)

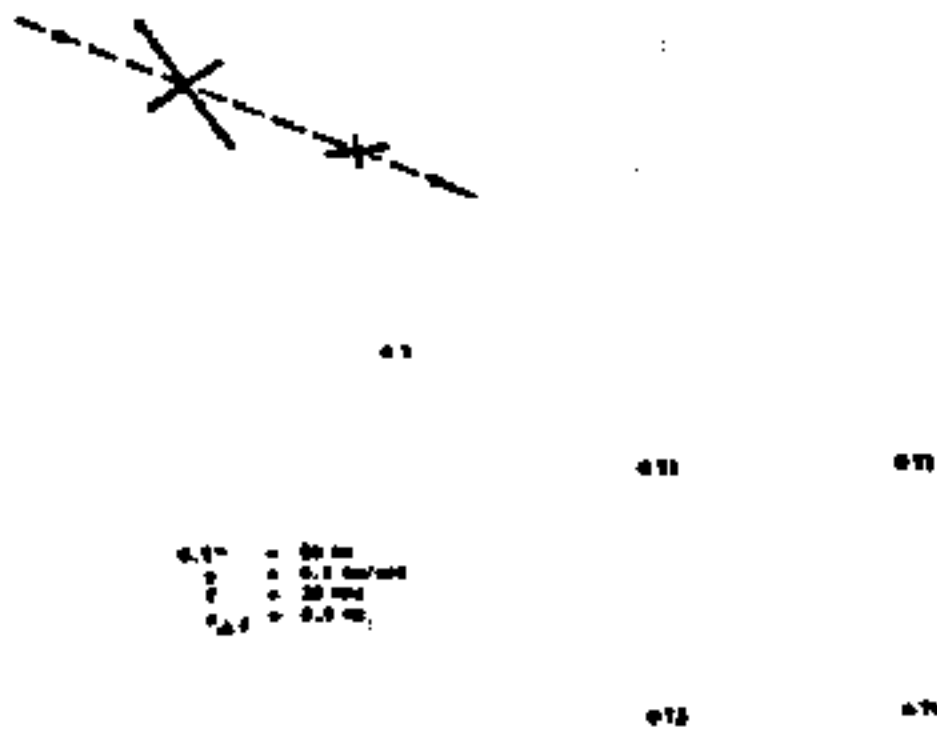


Figure 3-26 (U). Location Error for Doppler Location Finder--Geometry No. 8 (U)

UNCLASSIFIED

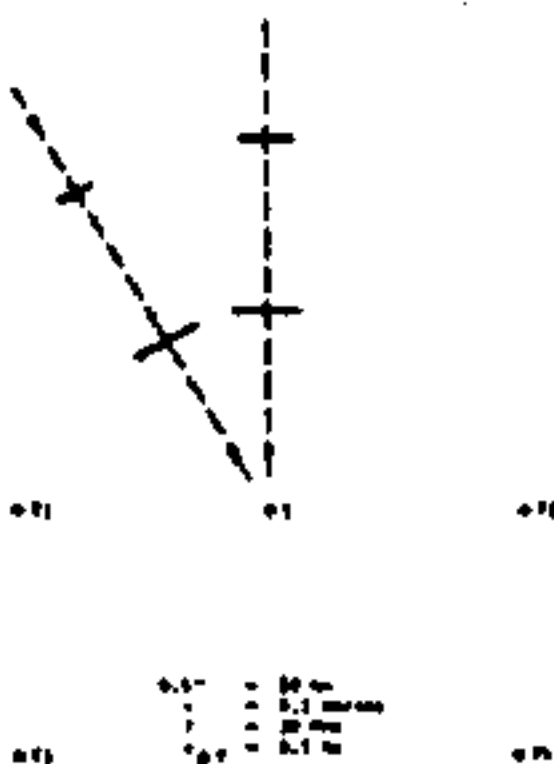


Figure 3-27 (U). Location Error for Doppler Location Finder-- Geometry No. 9 (U)

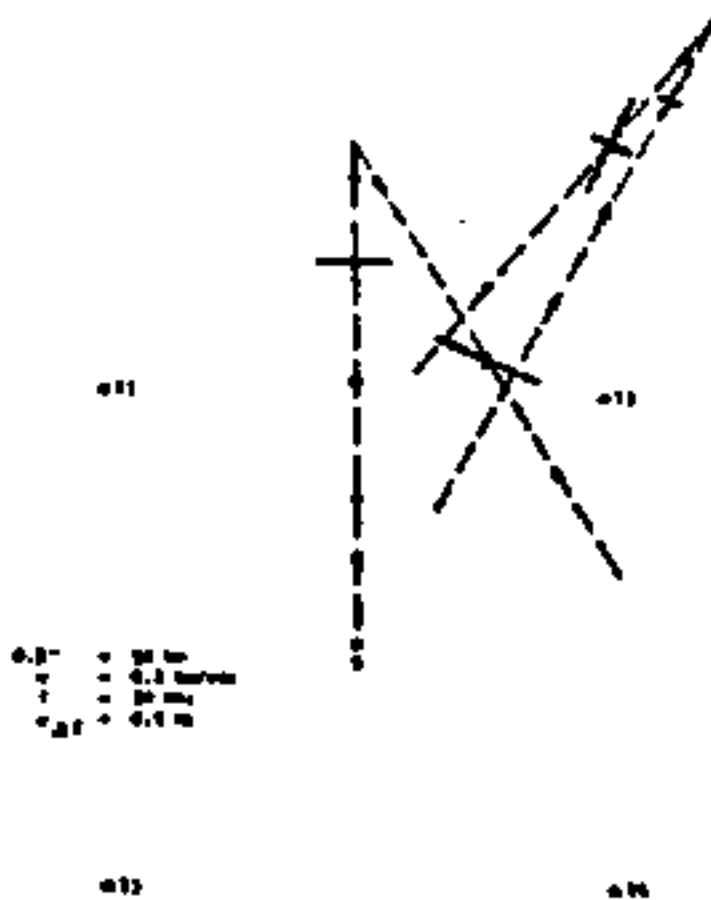


Figure 3-28 (U). Location Error for Doppler Location Finder-- Geometry No. 10 (U)

UNCLASSIFIED

UNCLASSIFIED

3.3.3.2 (U) -- Continued.

are less than 5 percent. This configuration can represent the use of transmitters on picket ships to protect a fleet aircraft carrier.

3.3.4 (U) Other Possible Sources of Error. (U)

The previous sections have discussed the RMS errors caused by measurement uncertainties and the bias errors due to equation approximations for the various estimation techniques. In this section several other possible sources of error are discussed; it is shown that errors from these sources are not significant compared to those described previously.

One of these sources of error is due to the period over which the bearings in the double and single baseline techniques are measured in practice. These are taken over a time duration of about ten seconds. The average value calculated is assigned as the bearing at the middle of the interval; in reality, due to non-linearities, the actual bearing at that middle time-point may be different. Yet, in all cases considered in this study, this bearing error was less than 0.1° , significantly smaller than the one degree uncertainty that was assumed for bearing measurements.

A second source of error comes from the use of a two-dimensional model for system geometries. In practice, targets may fly at higher altitudes above the ocean surface although the principal threats are expected to employ low altitudes to avoid line-of-sight radar detection. For these situations the actual Dopplers and bearing angles will not be the same as those used in a planar model. In most cases, however, the differences are masked by the measurement uncertainty. For example, a target 10 km high and 100 km from the ship is at a 6° elevation angle. According to the Doppler equation, the actual Doppler would be $\cos 6^\circ$ times the Doppler if the target were indeed flying in the plane of the transmitter and receiver. Because $\cos 6^\circ$ is greater than 0.99, the Doppler would be in error by less than 1 percent, which is about the accuracy of Doppler measurement. In a similar manner the slant range would differ from the planar range by less than 1 percent.

Another source of error is the determination of distance between the i^{th} transmitter and the ship (D_i). The accuracy of this measurement depends on the accuracy of the shipborne navigation system. Because the typical accuracies for the LORAN C and D systems are less than 1 km and this represents less than 1 percent at a target range of 100 km (compared to approximately 15 percent range accuracy for the location estimation techniques), the associated errors can be neglected.

UNCLASSIFIED

3.3.4 (U) -- Continued.

The measurement of transmitter frequencies (f_i) can also give rise to errors in the estimation techniques. However, with an RMS measurement accuracy of 0.1 Hz, the errors are less than one part in 10^8 in the HF band and is dominated by the limitations in computational accuracy.

Thus, the errors that arise from these other sources can be neglected compared to those examined in the previous sections.

3.3.5 (U) Conclusions of Error Analysis. (U)

The principal conclusion to be drawn from the error analysis is that all three techniques analyzed, the double-baseline, single-measurement technique, the single-baseline, double-measurement estimator, and the Doppler Location Finder, performs to within 15 percent range error for classes of target trajectories. The DLF, in particular, performs well over a wide range of trajectories and attains 5 percent accuracy for one of the geometries examined. In addition, it estimates bearing to an accuracy of 6° .

For all the estimation methods, however, expected errors strongly depend on both system geometry and system parameters. Because the three techniques perform reasonably well under different specific conditions, it appears that a hybrid location technique that employs the basic methods contained in the three techniques investigated can be developed that will perform satisfactorily (better than 15 percent accuracy) over a wider range of fleet operating geometries. This hybrid technique may rely on the DLF method as a basis, but include measurements of target bearing. Alternately, the hybrid technique may employ all three methods for estimating target range, but incorporate tests to discard estimates having large RMS values. Those estimates within an acceptable accuracy may then be weighted to provide the "hybrid" estimate of target range. Based on the potential of deriving a practical target location estimator for a wide range of transmitter, fleet, and target geometries it is recommended that a hybrid target location technique be investigated.

Section 4

EXPERIMENTAL TESTING OF FAD
POLYSTATIC TECHNIQUES

(U) In the previous sections the investigation of a polystatic radar technique that can be employed for FAD was presented. This investigation included an examination of detection regions, target location methods and a detailed error analysis. Because the results have been derived analytically there is a need to verify them experimentally and to demonstrate that a FAD early warning system using transmitters of opportunity is feasible. Experimental tests are therefore recommended for the FAD polystatic techniques.

(U) This section describes the experimental design considerations and a system designed particularly for these tests. The specific objectives of the experiments are first discussed. Then the factors that impact on the test design and the system design are described. Based on a tradeoff analysis of these factors a specific set of experiments and hardware are recommended.

4.1 (U) OBJECTIVES. (U)

The objectives of the FAD polystatic techniques experiments are to:

- a. demonstrate the detection range of the polystatic technique, and
- b. verify the predicted accuracies of the target location estimation methods.

The first objective is to show that the target detection ranges derived analytically using surface wave attenuation values and nominal radar cross sections agree with experimental values. This objective has been met partially when experiments were conducted for the early warning portion of the Aquarius study. (In these experiments a P3B aircraft was detected with a bistatic radar system using propagation modes comparable to those expected for FAD.) Also, target detection is necessary before the other experimental objectives can be met. Therefore, tests to satisfy this objective can be included with those to meet the other objectives.

The second objective is to verify that the target location accuracies of the estimation techniques agree with the analytic results. The majority of the experiments will be devoted to satisfying this objective because it includes

UNCLASSIFIED

4.1 (U) -- Continued.

the most tenuous area and contains numerous random variables (e.g., transmitter-target-receiver geometry, measurement accuracies, etc.)

4.2 (U) EXPERIMENTAL CONSIDERATIONS. (U)

In the design of experiments care must be taken to include all those system parameters that are crucial to the satisfaction of the test objectives. In addition, the experiments should be structured for performance at a nominal cost utilizing existing equipment and systems where possible. In the experimental design there are a number of factors that need to be considered. A list of the primary ones are included in Table 4-1. The majority of the factors (e.g., transmitters, targets, receivers) deal with the equipment/systems needed for the experiment. The use of existing equipment for the tests reduces the cost of the experiment. For some test elements (e.g., simulated targets, shipborne antenna arrays) it is not economically feasible to build or buy the system solely for the experiment and hence the time and location of the experiment is restricted to the availability of these systems.

4.2.1 (U) Transmitter Sources. (U)

To conduct the tests, sources of opportunity (i.e., broadcast transmitters) or cooperative transmitters (e.g., Carter Cay transmitters) can be employed. A partial list of candidate transmitters for the experiment are included in Table 4-2. A substantial number of HF sources are available with established transmitter powers and operational schedules. Lists of these sources can be found in the World Radio and TV Handbook.

Experimental HF transmitters and other radars may be employed to track the target during the tests and for calibration purposes, and ionospheric soundings and propagation measurements are desirable during the test to verify the use of HF propagation modes.

4.2.2 (U) Targets. (U)

For Fleet Air Defense the primary targets are enemy aircraft and missiles. The P3B aircraft has a radar cross section which is typical for enemy aircraft. Air-to-surface and surface-to-surface missiles generally have a smaller cross section and should be tested separately. Table 4-3 summarizes the estimates of operating characteristics for some of the Soviet aircraft and missiles that are threats to the U.S. Fleet.

UNCLASSIFIED

UNCLASS.

[REDACTED]
(This page is UNCLASSIFIED)

TABLE 4-1. (U) EXPERIMENTAL FACTORS. (U)

1. Transmitter Sources
 - a. Location
 - b. Operating Frequency
 - c. Schedule of Operation
 - d. Effective Radiated Power

2. Simulated Targets
 - a. Type and Size
 - b. Availability
 - c. Number

3. Receiving System
 - a. Platform: Shipborne/Landbased
 - b. Antenna Arrays
 - c. Receivers
 - d. Processing and Data Storage Equipment
 - e. Test Equipment

4. Test Location/Conditions
 - a. Sources Availability
 - b. Target(s) Availability
 - c. Receiver Ability
 - d. Similarity to Operational Environment
 - e. False Alarm/Noise Levels

[REDACTED]
UNCLASSIFIED

UNCLASSIFIED

TABLE 4-2. ^(U) CANDIDATE SOURCES FOR FAD POLYSTATIC EXPERIMENT. (U)

1.	<u>Atlantic Coast</u>
a.	<u>Broadcast Transmitters</u>
	CBC - Sackville, New Brunswick
	WNYW - New York, New York
	VOA - Greenville, North Carolina
b.	<u>Experimental HF Transmitters</u>
	MADRE Radar - Virginia
	Carter Cay - Bahamas
2.	<u>Pacific Coast</u>
a.	<u>Broadcast Transmitters</u>
	VOA - Dixon, California
	VOA - Delano, California
	KGEI - Belmont, California
b.	<u>Experimental HF Transmitters</u>
	Stanford University - Palo Alto, California

[Redacted]

UNCLASSIFIED

UNCLASSIFIED

TABLE 4-3. TYPICAL AIRCRAFT AND MISSILE THREATS. (U)

UNCLASSIFIED

In the experiments the aircraft and missiles need to be evaluated for a variety of operational profiles, including a number of scattering geometries and target altitudes. Soviet air-to-surface missiles, for example, are known to be capable of being launched at a range of altitudes but follow a low altitude profile for minimum detection. The typical aircraft approach is to fly close to the ocean surface to avoid line-of-sight radar detection. The targets used in the experiment should consist of two sizes (aircraft and missile) and be operated at velocities comparable to those of the expected threats. Turns and other aircraft maneuvers should be tested. Should the tests be constrained to a threat target, then the use of a P3 aircraft flying at 300 feet above the ocean surface for a variety of transmitters-target-receiver geometries is recommended. Should a number of test aircraft and missiles be available, single and multiple aircraft/missile signatures should be obtained for multiple signature and location evaluation.

Besides the intended targets, there may be commercial and military aircraft that are operating in the vicinity of the transmitters and receiver sites during tests. These aircraft will provide false alarms during the experiments. Schedules of such flights need to be obtained where possible for the evaluation of the experimentally collected data.

4.2.3 (U) Receiving Site. (U)

In the FAD polystatic radar system concept the receiving system is located on one or more of the ships of the fleet being protected. However, for experimental testing the receiving system can be located on a ship or at a landbased site. The use of a shipborne platform necessitates a ship having an accurate HF direction finding antenna system. It also would entail the assignment of a ship for the calibration and collection of experimental data and possibly the processing of ship navigational data to evaluate location estimation accuracies. In contrast, the use of a landbased receiving site simplifies the conduct of the experiments because the normal operational problems are circumvented and attention can be focused on the key facets of the FAD polystatic experiment. The destroyer DD714 (USS Gilbert Roan) contains an HF DF array and appears suitable as shipborne receiving platform. The potential landbased sites include the following:

- | | | | |
|----|------------------------|---|------------|
| a. | Vint Hill Farm Station | } | East Coast |
| b. | Madre | | |
| c. | White House | | |
| d. | Eastern Test Range | | |

UNCLASSIFIED

4.2.3 (U) -- Continued.

- | | | | |
|----|-------------------------|---|------------|
| e. | Stanford Antenna Array | } | West Coast |
| f. | Los Banos Antenna Array | | |

Of the two types of sites the landbased site is recommended because of operational simplicity in conducting the tests. For this alternative there is greater access to test equipment and the scheduling of data collection is not as severe as for shipborne operation. In addition, the collection and processing of ship navigational data is not required for experiments using a landbased site.

4.2.4 (U) Test Location/Conditions/Evaluation. (U)

The specific test location, conditions and evaluation depend on a combination of the factors described above. The availability of sources, targets, and receiving sites dictate the feasibility and cost of conducting tests on the Atlantic and Pacific coasts. When all three factors are considered, the principle test locations for consideration are the Pacific coast, Northern Atlantic area, and Southern Atlantic region. Of these regions the one that appears most suitable is the southern Atlantic region.

4.2.4.1 (U) Test Location. (U)

The southern Atlantic region is recommended for the FAD poly-static tests for a number of reasons. First there are a number of broadcast stations available. Second, forward-scatter geometry that is most representative for FAD can be achieved by using transmitters from Costa Rica, San Jose, Cuba, Paraguay and a receiving site at Vint Hill Farms Station, the Madre radar site, the White House site and/or the Eastern Test Range site. This allows a landbased site to be employed instead of a ship for the receiving system. The test region contains a sufficient amount of non-hostile aircraft so that false alarm signatures can be examined in conjunction with target signatures. In addition, most of the necessary receiving equipment is available and demonstrations can readily be made to Government personnel from the Washington, D.C. area. These reasons, plus others such as the availability of HF calibration equipment (e.g., ionospheric sounders), make the southern Atlantic region preferable to the others.

4.2.4.2 (U) Test Conditions. (U)

Once the test location is selected the test conditions that need to be delineated include primarily the transmitter frequencies to be used, target test trajectories, the equipment to be utilized, and the data to be collected.

UNCLASSIFIED

4.2.4.2

(U)

Continued.

UNCLASSIFIED

As mentioned previously, the targets must include both aircraft and missiles. The aircraft should be flown at various ranges, azimuths, and altitudes from the receiving site. Various aircraft maneuvers such as turns and dives should be included. A head-on approach to the receiver site as well as a fly-by-trajectory should be conducted. The time and location for each aircraft maneuver should be noted for correlation and with the collected experimental data. Missiles comparable to the Soviet AS-2 through AS-5 series should be fired, if possible, to obtain missile signatures at various ranges, altitudes and operating conditions. At least three signatures of missile trajectories should be obtained at different frequencies for the extrapolation of experimental data from aircraft targets and to demonstrate the system's ability to differentiate between aircraft and missile signatures. Table 4-4 summarizes the recommended transmitter source and target test parameters.

The receiving equipment system required to perform the experiment include an antenna system, receivers, a data processor, and associated peripheral equipment. If one of the landbased sites (e.g., Vint Hill Farms Station) is employed, then most of the antenna system equipment necessary for the experiments exist. Only the commitment of the equipment for the tests is required by the responsible agency to conduct the experiments.

The experimental data that needs to be collected include signal and noise measurements, Doppler signatures, and the DF information associated with the signatures for aircraft and missiles under various conditions. This data can be processed to:

- a. demonstrate the detection range of the polystatic technique, and
- b. verify the accuracies of the target location estimation method.

4.3

(U) SYSTEM DESIGN. (U)

In order to demonstrate the FAD target detection range capability and the accuracy of the location techniques described in previous sections of this report, a system as shown in the functional block diagram in Figure 4-1 may be used. By using both cooperative and noncooperative HF CW transmitters, this receiving system will be able to determine target Doppler and azimuth for test targets at beyond line-of-sight distances. This system would be capable of being operated in any of the three following modes:

UNCLASSIFIED

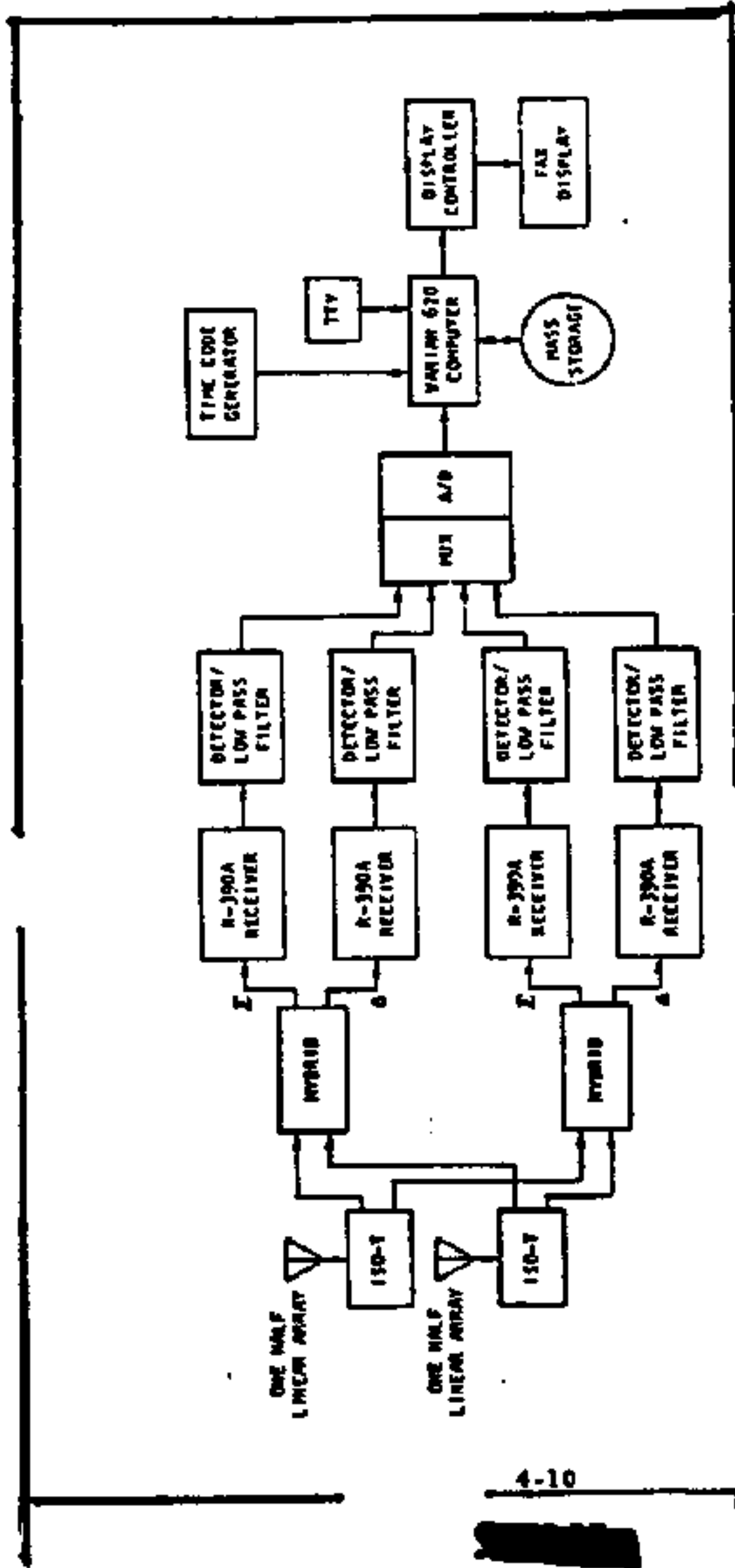
UNCLASSIFIED

TABLE 4-4. TEST PARAMETERS FOR EXPERIMENT. (U)

Transmitters:	Cooperative HF, and Noncooperative HF Broadcast
Target Types:	Aircraft, Missiles
Transmitter-Target Ranges:	50, 100, 200 N. M.
Target-Receiver Ranges:	50, 100, 200 N. M.
Aircraft Altitudes:	200, 500, 1000 feet above ocean level
Approaches:	Head-on, Fly by
Maneuvers:	Turn, Climb, Dive
Target Velocities:	250-400 ft/sec. (Aircraft) 700-7,000 ft/sec. (Missile)*

* At least three missile signatures at 100 NM range, 200 ft altitude with a head-on approach.

UNCLASSIFIED



4-10

Figure 4-1 (U) System Block Diagram. (U)

4.3

(U) -- Continued.

- a. the double baseline, single measurement mode;
- b. the single baseline, double measurement mode; and
- c. the four Doppler location mode.

Target tracking using the double-baseline technique would be accomplished by measuring the Doppler shift on two paths and the apparent angle-of-arrival to the target for each transmitter frequency. Both real-time Doppler and real-time azimuth would be displayed on a fax display. Similarly, the single baseline, two-measurement technique may also be used for target location by making two successive Doppler and two successive azimuth measurements separated by at least 10 and no more than 100 seconds. Finally, the four Doppler target location technique may also be tested with this system by using each of the four receivers to measure and display Doppler only.

The design goals of this system are to--

- a. measure azimuth to 1° and Doppler to 0.1 Hertz;
- b. be easy to operate by an untrained operator;
- c. be ultimately suitable for shipboard shock and vibration environment; and
- d. be principally composed of off-the-shelf hardware.

The one degree azimuth and 0.1 Hertz Doppler measurement accuracy are based upon the location technique and error analysis results. The required operator skill to use this system for target tracking is quite simple. The operator simply tunes each pair of receivers to the appropriate transmitter frequency of interest. During an event he observes and records the displayed Doppler and displayed azimuth signature for the target. Finally, the operator scales the Doppler and azimuth data, and inputs this information back into the computer to solve for range. The basic hardware items for this system are off-the-shelf and generally rugged enough for a shipboard environment. All of the electronics is solid state, except for the R390 receiver, which is used for shipboard HF communications.

4.4 (U) DESIGN CONCEPT. (U)

The following subsections discuss in detail the block diagram, techniques for Doppler and azimuth measurement, the required data displays and general operational procedures.

~~SECRET~~

(This page is UNCLASSIFIED)

UNCLASSIFIED

4.4.1 (U) System Description. (U)

As shown in Figure 4-1 the antenna array consists of a linear disposed antenna with one-half of the array connected to one of the two data channels. ISO-T's are used to divide the signal power between the two channels. In each data channel the signals are combined in a hybrid which produces sum (Σ) and difference (Δ) output signals. The particular transmitter to be spectrum analyzed is tuned up using standard R390A receivers. The paired receivers are gain matched to provide necessary monopole DF technique accuracy. The IF output of each receiver is envelope detected using high dynamic range AM detector, is low-pass filtered to approximately a 20 Hertz bandwidth to prevent aliasing during the sampling process in the A/D converter. Following sampling and A/D conversion the data is input in a recirculating buffer in the Varian 620/f computer. A total of four input buffers are used to store each 10-second duration signal to provide the 0.1 Hertz resolution required. One channel at a time is spectrum analyzed using the FFT algorithm and the voltage spectral density is calculated. The sum data signal is logarithmically compressed and matched to the dynamic range of the display and finally output to the display. The display matching process is used to automatically adjust the average level of a spectral data to the most sensitive range of the grey scale on the fax display. Each Doppler channel appears in the conventional time-frequency-intensity format on the display.

4.4.2 (U) Azimuth Angle-of-Arrival Calculations. (U)

The magnitude of the spectrum from the delta channel is combined with the previous spectrum from the sum channel to compute the angle-of-arrival of each time frequency cell for that spectrum. The angle-of-arrival from boresight for each time frequency cell may be expressed as:

$$\alpha_i = \sin^{-1} \left[\frac{\lambda \tan^{-1} (\Delta_i / \Sigma_i)}{\pi d \cos E} \right]$$

where

- λ is the operating wavelength,
- d is the physical separation between phase centers of the LDAA antenna,
- E is the elevation angle-of-arrival,

~~SECRET~~

UNCLASSIFIED

UNCLASSIFIED

4.4.2 (U) -- Continued.

Δ_i is the i^{th} frequency in the delta spectral array,

Σ_i is the i^{th} member of the sum spectral array, and

α_i is the azimuth angle-of-arrival of the i^{th} frequency time component.

Thus, we compute for each spectrum and each frequency, the angle-of-arrival of that bit of data. The α_i data is then formed into an alpha array, is amplitude compressed, display matched and displayed on the fax in a time-angle-intensity format.

The function $\alpha(t, f_i)$ is also stored in a mass-storage disk for later operator recall. This data is stored also in a recirculating buffer format so that the most recent 10 minutes of data is available to the operator. This same time-angle-amplitude data is computed for both channels and is displayed on a fax paper as well as being stored on the disk.

4.4.3 (U) Data Extraction. (U)

When a target detection is made as noted by observing the Doppler on the Doppler channel displays, the operator then manually measures the target Doppler frequency and target angle-of-arrival. If the double baseline, single-measurement technique is under test, measurements are made for both data channels. If the single baseline, double-measurement technique is under test, the operator first enters the time, frequency and target azimuth data at time T_1 , then on the order 10 to 60 seconds later the operator again measures the T_2 time, Doppler and target azimuth data on that same channel. Or, if the four Doppler target location technique is being employed, one frequency measurement is made for each of the four Dopplers. The appropriate data is then entered by the operator into the computer system via the teletype. For each set of data entered by the operator, the computer will solve the target range-azimuth algorithm and print out the results for the operator to review.

Although the operator has displayed for his viewing the computed target azimuth on the fax display, the operator scaling of the angle data will probably not be used in the actual range calculation. The appropriate angle information for each time-frequency cell entered by the operator will be retrieved from the disk storage device. This is because greater angular precision is stored on the disk and can be displayed on the fax display.

UNCLASSIFIED

4.4.3 (U) -- Continued.

An artist's concept of what this system might look like is shown in Figure 4-2. The rack at the left shows the four R390A receivers. The next rack contains the computer core memory, power supply, disk, A/D converter and other associated electronics. The operator is shown seated in front of the electrographic display with the teletype shown to the right.

4.5 (U) DETAILED DESIGN SPECIFICATIONS. (U)

4.5.1 (U) Spectrum Analysis Specifications. (U)

The specifications for the spectrum analysis portion of the system are given in Table 4-5.

Table 4-5 (U). Spectrum Analysis Specifications. (U)

<u>INPUT</u>	
Sample rate (per channel)	51.2 samples per second
Number of channels	4
Fast Fourier Transform size	512 points
Number of seconds of data per transform	10
<u>OUTPUT</u>	
Frequency resolution	0.1 Hz
Bandwidth (folded)	0-25.6 Hz
Displayed bandwidth	0-20 Hz
Approximate time required for FFT and angle calculations (per channel)	500 msec
<u>DUTY FACTOR</u>	
	500 percent

The requirement for a displayed bandwidth of 0-20 Hz is set by the back-scatter radar. Thus, the Doppler frequency shift equals --

$$\frac{2vf}{c}$$

UNCLASSIFIED

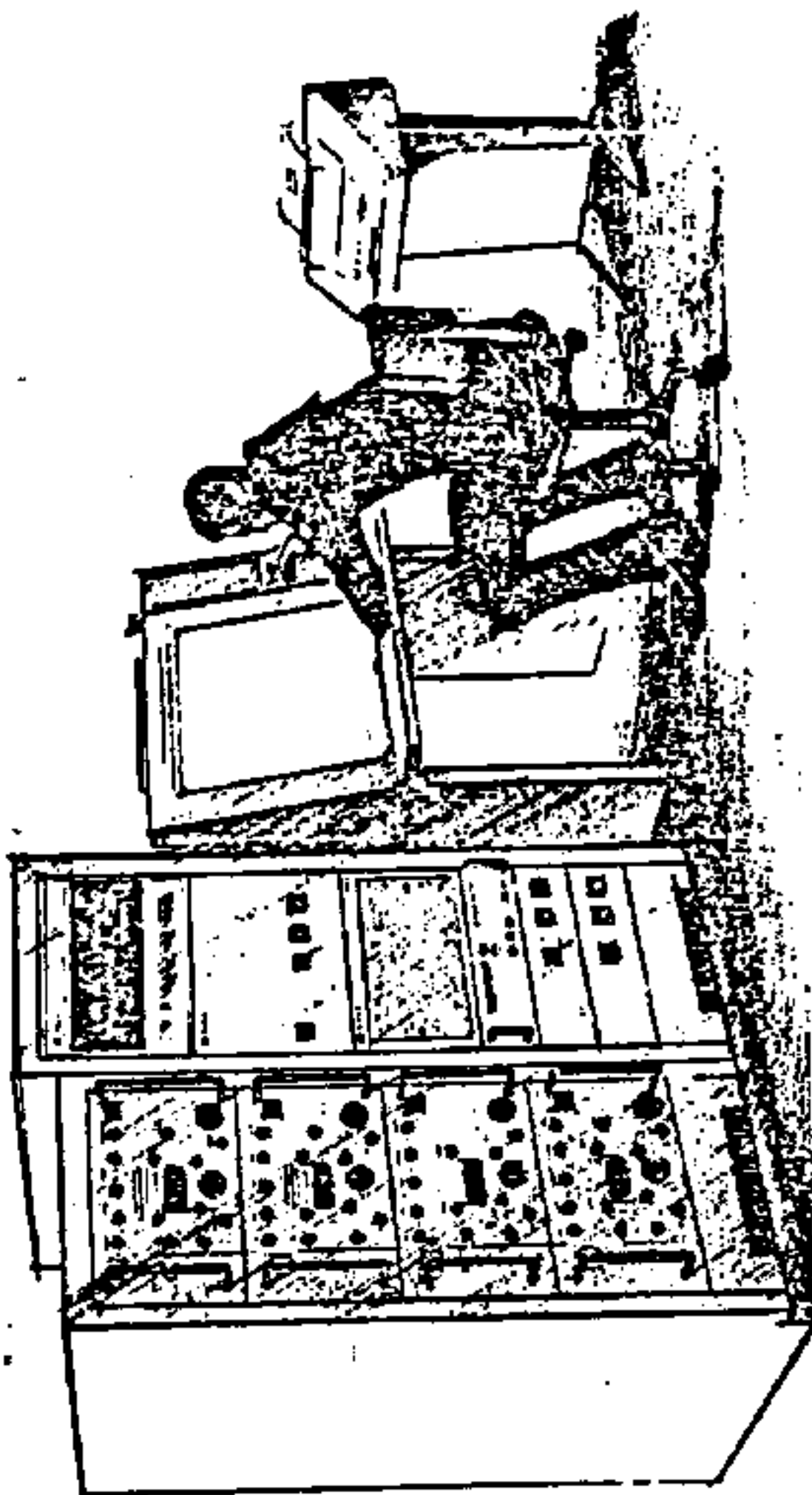


Figure 4-2 (U). Artist's Concept of Data Collection System (U).

-4-15-

UNCLASSIFIED

UNCLASSIFIED

4.5.1 (U) -- Continued.

where $c = 3 \times 10^8$ meters per second. If we assume $v = 600$ MPH, the maximum airspeed for the P3 aircraft recommended for the experiment and $f = 10$ MHz which will be a typical transmitter frequency used in the experiment, we get a frequency shift of 18 Hz. The backscatter case produces the largest frequency shift and shifts of 10 Hz or less are expected in most cases. Thus a displayed bandwidth of 0-20 Hz should adequately display all data collected in the experiment. The receiver output will be diode detected and the sidebands will be folded about zero Hertz in the 0-20 Hz displayed bandwidth, thus sideband sense will not be available from the display. However since the system will be used as part of an experiment, the sideband sense of the target Doppler will be known a priori to the operator. The chief advantage to the folded spectrum is that the time required for the Fast Fourier Transform and the disk and core storage are all halved by using the folded spectrum.

The requirement for 0.1 Hz resolution is set by the nature of the range estimation techniques.

Using the requirements for resolution and bandwidth, the A/D sample rate is 51.2 samples per second. The time samples are stored for 10 seconds and a Fast Fourier Transform (FFT) is performed on the 512 samples. The output of this transform is 256 frequency domain points which represent a bandwidth of 0-25.6 Hz with a resolution of 0.1 Hz. Since the low-pass filter used after the detector in the receiver is not an ideal low-pass filter, there will be some attenuation on the skirt of the filter and several frequency points will be affected. The displayed bandwidth has been set at 0-20 Hz for this reason.

The time required to perform the 512 point FFT and associated data manipulations is estimated to be 350 milliseconds. The time required for the azimuth angle calculations and associated data manipulations is estimated to be 300 milliseconds. The FFT estimate was obtained from a relative computational power and speed comparison between the SEL 810B computer and the computer proposed for this system, the Varian 620/i. Programs written for the 810B require 250 milliseconds to do the transform and the slightly slower 620/i should require 350 milliseconds or less. The estimate for the azimuth calculations was determined by coding a sample loop which computes the azimuth, and calculating the time to perform this operation on the 200 frequency domain points from each of the two channels used. A factor is then added to cover the overhead involved in the data manipulations.

UNCLASSIFIED

UNCLASSIFIED

4.5.1 (U) -- Continued.

This total of 700 milliseconds for the two FFTs and the 300 milliseconds for the azimuth angle calculations for each of the two receiver pair gives an average of 500 milliseconds per data channel. Thus, the system is able to process each sample of data with a duty factor of 500 percent. Duty factor is defined as the time duration of the transformed data divided by the time required to process that data for all the channels. Thus for 4 channels of data at 500 milliseconds per channel the duty factor is:

$$\frac{10.0}{(0.50)(4)} = \frac{10.0}{2.0} = 500 \text{ percent.}$$

Simply stated, each time sample of data is processed 5 times. Storing the time samples in a recirculating buffer permits the processing of the most recent 10 seconds of data. The higher the duty factor, the more smoothing and averaging of the data results, and the longer the Doppler-related data is displayed.

The two-tone dynamic range of the system will be 90 db which is the limit available with a 16-bit computer. This 90 db two-tone dynamic range is also approximately the dynamic range of the R390A receiver that is to be used in the experiment. In addition, atmospheric conditions are generally such that signals which necessitate a two-tone dynamic range of greater than 90 db are very rare.

4.5.2 (U) Azimuthal Specifications. (U)

The azimuth angle calculations will be done using the algorithm explained in Section 4.4. The azimuth calculated will have a range of -30° to +30° and will have a calculation resolution of 0.25°. The calculated azimuth can therefore be expressed as an 8-bit number which can represent up to 256 values, although only 240 values are required.

4.5.3 (U) Storage and Display Specifications. (U)

The computer core storage requirements for the programming and buffers required for the software implementation of the system are shown in Table 4-6. The total of 7,150 words will fit into the 8 K of core which is available on the Varian 620/f. If other features are added to the system or if the estimates given in Table 4-6 prove to be low, additional 4 K increments of memory are available.

UNCLASSIFIED

TABLE 4-6. (U) COMPUTER CORE REQUIREMENTS. (U)

<u>Programs</u>	<u>Words</u>
Signal Processing Programs	1500
Disc Handling	400
Teletype Handling	400
Range Algorithm	<u>2000</u>
	3900
<u>Buffers</u>	
Input Buffer	2048
Time-Weight Table	256
Sin/Cos Table	128
Work Area	512
Display Buffer	<u>275</u>
	3219 = 3250
<u>Total</u>	7150

UNCLASSIFIED

4.5.3 (U) -- Continued.

The azimuth calculations will result in an 8-bit number (8r byte). Each of two receiver pairs will compute 200 azimuthal points every 2.0 seconds. These azimuthal points will be stored 2 bytes to a 16-bit word on the disk. The disk to be used in the system has a storage capacity of 64,000 words; approximately 4,000 words will be used for program storage. At 200 words every 2 seconds, 600 seconds of data will be stored on the disk. The disk will always contain the most recent 10 minutes of data.

The spectral and azimuthal data will be displayed on an electrographic facsimile display. The display, shown in Figure 4-3, contains data from each of the two receiver pairs; these pairs are referred to as Channel A and Channel B in the figure. Each channel contains a spectral display of frequency, amplitude and time and an azimuthal display of angle, amplitude and time. The specification for the display are also given in the figure. At a sweep rate of one line per second and a resolution of 99 lines per inch, the most recent 30 minutes of data will be displayed on the fax at one time. In addition to the spectral and azimuthal display on the fax, the time code will be put on the fax. On the edges of the fax the time of day and the Julian day of the year will be encoded; this code will be put on once an hour. In the area between the spectrum and azimuth displays, marks will appear at every one and ten minute transition of the time code generator.

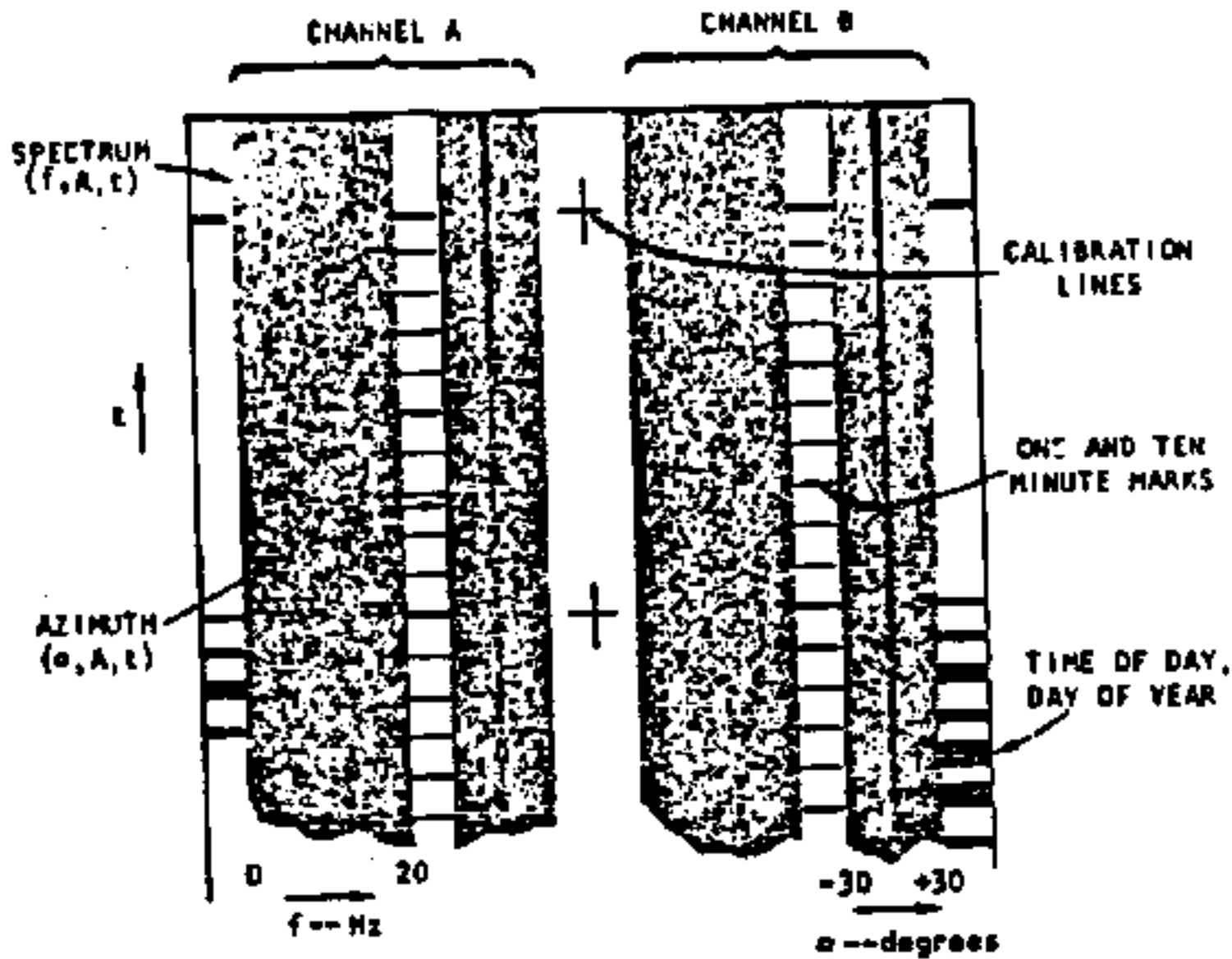
4.6 (U) COMPUTER HARDWARE DESCRIPTION. (U)

4.6.1 (U) Computer. (U)

The computer selected to perform the signal processing and related functions is the Varian 620/I. The Varian 620/I computer is a high-speed, general purpose, digital computer for scientific and industrial applications. Its features include--

Fast operation:	750-nanosecond memory cycle
Large instruction repertoire:	148 instructions
Word length:	16 bits
Modular core memory:	Expandable to 32,768 words in 4,096 increments
Automatic data transfer:	Direct memory access facility provides automatic data transfers with rates to 276,000 words per second

UNCLASSIFIED



SPECTRAL CHANNEL

0-20 Hz 0.1 Hz RESOLUTION
4 IN. WIDE 5 Hz PER INCH

AZIMUTHAL CHANNEL

-30° TO +30° 0.25° RESOLUTION
2.4 IN. WIDE 25° PER INCH

AMPLITUDE

32 LEVELS OF GREY SCALE

HORIZONTAL RESOLUTION
VERTICAL (TIME) RESOLUTION
SWEEP RATE

50 LINES PER INCH
99 LINES (SECONDS) PER INCH
1 LINE PER SECOND

Figure 4-3 (U). Fathometer Display. (U)

UNCLASSIFIED

4.6.) (U) -- Continued.

Multiple addressing: Direct, indirect, relative, index (pre and post), immediate, and extended

Flexible I/O: Ten devices may be placed on the I/O bus. The I/O system can easily be expanded to include features such as automatic block transfer, priority interrupt, and cycle-stealing data transfers

Extensive software: Complete package includes a symbolic assembler, subroutine library, A/D diagnostics, and an ASA FORTRAN compiler

The mechanical specifications for the 620/f are--

Dimensions: The mainframe and expansion frames are 10-1/2 inches high, 19 inches wide, and 21 inches deep.

Input voltage: 105 to 145V ac or 210 to 250V ac, 60 Hz

Input current: The mainframe power supply requires approximately 15 amperes ac; each expansion frame power supply requires approximately 4 amperes ac.

Temperature:

- Operating 0 to 50 degrees C
- Storage 20 to 70 degrees C

Humidity:

- Operating To 90 percent without condensation
- Storage To 95 percent without condensation

Vibration: 3 to 10 Hz at 1g force or 0.25 double amplitude, whichever is less. Exponentially-raised frequency from 3 to 10 Hz and back to 3 Hz over a 10 minute period, three complete cycles. This specifications applies for all three principal axes.

Shock: 4g for 11 milliseconds (all three principal axes)

UNCLASSIFIED

4.6.1 (U) -- Continued.

The 620/f was chosen on the basis of four factors--

- a. speed,
- b. capability,
- c. mechanical specifications, and
- d. cost.

The 750 nanosecond cycle time of the 620/f makes it one of the fastest 16-bit computers commercially available. This speed is combined with a powerful instruction set which permits fast execution of the FFT and azimuth angle calculation algorithms and thus gives a duty factor of over 500 percent in the processing. The temperature, vibration and shock specifications exceed most computers in the 620/f's price/performance field. The basic cost of the 620/f is below or comparable to most of the 16-bit computers in its performance field.

4.6.2 (U) Analog-to-Digital Converter. (U)

The analog to digital converter (A/D) selected for the system is the Raytheon Miniverter. The model of the Miniverter selected is a 12-bit A/D which has a throughput rate of 45 KHz, an aperture time of 50 nanoseconds and a resolution of 5 millivolts. The Miniverter is packaged in a very compact unit and has proven to be very reliable as a system component.

4.6.3 (U) Disk. (U)

The disk selected for the system is the Singer-Librascope, Model L107. The Singer-Librascope disk is a small, inexpensive and very rugged disk system which meets all the system requirements.

The specifications for the Model L107 are--

Maximum capacity bits:	1,080,000
Maximum capacity words:	67,000
Data heads:	45
Timing heads:	1

UNCLASSIFIED

4.6.3 (U) -- Continued.

Maximum bits/track: 24,000
Rotation speed, RPM: 3,600
Clock frequency, MHz Max.: 1.4

The mechanical specifications are--

Dimensions: 6 inches high x 9 inches diameter
Weight: 12 pounds (approximately)

Operating environment:

- Temperature 0°C to 55°C
- Humidity 90 percent R.H. without condensation
- Shock 10-Gs 11-msec rise time (no shock isolators required)
- Vibration 2-Gs acceleration max., 5 Hz to 50 Hz (no shock isolators required)

Nonoperating environment:

- Temperature -50°C to +75°C
- Humidity 95 percent relative humidity, no condensation.
- Shock 15-Gs 11-msec rise time (with no shock isolators)
- Vibration Mil-Std-810B, Method 514, Category (C) equipment specification used as a guideline. This equipment category is for shipment by common carrier, land or air.

Power requirements:

- Disk 115V ac, 50/60 Hz, single phase 1.5A
- Electronics +5V dc at 1.4A
-5V dc at 0.25A
+25V dc at 0.2A

UNCLASSIFIED

This Page Intentionally Blank

4-24

UNCLASSIFIED

UNCLASSIFIED

APPENDIX A

PROPAGATION PREDICTION PROGRAM. (U)

(U) The propagation prediction program used to estimate the system performance basically combines a modified version of the ITSA/ESSA HF propagation prediction program for mode and mode amplitude prediction; the bistatic radar range equation to predict the received scatter path power; and an ITSA/ESSA noise prediction program to estimate atmospheric, man made, and galactic noise at the receiver site.

(U) The prediction program package consists of individual computer programs that (a) compute a target trajectory; (b) predict propagation mode structure and mode amplitude; and (c) predict the doppler and missile cross-section.

(U) The trajectory simulation program estimates the missile or aircraft trajectory based upon fitting the flight profile to a functional form using a least-squares fit technique. The required inputs to generate the model profile are liftoff and burnout times, launch azimuth, apogee, and range. The program then computes altitude, range, latitude, longitude, velocity, the speed of sound, Mach number, Mach angle, local target bearings, local target elevation angles, and acceleration. The computed parameters serve as inputs to the propagation prediction program to determine mode structures with a time varying terminal point on the trajectory.

(U) The ITSA/ESSA propagation prediction program has been modified to allow for non-congruent hop structures and for propagation to and reflection from a point above the earth. The program predicts the mode structures that meet ionospheric propagation conditions on each of the three paths: the direct (transmitter-receiver) path, the transmitter-target half path, and target-receiver half path. In addition, the propagation losses and antenna gains for each mode are determined. For each mode predicted on the transmitter-missile half path, an "incident" (at the target) elevation angle, measured from the local horizon, is found. For each mode predicted on the target-receiver half path, the "scattered" elevation angle is also found. These parameters are then used with a modeled profile to predict doppler frequencies.


(U) Propagation predictions are based on empirically derived world-wide numerical maps of vertical ionosonde data. The results are monthly ionospheric coefficients which can be used with the parabolic layer assumption (parabolic electron density variations in the E and F layers) to predict monthly average ionospheric conditions affecting a specific ray path at any hour of the day.


A-1


UNCLASSIFIED


UNCLASSIFIED


App. A  --Continued.


(U)  In the prediction model, all line of sight, E and F propagating modes are determined between the transmitter and the target, between the receiver and the target, and between the transmitter and the receiver. The determination of these "half paths" is a generalization of the ground-to-ground prediction technique to include the case of ground-to-elevation-point predictions.

(U)  After the mode structures that meet the ionospheric conditions are identified, (those between horizontal screening and ionospheric penetration) propagation losses and antenna gains are determined. The losses calculated are free space loss (inverse square law), D-layer absorption loss, and ground reflection loss. The NBS empirical adjustment factor is included on the direct-path predictions to account for non-calculated losses. This factor is statistical and varies with season, path length, and earth location of the path. No similar adjustment factor is used or known for the half paths. The antenna types are specified for the system and the appropriate gain routines or gain tables are used.

(U)  The target scattering model for missile targets above 100 km is a hyperboloid compressed-ambient ionization in the exhaust-plume bow shock wave. The shock-wave scattering surface is considered hyperboloidal from photographic observations which have shown that the shock-wave surface could be described by a second order function and that the shock-wave surface should be asymptotic to the Mach cone.

(U)  The direction of the rays for the transmitter-missile and receiver-missile propagation paths uniquely define a plane tangent to the hyperboloidal surface which has the proper orientation for a reflection, provided the incident ray encounters a high enough electron density for reflection.

(U)  Since little definitive work has been done to accurately model missile cross sections below 100 km or aircraft cross sections at HF, a constant (adjustable) cross section is used for aircraft and missile targets below 100 km.

(U)  The antenna gain patterns for both the monopole transmitter antennas and the LDAA receiving antenna are part of the program. The gain pattern for the LDAA was obtained from data supplied by ITT by using azimuth patterns predicted by the array factor technique for 16 monopole elements and the elevation patterns from scaled model measurements.

UNCLASSIFIED

END

DATE
FILMED

6 - 71